3-10-2022

Volitional Control of Lower-limb Prosthesis with Vision-assisted Environmental Awareness

S M Shafiul Hasan
Florida International University, shasa022@fiu.edu

FLORIDA INTERNATIONAL UNIVERSITY

Miami, Florida

VOLITIONAL CONTROL OF LOWER-LIMB PROSTHESIS WITH VISION-ASSISTED ENVIRONMENTAL AWARENESS

A dissertation submitted in partial fulfillment of the

requirements for the degree of

DOCTOR OF PHILOSOPHY

in

ELECTRICAL AND COMPUTER ENGINEERING

by

S M Shafiul Hasan

2022

To: Dean John L. Volakis
College of Engineering and Computing

This dissertation, written by S M Shafiul Hasan, and entitled Volitional Control of Lower-Limb Prosthesis with Vision-assisted Environmental Awareness, having been approved in respect to style and intellectual content, is referred to you for judgment.

We have read this dissertation and recommend that it be approved.

Armando Barreto

Jean Andrian

Hai Deng

Wei-chiang Lin

Ou Bai, Major Professor

Date of Defense: March 10, 2022

The dissertation of S M Shafiul Hasan is approved.

Dean John L. Volakis
College of Engineering and Computing

Andrés G. Gil
Vice President for Research and Economic Development
and Dean of the University Graduate School

Florida International University, 2022

DEDICATION

To my two stars- Samira and Sarina, and my loving parents.

ACKNOWLEDGMENTS

First and foremost, I want to thank my advisor, Dr. Ou Bai, for his patience, enthusiasm, and vast expertise. His guidance aided my personal and professional development. He never hesitated to commit his time to discussing the research, regardless of the time of day or night.

Dr. Deng, Dr. Barreto, Dr. Andrian, and Dr. Lin, members of the committee, thank you for taking the time to review and remark on this dissertation.

Roozbeh, Sebastian, Sai, Masud, Rodrigo, Tong, Robin, Kaida, Chaohao, my friends and colleagues in the Human Cyber Physical Systems (HCPS) lab, deserve a special thanks for their support and assistance throughout the journey.

My heartfelt appreciation goes out to my parents and brother, Tuhin, without whom none of this would have been possible. Thank you, Sohana, Imran, Arka, Saima, Rafi, Nadia, Proyash, Prianka for being there for me through thick and thin. Last but not the least a special word of gratitude to my wife, who held everything together for me; and my little angel, Sarina for bringing the much needed joy in these trying times.

This dissertation project was funded by a graduate assistantship from Florida International University's Department of Electrical and Computer Engineering, the Dissertation Year Fellowship and Graduate Student Research Support Program by Florida International University's University Graduate School and the National Science Foundation (CNS-1552163).

ABSTRACT OF THE DISSERTATION

VOLITIONAL CONTROL OF LOWER-LIMB PROSTHESIS WITH VISION-ASSISTED ENVIRONMENTAL AWARENESS

by

S M Shafiul Hasan

Florida International University, 2022

Miami, Florida

Professor Ou Bai, Major Professor

Early and reliable prediction of user's intention to change locomotion mode or speed is critical for a smooth and natural lower limb prosthesis. Meanwhile, incorporation of explicit environmental feedback can facilitate context aware intelligent prosthesis which allows seamless operation in a variety of gait demands. This dissertation introduces environmental awareness through computer vision and enables early and accurate prediction of intention to start, stop or change speeds while walking. Electromyography (EMG), Electroencephalography (EEG), Inertial Measurement Unit (IMU), and Ground Reaction Force (GRF) sensors were used to predict intention to start, stop or increase walking speed. Furthermore, it was investigated whether external emotional music stimuli could enhance the predictive capability of intention prediction methodologies. Application of advanced machine learning and signal processing techniques on pre-movement EEG resulted in an intention prediction system with low latency, high sensitivity and low false positive detection. Affective analysis of EEG suggested that happy music stimuli significantly ($p<0.05$) enhanced movement related neural phenomena and thus could enhance the state-of-the-art brain computer interface technologies. To enable vision assisted environmental awareness, approximately an hour-long video of five types of terrains, e.g., asphalt, brick, concrete, grass, gravel was recorded using a wearable camera system placed on a

subject's ankle. A deep convolutional neural network was trained on the collected image database using a transfer learning approach and it showed significant accuracy and early prediction time in predicting terrain type and an oncoming transition of terrain before the first heel strike on the new terrain. The outcomes of the dissertation suggest that the proposed methodologies can provide highly accurate neural decoding of movement intention and facilitate environmental context awareness by recognizing terrain type and incoming transition. Therefore, the combination of neural decoding and computer vision can enable seamless operation of lower limb prosthetic systems in the event of changing terrain and speed demands.

TABLE OF CONTENTS

CHAPTER PAGE

1. INTRODUCTION 1
1.1 Background 1
1.2 Motivation 2

2. FEASIBILITY OF PREDICTING GAIT INTENTION 6
2.1 Background 6
2.1.1 Neural Phenomenon Related to Movement Intention 6
2.1.2 Related Work 7
2.2 Current Work 9
2.3 Methods 10
2.3.1 Experimental Procedure 10
2.3.2 Data Acquisition 12
2.3.3 Motion Capture System 13
2.3.4 Data Preprocessing 14
2.3.5 Discrete Wavelet Transform 17
2.3.6 Data Segmentation 17
2.3.7 Feature Extraction 19
2.3.8 Feature Selection 21
2.3.9 Offline Classification 21
2.4 Results 22
2.5 Discussion 30
2.6 Conclusion 36

3. EXPLORING THRESHOLD RESGULATION AND MAJORITY VOTING FOR ASYNCHRONOUS INTENTION DETECTION 38
3.1 Background 38
3.2 Current Work 38
3.3 Methods 39
3.3.1 Data Segmentation 39
3.3.2 Feature Extraction and Selection 40
3.3.3 Asynchronous Detection 40
3.3.4 Evaluation of the model and thresholds 41
3.4 Results and Discussion 42
3.5 Conclusion 44

4. ASYNSCHRONOUS PREDICTION OF GAIT INTENTION 45
4.1 Background 45
4.2 Current Work 46
4.3 Materials and Methods 47
4.4 Computational Methods for Prediction 48

4.4.1 Data segmentation and epoching . . . 48
4.5 Signal Processing for Time-frequency Analysis . . . 48
4.5.1 Discrete wavelet transform . . . 48
4.5.2 Empirical Wavelet Transform . . . 49
4.5.3 Wavelet synchrosqueezed transform . . . 50
4.6 Feature extraction and prediction . . . 51
4.6.1 Feature extraction . . . 52
4.6.2 Modeling . . . 53
4.6.3 Determining a working threshold . . . 54
4.6.4 Majority voting . . . 54
4.6.5 Neurophysiological Data Analysis . . . 55
4.7 Results . . . 56
4.7.1 Evaluation indices . . . 56
4.7.2 Offline Analysis . . . 58
4.7.3 Pseudo-Online Analysis . . . 61
4.8 Discussion . . . 64
4.9 Conclusion . . . 72

5. VMD-WSST: A COMBINED BCI FOR MOVEMENT INTENTION DETECTION . . . 73
5.1 Background . . . 73
5.2 Materials and Methods . . . 74
5.2.1 Variational Mode Decomposition . . . 74
5.3 Wavelet Synchrosqueezing Transform . . . 75
5.4 Feature extraction and Classification . . . 76
5.5 Results and Discussion . . . 78
5.5.1 Classification Results . . . 78
5.6 Conclusion . . . 80

6. REAL-TIME PREDICTION OF GAIT ACCELERATION INTENTION 82
6.1 Background . . . 82
6.2 Related Work . . . 82
6.3 Current Work . . . 84
6.4 Materials and Methods . . . 85
6.4.1 Subject . . . 85
6.4.2 Experimental Procedure . . . 85
6.4.3 EEG Data Acquisition . . . 86
6.4.4 Event Detection . . . 87
6.4.5 Data Preprocessing . . . 88
6.4.6 Data Segmentation . . . 89
6.4.7 Neurophysiological Data Analysis . . . 89
6.5 Binary Classification and continuous decoding . . . 91
6.5.1 Feature Extraction and Selection . . . 91

6.5.2 Offline Evaluation . . . 92
6.5.3 Pseudo-Online Evaluation . . . 93
6.5.4 Real-time testing . . . 94
6.6 Results . . . 95
6.6.1 Result of Neurophysiological Data Analysis . . . 95
6.6.2 Performance Metrics . . . 96
6.6.3 Offline Classification Results . . . 98
6.6.4 Pseudo-online Classification Results . . . 98
6.6.5 Real-time classification results . . . 99
6.7 Discussion . . . 99
6.8 Conclusions . . . 102

7. ENHANCEMENT OF MOVEMENT INTENTION DETECTION BY AFFECTIVE STIMULI . . . 103
7.1 Background . . . 103
7.2 Materials and Methods . . . 107
7.2.1 Subjects . . . 107
7.2.2 Emotion Stimulus Database . . . 107
7.2.3 Experimental Protocol . . . 108
7.2.4 Analysis of Subjective Emotional Stimuli . . . 109
7.2.5 Data Collection and Event Detection . . . 110
7.2.6 Data Preprocessing . . . 112
7.2.7 Data Segmentation . . . 113
7.2.8 Binary Classification Problem . . . 114
7.2.9 Signal Processing for Feature Extraction . . . 115
7.2.10 Offline and Pseudo-online Training . . . 117
7.2.11 Parameter Tuning . . . 118
7.2.12 Pseudo-online Testing . . . 119
7.2.13 Performance Metrics . . . 120
7.3 Results . . . 121
7.3.1 Neurophysiological Data Analysis . . . 121
7.3.2 Offline Classification Results . . . 128
7.3.3 Pseudo Online Classification Results . . . 133
7.4 Discussion . . . 135
7.5 Conclusion . . . 145

8. VISION-ASSISTED TERRAIN TRANSITION PREDICTION . . . 146
8.1 Background . . . 146
8.2 Related Work . . . 147
8.3 Current Study . . . 150
8.4 Materials and Methods . . . 151
8.4.1 Experimental Protocol . . . 151
8.4.2 Image Preprocessing . . . 153

8.5 Offline Training and testing 155
8.5.1 Pseudo Online Testing 156
8.6 Results and Discussion 158
8.7 Conclusion 166

BIBLIOGRAPHY 168

VITA 185

LIST OF TABLES

TABLE PAGE

2.1 Demographic characteristics of the subjects. 11

2.2 Different levels of coefficients and their corresponding brain waves. . . . 18

2.3 'Rest' vs. 'Start' classification accuracy, sensitivity and specificity for all the subjects using different data windows. 25

2.4 'Walk' vs. 'Stop' classification accuracy, sensitivity and specificity for all the subjects using different data windows. 26

2.5 Mean classification accuracy, sensitivity and specificity with standard deviation for 'Rest' vs. 'Start' classification 27

2.6 Mean classification accuracy, sensitivity and specificity with standard deviation for 'Walk' vs. 'Stop' classification 28

2.7 Result of t-test with Bonferroni-Holm correction performed on classification results. 28

3.1 Classification performance for different subjects with threshold regulation 42

3.2 Cross subject average performance metrics with standard deviation. . . 43

4.1 Offline 'Start' of Gait Prediction Results (Mean±Standard Deviation) . 59

4.2 Offline 'Stop' of Gait Prediction Results (Mean±Standard Deviation) . . 60

4.3 Pseudo-online 'Start' of Gait Prediction Results (Mean±Standard Deviation). 62

4.4 Pseudo-online 'Stop' of Gait Prediction Results (Mean±Standard Deviation). 63

4.5 Comparison of Results with Existing Works. 71

5.1 'Rest' vs. 'Start' Classification Results using VMD+WSST 79

5.2 'Walk' vs. 'Stop' Classification Results using VMD+WSST 80

6.1 Offline Performance Metrics. 98

6.2 Pseudo-online Performance Metrics. 98

6.3 Real-time Testing results. 99

7.1 Subjective Emotion Stimuli. 110

7.2 Comparison of Baseline EEG Powers ($10^{-9}V^2$) across Subjects 126

7.3 Comparison of Average EMG Powers (V^2) across Subjects 128

7.4 Offline Classification Results in Different Emotion States (ERD) 129

7.5 Offline Classification Results in Different Emotion States (ERD+MRCP) 130

7.6 Comparison of Classification Results obtained using Different Feature Combinations. 132

7.7 Pseudo-online Classification Results in Different Emotion States(ERD) . 134

8.1 Comaprison of Pseudo-online Transition Prediction Performance using proposed method and conventional method. 159

8.2 Comaprison of Pseudo-online Terrain Recognition Performance using Different Frame Rates. 160

LIST OF FIGURES

FIGURE PAGE

2.1 The experimental protocol of the study. 12

2.2 The entire body area sensor network for data collection. 14

2.3 The cleaning process of EEG data from subject 5. 16

2.4 Sample data segment from the pressure sensor and right TA EMG. . . . 18

2.5 'Rest' vs. 'Start' classification performance with standard deviation using different data windows. 23

2.6 'Walk' vs. 'Stop' classification performance with standard deviation using different data windows. 24

3.1 Block diagram of the proposed methodology. 39

4.1 Data windows used for offline classifier training and validation, and pseudo-online testing. 49

4.2 Pseudo Online testing procedure. 55

4.3 ERD activity from C3, Cz and C4 channels corresponding to 'stop' of gait. 57

4.4 ERD activity from C3, Cz and C4 channels corresponding to 'start' of gait. 57

5.1 The instantaneous frequencies of the IMFs obtained from a 10-second window. 76

5.2 Comparison of ERD activity obtained by VMD+WSST and a 4th order Butterworth bandpass filtering correspoding to start of gait. 77

5.3 Comparison of ERD activity obtained by VMD+WSST and a 4th order Butterworth bandpass filtering correspoding to stop of gait. 78

6.1 The offline and real-time protocol of the study. 87

6.2 Segment of pressure sensor, top and bottom spine Inertial Measurement Unit (IMU) sensor data 90

6.3 Time-frequency analysis of EEG signals obtained from C3. 95

6.4 Time-frequency analysis of EEG signals obtained from C3. 96

6.5 MRCP plots obtained from C3. 97

6.6 MRCP plots obtained from C4. 97

7.1 Experimental protocol of the study in summary. 108

7.2 EEG and EMG sensor locations. 111

7.3 Wrist extension event detection. 112

7.4 Windowing and segmentation method. 116

7.5 Pseudo online testing procedure. 120

7.6 Comparison of ERD corresponding to the intention of wrist extension in three different affective states, namely neutral, happy and sad. . . 122

7.7 Results of a pairwise permutation test performed on ERD in the range of (-2,2) seconds in three different emotional states at 0.01 confidence level. 123

7.8 Comparison of MRCP in contralateral, medial, and ipsilateral electrodes (from left to right) under three difference affective states. 124

7.9 Result of statistical significance testing at $p<0.05$. 125

7.10 Comparison of EMG activity in three different emotional states. 127

8.1 Example of two types of transitions. 149

8.2 The portable camera system used in this study. 152

8.3 Example of outdoor sites for data collection. 153

8.4 Image Preprocessing Pipeline. 154

8.5 Flowchart of Pseudo-online terrain transition prediction pipeline. 157

8.6 Offline Classification Results using modified Shufflenet. 160

8.7 Pseudo-online terrain transition prediction example between asphalt and gravel. 162

LIST OF ABBREVIATIONS

EEG	Electroencephalography
BCI	Brain-Computer Interface
CDC	Centers for Disease Control and Prevention
GRF	Ground Reaction Force
EMG	Electromyography
VMD	Variational Mode Decomposition
DWT	Discrete Wavelet Transform
EWT	Empirical Wavelet Transform
WSST	Wavelet Synchrosqueezed Transform
SVM	Support Vector Machine
IMF	Intrinsic Mode Function
IMU	Inertial Measurement Unit
RBF	Radial Basis Function
ADMM	Alternating Direction Method of Multipliers
ERD	Event Related Desynchronization
TPR	True Positive Rate
BMI	Brain-Machine Interfaces
ERP	Event-Related Potentials
MRCP	Movement-Related Cortical Potential
ERS/ERD	Event-Related Synchronization/ Desynchronization
BP	Bereitschafts Potential
FFT	Fast Fourier Transform
STFT	Short Time Fourier Transform
IRB	Institutional Review Board
TA	Tibialis Anterior
ASR	Artifact Subspace Reconstruction
ICA	Independent Component Analysis
SD	Standard Deviation
AMICA	Adaptive Mixture Independent Component Analysis
FPR	False Positive Rate
EMD	Empirical Mode Decomposition

EWT	Empirical Wavelet Transform
MRMR	Minimum Redundancy Maximum Relevance
TP	True Positive
TN	True Negative
FP	False Positive
FN	False Negative
ERS	Event Related Synchronization
REST	Real-time EEG Source-mapping Toolbox
MFLOPS	Million Floating Point Operations Per Second
FPS	Frames Per Second

CHAPTER 1

INTRODUCTION

1.1 Background

Locomotion impairments resulting from cerebrovascular accidents, stroke and brain trauma create a severe handicap for many people, especially the elderlies [1, 2]. Besides, lower limb amputation due to trauma or diabetes results in reduced mobility, thus severely affecting people's quality of life. According to the Centers for Disease Control and Prevention (CDC) 19.4 million American adults are unable or find it difficult to walk a quarter of a mile [3]. Moreover, there are 2.1 million people living with limb loss in the USA [4] with an additional 185,000 new cases every year, and that number is expected to double by 2050 [5]. This highly increasing number of people with motor disabilities has made it a critical research question to determine and use proper methods that prove to provide the best rehabilitative outcomes for the impaired people.

Neurorehabilitation, a complex therapeutic approach, is used traditionally to facilitate recovery of neuroplasticity to the motor impaired [6, 7]. However, such therapies only provide passive support to the motor impaired [8, 9, 10]. This issue coupled with the enhancement of computational power and improvement in design have resulted in the emergence of various assistive devices as an alternative pathway to assist people with motor disabilities. Various assistive orthosis and prosthesis devices have been developed in recent years to help people with diminished motor abilities [11, 12, 13, 14, 15, 16]. For an effective prosthetic system, the human and the device must work together in an intuitive and synergistic way: the device must recognize the user's motion intentions and act to assist with that movement with minimal cognitive disruption and required compensatory motion. Failure to

incorporate and adapt to the user's intent leads to an incomprehensive assistive experience for the user which might include execution delay, staggered or labored movement, inefficient expenditure of metabolic energy, and even safety hazards due to frequent falls. Thus, a well-designed and interactive Prosthetic controller must begin with understanding and predicting the human locomotion intent. Meanwhile, environmental properties have a great influence on the stability, balance, and energy consumption of the device and of the user [17] and thus should be considered in the overall control scheme. Moreover, knowledge regarding the environment through which the user would move is useful for strategic control planning because it constrains the likelihood of encountering a terrain feature and the degree to which the environment is structured. Such knowledge is also useful in a shared-control context, where the device is responsible for execution of the user's high-level commands.

1.2 Motivation

Despite efforts to enhance the performance of robotic assistive devices, the current state of the art methodologies fails to provide context-aware situation specific prosthetic solutions to users with limited mobility. A major challenge in the design process of a powered prosthesis for the lower limb is the development of a robust and versatile adaptive control approach. Most of the traditional mechanical control mechanisms provide passive control of assistive devices and lack the incorporation of user's intention and motivation which is essential for proper recovery of neuroplasticity. In a recent review on the control strategies of lower limb prosthesis systems implemented in 2020 [18], most studies used mechanical sensors, i.e. load cell, motor current measurement [19, 20, 21, 22, 23, 24, 25, 26, 27], IMU [19, 20, 21, 22, 23, 24, 25, 26, 27, 28], pressure-sensitive in-soles [28] to measure knee

ankle angle, angular velocity and other kinematic information to recognize activity modes. Although, these methods resulted in good outcomes using different machine learning algorithms, the major setback is that these methods detect the activity modes or intentions rather than predicting them. The detection latencies appear since the kinematic changes which are indicative of change in gait mode appear immediately at the onset or after the change of locomotion mode when the body is about to move or already on the move. Therefore, there is hardly any time for the prosthetic system to recognize such changes and adapt the control parameters accordingly. As a result, these systems very often lead to delayed response. Such detection latencies can pose serious safety hazards for the users in transitioning between gait modes with substantially different characteristics. This creates a serious drawback in providing seamless transitions in the event of changing gait demands. Presumably, therefore many commercial devices favor the manual mode switching [29, 30]. This switching mechanism results in safe and accurate outcomes to the user. However, a human being with unharmed motor ability can change locomotion modes volitionally with minimal cognitive effort and never requires an interruption or additional effort to switch on or off their motor function. As a result, the switching mechanism, although accurate, is prone to delays and does not provide a natural and volitional movement experience which is a critical setback. Some studies also utilized surface EMG sensors placed on the residual limb to recognize intentions to perform different lower limb tasks in different terrains [22, 24, 25, 31, 32]. However, myoelectric interfaces create the extra step of muscle activation to control prosthetic functions which can be a tedious task for people with amputation [33]. Furthermore, the EMG or mechanical sensor-based control is only reactive to the kinematic movement on residual or healthy limbs which still creates the problem of detection latency and safety hazards. Additionally, there is an electromechanical delay between the

motor commands and the generation of force in the muscle, which may result in instability when a device with a fast control loop is coupled to the user to provide high levels of assistance [34]. On the other hand, the intents to change locomotion modes originate at the brain and scalp EEG is a very convenient and noninvasive way to decode neural correlates related to change in locomotion modes for enabling prediction of the intent before the event. However, the predictions are not quite reliable due to the noisy and nonstationary nature of Electroencephalography (EEG). Therefore, a reliable, early and accurate prediction of human locomotion intention is still a daunting challenge.

Additionally, current state-of-the-art prosthetic systems lack the integration of effective environmental feedback for providing context aware assistance to the user. Traditional approaches include the utilization of mechanical measurements [19, 32] (e.g., forces and motions), Electromyography (EMG) signals [24], or inertial measurement units (IMUs) [35] for detection of locomotion mode transition. But these methods are affected by delay, user-dependence, and sensor location sensitiveness. Recent approaches to detect terrain information and provide an environmental context used computer vision and edge detection by depth sensing. However, the documented devices are still confined to well-defined and controlled environments as imposed by hardware and experimental constraints, for example stairs and ramps [32, 36, 37] and does not properly address real life environmental scenario like different types of surfaces and various decision demanding scenarios that humans face regularly. Additionally, such systems often utilized several cameras placed at different locations of the body for capturing reliable images of the terrains for classification. The usage of multiple cameras leads to decreased portability and increase system complexity, reducing the real-time applicability of such systems. Studying variations in the real-life environment and adding environmental context to the pros-

thetic device using a portable, low energy, properly sized computer vision system in a real-time manner remains a topic of research.

The dissertation will focus on implementing volitional control of a lower limb prosthetic device equipped with computer vision and multi-sensor technology for intention recognition and terrain adaptation through environmental feedback. To achieve the goal of the dissertation, the following specific questions will be investigated.

• Is it possible to enable volitional control of the prosthetic system through early and accurate prediction of the user's intention to change locomotion mode or speed before the occurrence of the change?

• Can a computer vision system predict incoming terrain transition to facilitate in-time parametric adaptation of the prosthetic system?

For that purpose, the rest of the dissertation has been structured as follows. Chapter 2 discusses the feasibility of gait intention prediction from pre-movement EEG only. Chapter 3 explores score threshold regulation and majority voting for introducing asynchronous movement intention detection. Next, chapter 4 discusses asynchronous movement intention prediction in offline and pseudo-online scenarios. In chapter 5, a combination of variational mode decomposition and wavelet synchrosqueezed transfrom was used for detecting movement intention from movement-related EEG. Chapter 6 includes discussion on real-time acceleration intention prediction from pre-event EEG, IMU and GRF data. The following chapter focuses on the effect of emotional music stimuli on movement related neural phenomena and investigates how they affect intention prediction performance. Chapter 8 includes discussion about a computer vision technology designed to predict terrain types and oncoming terrain transition to facilitate smooth transition between different terrains.

CHAPTER 2

FEASIBILITY OF PREDICTING GAIT INTENTION

2.1 Background

Locomotion impairments resulting from cerebrovascular accidents or stroke and brain trauma create a severe handicap for many people, especially the elderlies [1]. Besides, lower limb amputation due to trauma or diabetes results in reduced mobility, thus severely affecting people's quality of life. Various assistive orthosis and prosthesis devices have been developed in recent years to help people with diminished motor abilities [11, 12, 13, 14, 15, 16]. Although several Electromyography (EMG)-based studies have been carried out [38, 39], Brain-Computer Interface (BCI) or Brain-Machine Interfaces (BMI) have been more extensively investigated in the recent years in the scope of gait rehabilitation due to their great prospect in understanding and analyzing gait-related brain rhythms and Event-Related Potentials (ERP)s. As EEG signals can act as a real-time projection of brain's motor activity during gait, EEG- based gait studies hold significant potential in achieving early prediction of future movement plans which researchers can readily utilize for more effective rehabilitation of motor-impaired persons providing them with necessary motor capabilities.

2.1.1 Neural Phenomenon Related to Movement Intention

Prediction of human movement intention is highly significant for successful gait rehabilitation. In a BCI-based rehabilitation system, the brain waves are extracted, processed, and translated to control an assistive device. For an effective assistive system, it is critical to detect the movement intention as early as possible to provide

the system with enough time to adapt to the requirement of the individual. There have been two majorly reported neural features related to movement intention detection. Those are Movement-Related Cortical Potential (MRCP) [40, 41, 42] and Event-Related Synchronization/ Desynchronization (ERS/ERD) [43, 44]. MRCP corresponding to self-paced movement is known as Bereitschafts Potential (BP), and it is characterized by a slow decrease in EEG amplitude over the primary motor cortex within at least 0.5 seconds preceding the movement initiation. On the other hand, ERD is defined as a decrease in spectral power 0.5- 2 seconds before movement onset reported most in the mu (8-12 Hz) and beta (13-30 Hz) frequency bands of the brain wave [45, 46, 47]. The limits of the frequency bands may differ across different authors. These features have been used as physiological triggers to activate and operate various assistive devices [19, 20, 48].

2.1.2 Related Work

Although Event Related Desynchronization (ERD) [49, 50] and MRCP [51, 52, 53] based studies have been carried out quite extensively in understanding unique aspects of motor cortex activation, both of these modalities have some drawbacks. MRCP provides timing information about different stages of movement planning and execution. But it is a very subtle change in near DC frequencies and it takes multiple repetitions of the same trial to extract useful and reliable gait-related information from MRCP [54]. On the other hand, ERD has been shown to be detectable from single trial EEG, but the main disadvantage of using ERD as a control signal for assistive devices is that it does not provide precise timing information about different stages of movement planning, preparation, and execution. Moreover, ERD/ERS requires a reliable steady state baseline to correctly detect power changes correlated

to movement intention. Few studies, therefore, have focused on combining these two frequently used modalities to enhance the performance of movement intention detection systems to create a useful Brain-Computer Interface for proper neurorehabilitation [55, 56]. However, all these studies either use EEG signal from both before and after the movement initiation and termination or use a large portion of pre-movement EEG data for proper baseline information. Such systems are, therefore, impractical in online real-time BCI application and may become prone to erroneous or delayed detection of intention in the presence of sudden intention to move. To address the shortcoming of the traditional features, in this paper Hjorth parameters, namely activity, mobility and complexity are proposed as features to obtain instantaneous time-frequency information related to gait intention in a window by window approach without the necessity of baseline selection.

Besides, very few studies have explored pre-movement state for healthy subjects in the context of upper or lower limb function [55, 10, 57, 58, 59, 60, 61]. Although the pre movement neurological changes in the EEG signal has been identified and studied, whether it is possible to detect those phenomena to predict human voluntary gait intention in a real-time BCI scenario is yet to be extensively investigated. Also, understanding the exclusive pre-movement EEG signal parameters for healthy subjects as well as amputees is yet to be explored. Moreover, detecting gait intention before the movement onset or termination would be a very critical feature for online BCI systems for rehabilitation. Currently, early and accurate detection of self- paced movement intention for real-time BCI application remains a daunting challenge. Early and accurate detection of gait intention would give the BCI system necessary time to validate the authenticity of the predicted intention and adapt the parameters of corresponding assistive devices thus ensuring safe and natural gait rehabilitation. That is why a fully predictive BCI would always be preferred over

a BCI which would only detect gait intention after the gait had already happened. As such this study would explore the feasibility of predicting gait intention from pre movement EEG data only. The data analysis and classification were done in an offline scenario to investigate whether it is possible to separate EEG data corresponding to gait 'start' or 'stop' intention from EEG data related to steady state 'walking' or 'resting' respectively. Moreover, a trans-movement EEG data structure was also evaluated for the same classification task to analyze whether use of only pre movement EEG data caused any statistical decline in system performance. This study would work as a good starting point for future online implementation of BCI for gait rehabilitation.

2.2 Current Work

In this chapter, a Wavelet Transform based intention detection methodology was proposed to address the challenges discussed in the above paragraphs by utilizing Hjorth parameters as features. Several time windows before movement initiation and termination were used for classification, which is more similar to real life situations where the intention to move or stop can be abrupt. Moreover, a brief duration of data after the movement initiation or termination were also included with the pre-movement data windows in a separate classification scheme to examine the change in detection performance and to validate the feasibility of the proposed fully predictive system. Wavelet Transform is chosen due to its ability to provide better time-frequency resolution than conventional signal processing tools like Fast Fourier Transform (FFT). The Hjorth parameter is a convenient tool to extract useful information in the time-frequency domain and also has the advantage of minimal computational complexity compared to other time-frequency analysis tools, e.g., Short

Time Fourier Transform (STFT) [62]. These parameters have been used in several EEG– based studies across various applications, such as upper body movement intention detection [62] Alzheimer's study [63], seizure lateralization [64], emotion recognition [65], mental task classification [66]. However, the Hjorth parameters have not been utilized in the scope of self-paced movement intention detection to the knowledge of the authors. From that background, the performance of Hjorth parameters was investigated in detecting self-paced lower limb movement intention. The hypothesis of this study is: It is possible to predict intention of voluntary gait initiation and termination by using pre-movement EEG signals only.

2.3 Methods

2.3.1 Experimental Procedure

Seven healthy individuals and two amputees (Seven male and two female, mean age = 32.6 years and SD = 10.41 years) participated in the experiment. None of the participants had any known history of neurological disorder. The experimental protocol was approved by the Institutional Review Board (IRB) of Florida International University, and Hunter Holmes McGuire VA Medical Center. Also, signed consent papers were obtained from subjects. The demographic and physiological information of the subjects is summarized in Table 2.1.

The experiments on healthy subjects were carried out in the Human Cyber-Physical Systems (HCPS) Laboratory at Florida International University. While, the amputee subjects carried out the experiment in Hunter Holmes McGuire VA Medical Center, Richmond, Virginia. The experimental procedure was designed to detect the intention of movement starting and stopping. For this purpose, all the

Table 2.1: Demographic characteristics of the subjects.

Subjects	Gender	Age	Weight (kg)	Height (cm)	Amputated limb
S1	Male	26	96	171	N/A
S2	Female	23	62	158	N/A
S3	Male	29	71	170	N/A
S4	Male	33	62	152	N/A
S5	Male	30	98	185	N/A
S6	Male	26	61	170	N/A
S7	Female	26	61	165	N/A
A1	Male	47	92	170	Right foot; Trans-Tibial
A2	Male	53	115	167	Right foot; Trans-Tibial

participants were asked to execute several starts and stops of gait while walking on level grounds in a self-paced manner. There were no audio or visual cues offered to the participants because the presence of audio or visual cues might corrupt the gait-related EEG signals.

The subjects were allowed to start and stop walking according to their will. However, it was made sure that the duration of walking and resting periods were at least 5 seconds. This duration was set to ensure the extraction of uncorrupted and distinctive features. To ensure the minimum duration of walking and resting, the subjects were instructed and trained about the duration in a separate short session before the beginning of the actual experiment. In this session, the subjects were asked to complete 5 cycles of gait and then stop walking. While in the rest state, they were instructed to count from 1 to 10 before starting to walk again. In the introductory session, when the subjects could walk and rest for the minimal amount of time according to the instruction they were given, they were then allowed to start the experimental session.

In the experimental session, each of the subjects carried out approximately 140 repetitions of gait cycles in as many runs as they needed. The number of necessary

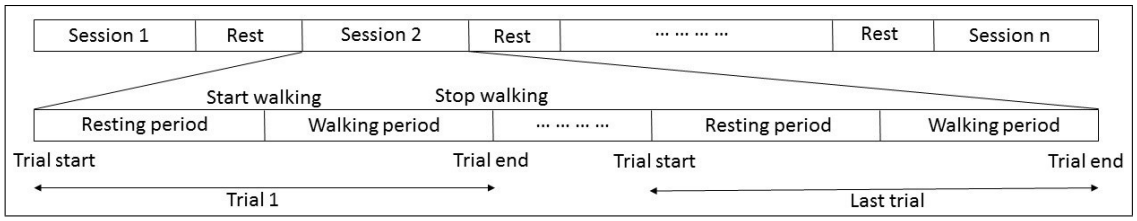

Figure 2.1: The experimental protocol of the study. Data were collected in multiple sessions with rest period between two consecutive sessions. In each session, multiple trials were performed by the subjects. Each trial consisted of resting period, self-paced initiation of walking, stop walking and resting again
.

runs varied across the participants. In each run, the following tasks were repeated periodically: Rest, Start walking, Stop, and Rest again. The subjects were allowed to take a rest after every run for as long as they needed. The whole experimental procedure consisted of 6-7 sessions varying across the subjects. Each session lasted about 7-8 minutes, with 3-5 minutes break between two consecutive sessions. The total experimental procedure took about one and a half hours, including the experimental setup. In total, the participants executed approximately 140 repetitions of self-paced gait trials without the help of any external stimuli. Moreover, as the amputated subjects would find it challenging to complete too many starting and stopping cycles due to probable fatigue, discomfort and more extended inter-session rest periods, they were asked to continue the experiment for as long as they feel comfortable to carry on. That is why the number of gait initiation and terminations trials for the amputated subjects were less than that for the healthy subjects. The experimental protocol has been briefly presented in figure 2.1.

2.3.2 Data Acquisition

EEG signal was recorded from the central motor cortex to capture information about gait preparation and execution for reliable gait intention detection. An active

electrode system (actiCAP developed by Brainproducts GmbH) was used to collect eight-channel EEG data from all the subjects. A custom made data acquisition board utilizing ADS1299 (Texas Instruments) amplifier was used to amplify the EEG data. The electrodes were placed at Cz, C3, C4, CP3, CP4, FCz, CPz, and Pz, according to the International 10-20 system. The reference and ground electrodes were placed at FPz and AFz, respectively. Figure 2.2 shows the placement of the electrodes. Before data acquisition, a proper amount of conductive gel was applied to ensure that the impedances of all the electrodes were below a manufacturer-recommended value. The sampling frequency of the EEG data acquisition system was set at 500 Hz.

2.3.3 Motion Capture System

Both Electromyography (EMG) and Ground Reaction Force (GRF) were recorded throughout the experiment to monitor the current stage of the gait cycle (Figure 2.1). A two-channel EMG sensor was also used to record muscle activity using an ADS1292 amplifier at 1000 samples per second. The EMG electrodes was placed at the mid-belly of right leg Tibialis Anterior (TA) muscle with the reference electrode placed on the bony surface of the right knee. TA was chosen because it is one of the muscles which activates the earliest during a gait cycle [67]. The EMG signal was bandpass pass filtered with cut off frequencies at 20 and 400 Hz using a 4th order Butterworth filter.

A custom made pair of in-sole pressure sensors which was used in a previous study reported in [68] were placed inside the shoes of the subjects to capture which phase of gait they were in at any particular moment. All the boards were also equipped with built-in nine-axis IMU sensors (MPU-9250, InvenSense) for detecting

motion artifacts so that adaptive filtering could be used [69]. The sensors included an accelerometer, a gyroscope, and a magnetometer. The timing information of starting and stopping of gait was acquired from the in-sole pressure sensors, and the corresponding EMG of Tibialis Anterior used to verify the time information acquired from the pressure sensor. The placement of all sensors and electrodes are shown in figure 2.2.

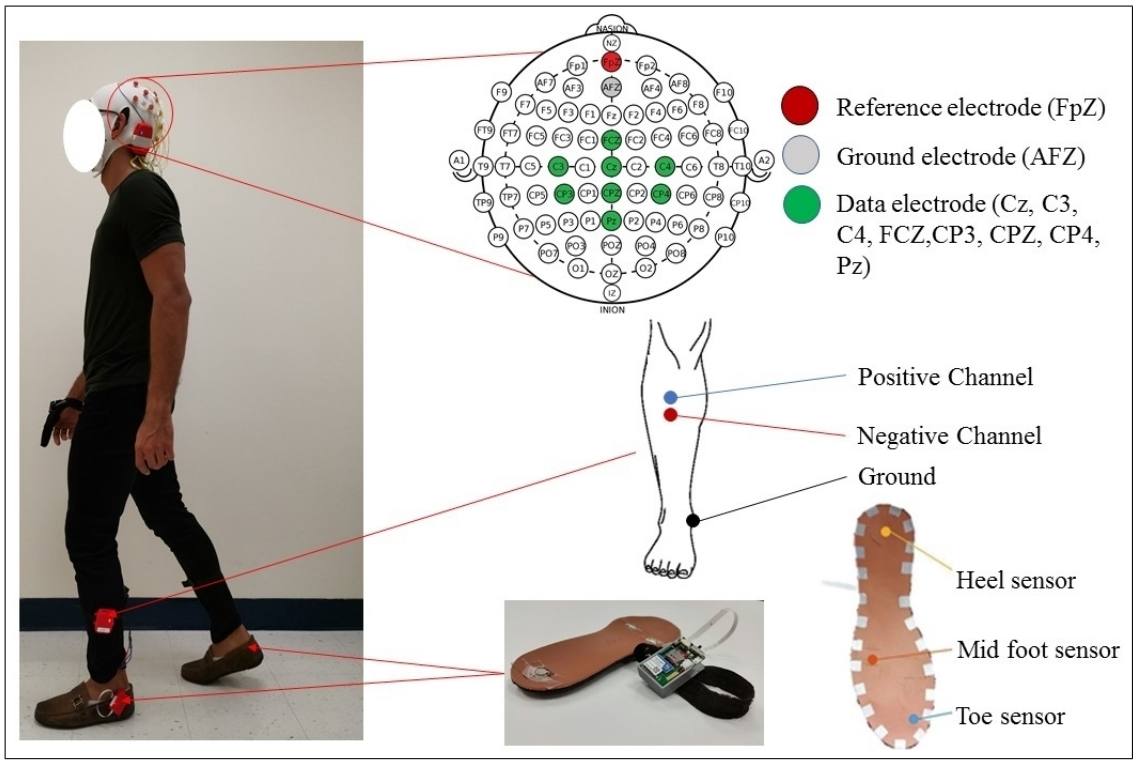

Figure 2.2: The entire body area sensor network for data collection. The placement of EEG, EMG and in-sole pressure sensors are shown in the figure.
.

2.3.4 Data Preprocessing

As EEG signal is highly prone to noise and also is non- stationary, proper preprocessing tools are needed to extract valuable event related information. In this work, a well-known MATLAB-based EEG processing toolbox EEGLAB [70] was utilized

to preprocess the acquired EEG data. For increasing computational efficiency, the signal was downsampled to 250 Hz. Then, the data were high pass filtered by a primary FIR filter with 1 Hz cutoff frequency to get rid of the DC drift in the data. The signal was cleared off line noise at 60 Hz by using a notch filter. The cleansing process of the EEG signal was carried out in two steps using the EEGLAB toolbox: Artifact Subspace Reconstruction (ASR) [71] and Independent Component Analysis (ICA). The ASR algorithm is a non-stationary method which uses sliding window PCA to remove unusual large-amplitude noise or artifacts. The usage of ASR increases data stationarity and makes the data suitable for ICA operation.

In this paper, ASR was used for two purposes: bad channel rejection and removal of short-time high-amplitude artifacts in continuous data. A channel was rejected if (1) it had a flat signal for more than 5 seconds or (2) was poorly correlated with adjacent channels. The threshold of the cross-correlation was set at 0.7 for all the subjects. To estimate the signal of one channel from contaminating signals of adjacent channels, the Standard Deviation (SD) value for repair bursts using ASR was set to 10. The value was chosen in such as a way that it was 'small enough to remove activities from artifacts and eye-related components and large enough to retain signals from brain-related components' according to the study in [72].

After the ASR operation, the processed EEG signal was re-referenced to a common average as a part of the preprocessing process. The re-referenced EEG signal was then ready for ICA operation. A study in [73] reviews some of the most used Independent Component Analysis method for artifact removal from EEG signals. In the proposed methodology, a variant of ICA called the Adaptive Mixture ICA knows as Adaptive Mixture Independent Component Analysis (AMICA) was used for processing. AMICA is a binary program for performing ICA decomposition on the input signal with multiple ICA models [74]. AMICA achieves better ICA de-

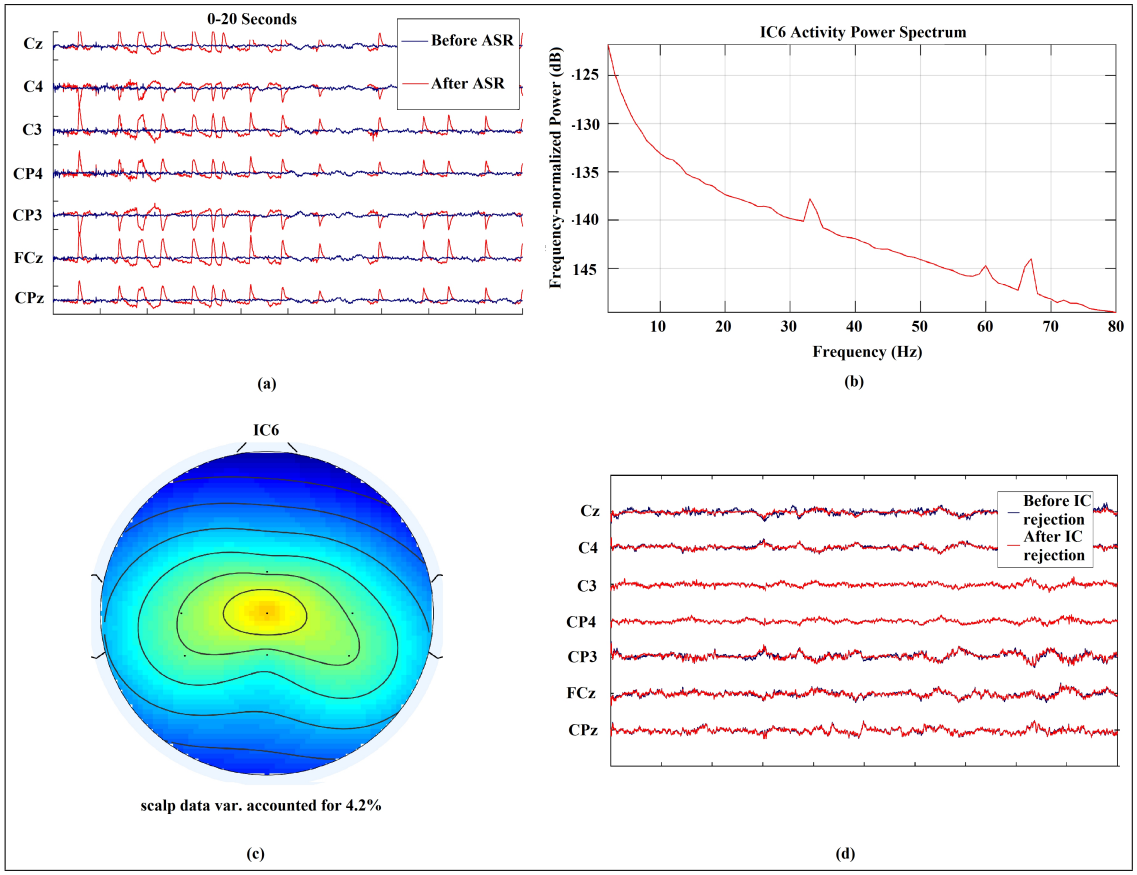

Figure 2.3: **(a)** Shows the performance of ASR in removing eye movement artifacts and unnatural high amplitude noise. Moreover, channel Pz was marked as a flat channel and was rejected by the algorithm. **(b)** and **(c)** shows the power spectrum and scalp distribution of a rejected Independent Component. The IC was rejected due to its low contribution to the scalp data variance and unusual peaks at higher frequencies like 60 and 70 Hz. **(d)** shows the EEG signal obtained after ASR operation and artifactual IC rejection.

composition than other ICA approaches as reported in [75]. Moreover, multi-model AMICA can be used as a data-driven approach to address the non-stationarity and dynamic changes of continuous EEG data [76]. The resulting independent components thus obtained were then inspected, and artefactual IC's were rejected by visual inspection. The artifacts might include muscle or heart components, channel noise, line noise, or others. After the rejection of artifacts, the cleaned data were used for further processing and classification scheme. Figure 2.3 shows different stages of cleaning of the artifact-laden EEG data.

2.3.5 Discrete Wavelet Transform

The EEG signal cleaned by ASR and ICA was then analyzed by discrete wavelet transform to look into the signal properties in the time-frequency domain. A 5-level decomposition of the EEG data was carried out using the Daubechies 4 or 'db4' as the mother wavelet, and the corresponding frequency ranges are shown in Table 2.2. The detail coefficients of the third and fourth level of decomposition correspond to the beta and alpha band of brain waves, respectively. As these two brain waves are the most informative about human gait stages as reported in multiple studies, the second and third level detail coefficients were reconstructed to get the beta and alpha band EEG signals. The resulting alpha and beta band signals were used for further processing and feature extraction.

2.3.6 Data Segmentation

The overall data segmentation procedure is summarized in Figure 2.4. The red and black lines line in the figure corresponds of gait starting and stopping respectively. Equidistant points from two adjacent gait starting and stopping times were recorded

Table 2.2: Different levels of coefficients and their corresponding brain waves.

Coefficients	Frequency Range (approx.)	Sub-band
First level detail coefficient (cD1)	62.5-125 Hz	-
Second level detail coefficient (cD2)	31.25-62.5 Hz	Gamma
Third level detail coefficient (cD3)	15.63-31.25 HZ	Beta
Fourth level detail coefficient (cD4)	7.81-15.63 Hz	Alpha
Fourth level approximate coefficients (cA4)	0-7.81 Hz	Delta and theta

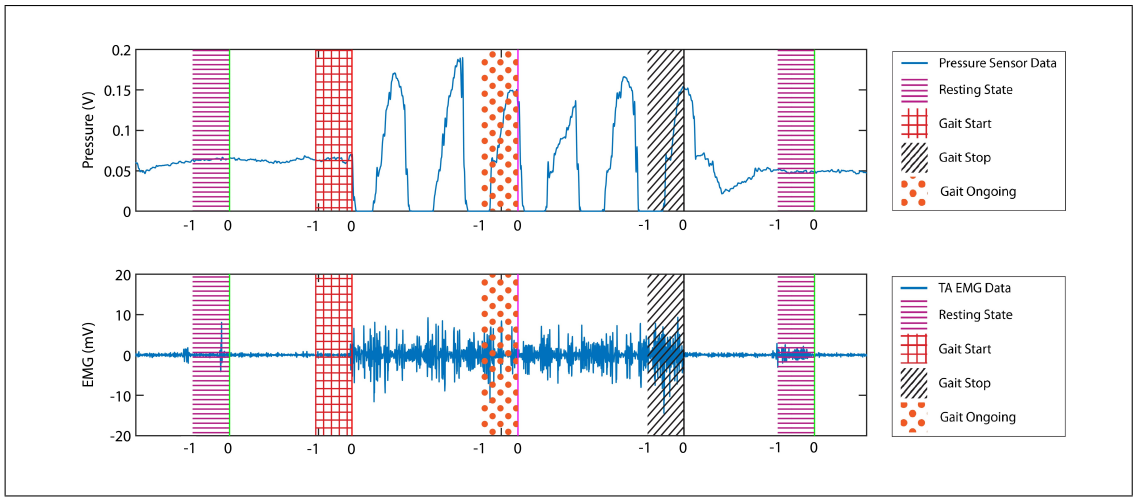

Figure 2.4: A 20-second segment of pressure sensor and right TA EMG data from Subject 1.The red line in the figure corresponds to the time of gait starting, while the black line corresponds to the time of gait stopping. The resting and walking times were chosen by taking equidistant points from two adjacent gait starting and stopping times. After marking all crucial time points, data windows of different lengths, and relative positions corresponding to those events were taken for further processing and feature extraction. In the figure, the segmentation procedure of [-1,0] data interval is shown. The data windows were marked by -1 and 0 where 0 denotes the extracted event times and -1 denotes the time points one second before the event. The extracted data windows were labeled to the corresponding events. After that, two two-class classification problems were addressed: 'Rest vs. Start' and 'Walk vs. Stop.' This segmentation and windowing approach ensured no overlapping between data windows corresponding to different classes reducing the chance of data contamination.

as walking and resting points. This data segmentation procedure was inspired by similar approaches reported in [49, 50, 77]. Windows of different time lengths were chosen to correspond to the starting, stopping, walking and resting times thus obtained. To analyze the feasibility of a fully predictive intention recognition system, two kinds of data windows were extracted for classifier training and cross-validation. For fully predictive system, three types of windows were evaluated: [-1, 0], [-1.5, 0] and [-2, 0] second windows where no data after the movement initiation were used. Also, [-1, 1] and [-1.5, 0.5] second windows were extracted and validated where a brief portion of data after the occurrence of movement starting or stopping was used for feature extraction and classification. The numbers represent the starting time and ending time of the window corresponding to the event onset time, i.e. [-1,1] second window represents a two-second window starting one second before and ending one second after the 'starting' and 'stopping' of gait events. For the sake of balanced and unbiased classification, the length of 'resting' and 'walking' data samples were set as equal to that of the 'starting' and 'stopping' classes. It was made sure that there was no overlap between consecutive data samples belonging to different classes After that, two two-class classification problems were addressed: 'Rest vs. Start' and 'Walk vs. Stop.' This segmentation and windowing approach ensured no overlapping between data windows corresponding to different classes reducing the chance of data contamination.

2.3.7 Feature Extraction

For extracting distinguishing features from the non-stationary EEG data; the segmented data windows obtained in the previous subsection were further divided into 0.5-second long data windows with 50 milliseconds overlap. Thus, each one-second

epoch was divided into 11 windows, 1.5 second windows were divided into 21 sub windows and 2 second windows yielded 31 sub windows. All three Hjorth parameters were computed for both alpha and beta band signals for the resulting sub windows. Thus, for every one-second data window, a total of 11 windows $\times$ 2 sub-bands $\times$ 3 parameters = 66 features were calculated per channel. Similarly, a total of 126 and 186 features were generated for 1.5 second and 2 second data windows. All the features corresponding to all the channels were then concatenated to form the final feature vector. Equations (2.1)-(2.6) summarizes the feature extraction, and the subsequent paragraph discusses feature vector formation. Equations (2.1) and (2.2) shows the activity parameters, equations (2.3) and (2.4) defines the mobility parameters and equations (2.5) and (2.6) describes the complexity parameters.

$$A^i_{j,k,\alpha} = \sigma^2_{x^i_{j,k,\alpha}} \tag{2.1}$$

$$A^i_{j,k,\beta} = \sigma^2_{x^i_{j,k,\beta}} \tag{2.2}$$

$$M^i_{j,k,\alpha} = \frac{\sigma_{\frac{dx^i_{j,k,\alpha}}{dt}}}{\sigma_{x^i_{j,k,\alpha}}} \tag{2.3}$$

$$M^i_{j,k,\beta} = \frac{\sigma_{\frac{dx^i_{j,k,\beta}}{dt}}}{\sigma_{x^i_{j,k,\beta}}} \tag{2.4}$$

$$C^i_{j,k,\alpha} = \frac{\sigma_{\frac{d^2x^i_{j,k,\alpha}}{dt}}}{\sigma_{\frac{dx^i_{j,k,\alpha}}{dt}}} M^i_{j,k,\alpha} \tag{2.5}$$

$$C^i_{j,k,\beta} = \frac{\sigma_{\frac{d^2x^i_{j,k,\beta}}{dt}}}{\sigma_{\frac{dx^i_{j,k,\beta}}{dt}}} M^i_{j,k,\beta} \tag{2.6}$$

Here x denotes the EEG signal. A, M and C denote the activity, mobility and complexity parameters, and σ denotes standard deviation of x. While i, j and k, denote the channel number, sample number, and window number respectively. All

the features corresponding to a single sample from all the channels are concatenated to form the initial feature vector.

2.3.8 Feature Selection

As the number of features is too high compared to the number of samples, there is a high chance of having redundant and noisy features in the feature set. That is why a feature selection method is necessary to get rid of the redundant features. In this work, the absolute value of the standardized u-statistic of a two-sample unpaired Wilcoxon test [78], (also known as the Mann-Whitney test) was chosen to be the criterion to select distinctive and informative features. To further reduce the number of features, the average of the absolute values of the cross-correlation coefficient between the candidate feature and all previously selected features were calculated, and features that were highly correlated with the features already picked were less likely to be included in the output list. This procedure ensured the formation of a reduced and more distinctive set of features for successful classification. After feature selection, the number of selected features was reduced to 20 for all the subjects and classes.

2.3.9 Offline Classification

The ultimate goal of this study is to come up with a feasible methodology to apply in real-time BCI systems. For a proper real-time BCI system, the classifiers must have high sensitivity as well as high specificity to avoid accidents while using a prosthesis or orthosis system. With that in mind, in this work, we used an Support Vector Machine (SVM) classifier [79] with RBF kernel to solve two two-class classification problems. For each subject, one classifier was trained to classify between 'rest' and

'start' classes while another classifier was trained to classify between 'walk' and 'stop' classes. The performance of the classifiers was evaluated by ten-fold cross-validation. In each step of classification, one fold was used as the test set while all the other folds were used to train the classifier. Each fold was used only once as the test set, and finally, the performance metrics were average across all the folds.

2.4 Results

For performance evaluation of the offline classification, the following metrics were calculated in this study: Accuracy, sensitivity, specificity. Accuracy shows the performance of the classifier in predicting start or stop and walk or rest classes. Sensitivity is the measure of the capability of the classifiers of correctly predicting the start or stop class, while specificity is the measure of the classifier performance in successfully predicting the walk or rest classes. The definition of these parameters are included in the following equations:

$$Accuracy = \frac{TP + TN}{TP + TN + FP + FN} \tag{2.7}$$

$$Sensitivity = \frac{TP}{TP + FN} \tag{2.8}$$

$$Specificity = \frac{TN}{TN + FP} \tag{2.9}$$

Here TP, TN, FP, FN denotes true positive, true negative, false positive and false negative detection where the 'start' and 'stop' windows belong to 'positive' class and 'resting' and 'walking' data windows belong to the 'negative' class. Another informative metric is FP/min. FP/ min is the ratio of the number of false detection of intention to start or stop and the number of rest or walk trials per minute. The resulting average performance parameters are summarized in this section.

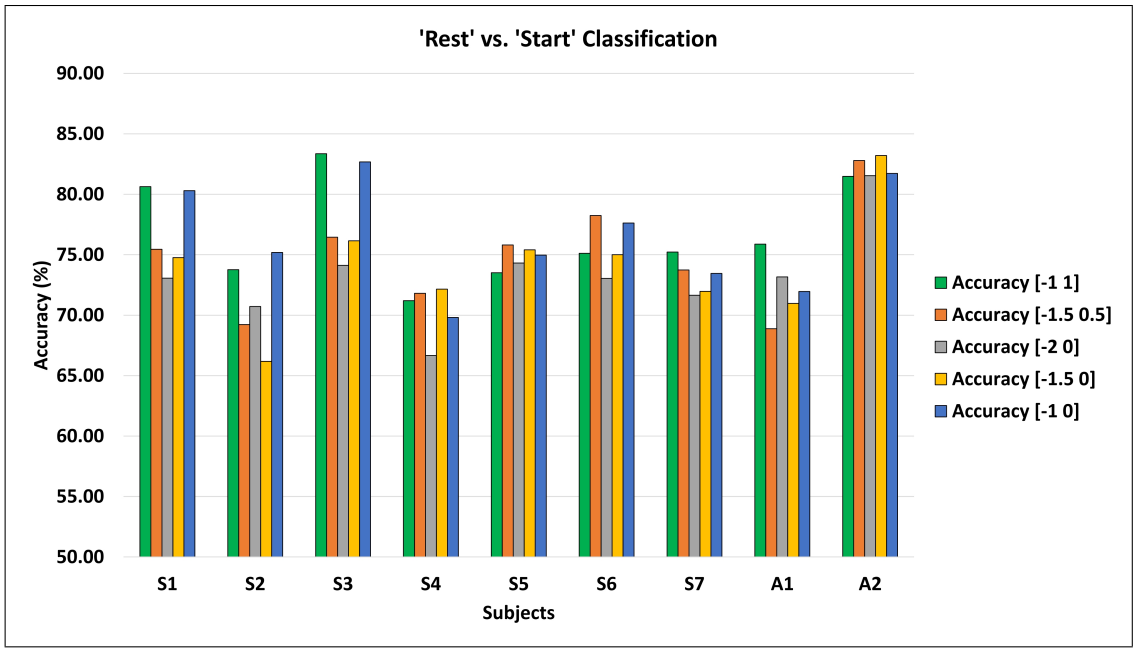

Figure 2.5: 'Rest' vs. 'Start' classification performance with standard deviation using different data windows.

Table 2.3 and Table 2.4 summarizes the accuracy, sensitivity, and specificity for the 'Rest' vs. 'Start' and 'Walk' vs. 'Stop' classification respectively for different data windows across all the subjects. Table 2.5 and table 2.6 show the average classification accuracy, sensitivity, and specificity across the subjects along with the standard deviations. In all of these tables, the first two columns represent the performance of the trans-event windows, while the latter three show the classification performance of the pre-event data windows only. The highest performance metrics obtained in both cases are highlighted in bold fonts. For the sake of understanding the results better, the results are also presented in Figure 2.5 and Figure 2.6.

From table 2.3, it is evident that the highest accuracy for 'Rest' vs. 'Start' classification among the healthy subjects was achieved for S3 which was 83.35% with a sensitivity of 80.14% and a specificity of 86.29% using [-1 1] data window which consisted of EEG data both before and after event occurrence. However,

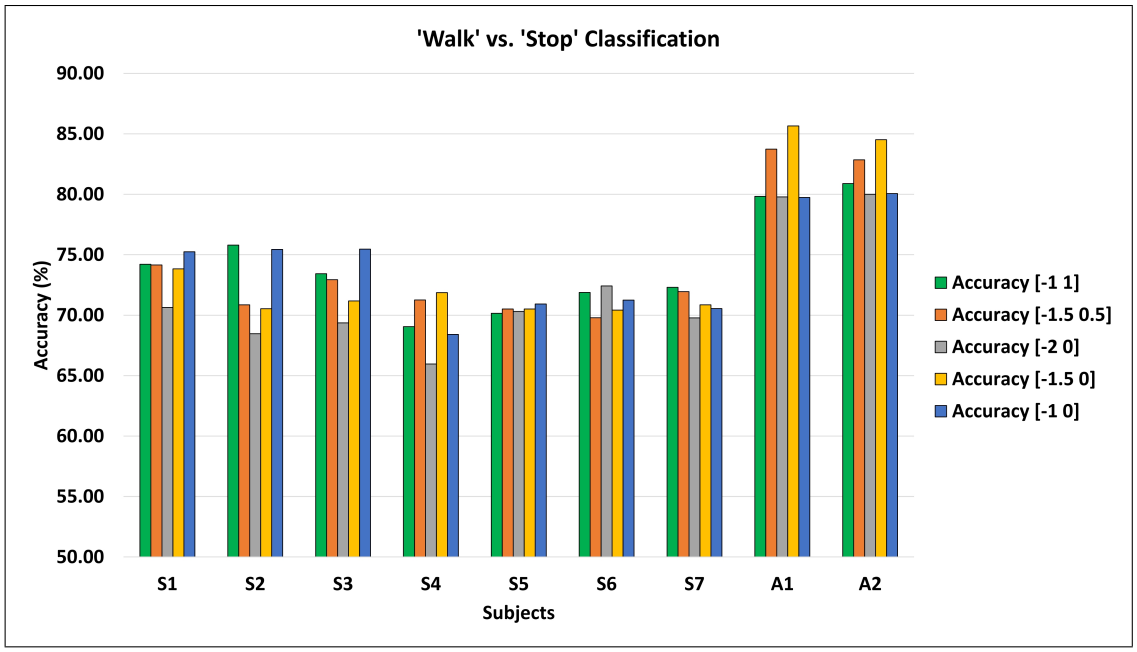

Figure 2.6: 'Walk' vs. 'Stop' classification performance with standard deviation using different data windows.

a similar classification accuracy of 82.67% was achieved using a pre-movement [-1 0] data window with balanced sensitivity and specificity of 83.67% and 81.43% respectively. Among the amputated subjects, the highest accuracy was reached for A2, which was 83.21% with a sensitivity of 69.17% and a specificity of 96.67% using [-1.5 0] data window. The highlighted results in Table 2.3 suggests that for every subject, there were one or more pre-movement data windows, which were resulting in almost similar classification results compared to the data window comprising both pre-movement and post-movement EEG signals. Table 2.5 shows that [-1 1] window yielded slightly better accuracy than the [-1 0] window with an overall accuracy of $76.69 \pm 4.14\%$, which was the highest among all the data windows. In terms of sensitivity, the highest value was obtained from [-1 0] data window, and the highest specificity was achieved for [-1.5 0.5] window. Figure 2.5 shows the pictorial representation of the information mentioned above.

Table 2.3: 'Rest' vs. 'Start' classification accuracy, sensitivity and specificity for all the subjects using different data windows.

	Subjects	Data windows				
		[-1 1]	[-1.5 0.5]	[-2 0]	[-1.5 0]	[-1 0]
Accuracy(%)	S1	**80.63**	75.46	73.07	74.77	**80.30**
	S2	**73.76**	69.23	70.71	66.18	**75.19**
	S3	**83.35**	76.45	74.12	76.15	**82.67**
	S4	71.20	**71.82**	66.66	**72.16**	69.81
	S5	73.52	**75.81**	74.31	**75.41**	74.97
	S6	75.13	**78.25**	73.04	75.00	**77.63**
	S7	**75.22**	73.74	71.65	71.97	**73.45**
	A1	**75.88**	68.88	**73.17**	70.98	71.96
	A2	81.49	**82.80**	81.55	**83.21**	81.73
Sensitivity(%)	S1	**75.14**	63.00	58.71	58.90	**73.71**
	S2	68.30	**68.35**	49.29	59.56	**77.80**
	S3	**80.14**	78.90	69.57	80.95	**83.67**
	S4	**65.43**	58.05	55.00	**69.48**	66.24
	S5	60.05	**71.65**	**81.59**	72.20	66.48
	S6	**70.54**	64.46	**76.43**	53.93	68.21
	S7	**73.52**	66.04	63.85	59.62	**72.80**
	A1	**71.61**	56.96	**73.21**	64.11	63.39
	A2	**77.50**	67.50	70.00	69.17	**83.33**
Specificity(%)	S1	86.19	**87.48**	87.52	**90.29**	86.95
	S2	**79.23**	70.11	**92.14**	72.80	72.58
	S3	**86.29**	74.05	78.43	71.29	**81.43**
	S4	76.95	**85.57**	**77.86**	74.95	73.57
	S5	**86.76**	79.95	67.14	78.41	**83.30**
	S6	79.46	**92.14**	68.93	**95.89**	86.96
	S7	76.92	**81.26**	79.29	**84.12**	74.07
	A1	**80.36**	80.18	73.21	77.32	**79.64**
	A2	90.00	**93.33**	91.67	**96.67**	80.83

Table 2.4: 'Walk' vs. 'Stop' classification accuracy, sensitivity and specificity for all the subjects using different data windows.

	Subjects	Data windows				
		[-1 1]	[-1.5 0.5]	[-2 0]	[-1.5 0]	[-1 0]
Accuracy(%)	S1	**74.21**	74.15	70.64	73.83	**75.24**
	S2	**75.80**	70.85	68.46	70.54	**75.44**
	S3	**73.43**	72.94	69.36	71.18	**75.46**
	S4	69.05	**71.26**	65.96	**71.86**	68.41
	S5	70.15	**70.51**	70.30	70.51	**70.92**
	S6	**71.88**	69.79	**72.42**	70.42	71.25
	S7	**72.30**	71.94	69.78	**70.86**	70.54
	A1	79.83	**83.74**	79.79	**85.65**	79.74
	A2	80.89	**82.86**	80.00	**84.52**	80.06
Sensitivity(%)	S1	60.57	**68.52**	65.29	67.71	**72.05**
	S2	**72.97**	65.05	52.42	67.36	**74.40**
	S3	**74.81**	71.86	66.00	70.33	**82.19**
	S4	**72.43**	64.57	60.81	65.95	**60.71**
	S5	**72.09**	54.56	**70.82**	69.78	64.67
	S6	**71.79**	53.57	67.68	56.25	**72.86**
	S7	**61.81**	57.36	**64.89**	51.65	64.01
	A1	**76.79**	72.32	69.82	**76.07**	69.64
	A2	**79.17**	73.33	**77.50**	73.33	71.67
Specificity(%)	S1	75.67	**88.33**	**80.10**	80.05	78.52
	S2	**84.67**	78.68	**76.65**	73.68	76.37
	S3	72.24	**72.29**	**74.24**	72.10	68.76
	S4	**70.86**	65.76	77.86	**78.05**	75.62
	S5	**70.11**	68.02	**85.93**	70.82	77.25
	S7	82.80	**86.43**	74.89	**90.00**	77.09
	S6	**76.96**	71.43	**85.36**	84.46	69.29
	A1	**88.93**	82.32	**94.64**	**94.64**	88.75
	A2	80.83	**82.50**	90.83	**94.17**	88.33

In case of 'Walk' vs. 'Stop' classification, the highest accuracy of 75.80% was obtained for S2 among the healthy subjects using the [-1 1] data window comprising both trans-event data. The corresponding sensitivity and specificity values were 72.97% and 84.67%, respectively. Almost equal accuracy, sensitivity, and specificity values of 75.44%, 74.40%, and 76.37% were achieved for the same subject using only the pre-event [-1 0] data window. Among the amputated subjects, the best results were obtained for pre-event [-1.5 0] window for subject A1. The classification model achieved an accuracy of 85.65%, a sensitivity of 76.07% and a specificity of 94.64%. A slightly decreased classification accuracy was achieved for this subject using trans-event window [-1.5 0.5]. The resulting accuracy, sensitivity, and specificity values were 83.74%, 72.32%, and 82.32%. Highlighted results in Table 2.4 suggest that the best performing trans-event data window had a similar or better performing pre-event data window for all the subjects. From Table 2.6, it can be seen that the highest mean accuracy for 'Walk' vs. 'Stop' classification was achieved using [-1.5 0] data window, which was $74.38 \pm 6.17\%$. The highest sensitivity was achieved using the [-1 1] window, and the highest average specificity was achieved using [-1.5 0] window.

Table 2.5: Mean classification accuracy, sensitivity and specificity with standard deviation for 'Rest' vs. 'Start' classification

	Data windows				
	[-1 1]	[-1.5 0.5]	[-2 0]	[-1.5 0]	[-1 0]
Mean accuracy(%)	**76.69±4.14**	74.72±4.42	73.14±3.92	73.98±4.62	**76.41±4.47**
Mean sensitivity(%)	**71.36±6.19**	66.10±6.73	66.41±10.54	65.32±8.38	**72.85±7.48**
Mean specificity(%)	82.46±4.86	**82.67±7.77**	79.58±9.22	**82.41±9.77**	79.93±5.50

Table 2.6: Mean classification accuracy, sensitivity and specificity with standard deviation for 'Walk' vs. 'Stop' classification

	Data windows				
	[-1 1]	[-1.5 0.5]	[-2 0]	[-1.5 0]	[-1 0]
Mean accuracy(%)	74.17±4.05	**74.23±5.31**	71.86±4.88	**74.38±6.17**	74.12±4.12
Mean sensitivity(%)	**71.38±4.14**	64.57±7.74	66.14±6.95	66.49±7.84	**70.24±6.45**
Mean specificity(%)	76.90±7.77	**83.56±6.82**	77.24±6.42	**82.00±9.28**	77.78±7.01

Table 2.7: Result of t-test with Bonferroni-Holm correction performed on classification results.

'Rest' vs. 'Start'	Data Window	[-2 0]	[-1.5 0]	[-1 0]
	[-1 1]	H1	H1	H0
		p=0.0011	p=0.0080	p=0.3990
	[-1.5 0.5]	H0	H0	H0
		p=0.0744	p=0.2474	p=0.9398
'Walk' vs. 'Stop'	[-1 1]	H1	H0	H0
		p=0.0067	p=0.5901	p=0.4762
	[-1.5 0.5]	H1	H0	H0
		p=0.0058	p=0.5658	p=0.4514

A two-sample t-test with Bonferroni-Holm correction [80] was also performed between the classification results obtained from the trans-event data windows and those obtained from only the pre-event data windows. The hypotheses of the test were:

H0: Mean classification performance of trans-event data windows is equal to that of pre-event data windows.

H1: Mean classification performance of trans-event data windows is greater than that of pre-event data windows.

For 'Rest' vs. 'Start' classification, the t-test result yielded that the mean accuracy obtained by only the [-1 1] data window was significantly better than those of [-2 0] and [-1.5 0] data windows at $p<0.05$ significance level. All the other pairs could not reject the null hypothesis. This result indicates to the idea that the pre-movement window of [-1 0] seconds can lead to statistically similar gait start intention detection accuracy compared to the trans-event data windows namely [-1 1] and [-1.5 0.5] data windows. On the other hand, for 'Walk' vs. 'Stop' classification, the t-test result showed that the mean detection accuracy obtained by using the [-1 1] and [-1.5 0.5] windows are only significantly better than that of the pre-event [-2 0] data window. The other pre-event data windows have statistically similar detection accuracy compared to the trans-event data windows. The t-test results are summarized in Table 2.7. The results of the statistical analysis show that it is possible to obtain similar gait start or stop intention detection by using either the combination of data windows before and after the event or only the data windows before the events at $p<0.05$ significance level and hence support the hypothesis of the study.

Overall average true positive rate achieved in the study was $72.06 \pm 8.27\%$. For all the participants, the total number of rest or walk trials was 1564, and the total recording time was 227.4 minutes. This calculation amounts to 6.88 rest or walk trials per minute. The resulting False Positive Rate (FPR) was approximately 1.45/min on an average.

2.5 Discussion

This study aims to analyze the performance of the pre-movement EEG signals in predicting human intention for gait initiation or termination. Also, this study hypothesized that it is possible to obtain similar intention detection performance, whether post-event EEG data were used for classification or not. The ability to predict gait intention is a very significant feature to have to design and implement a prosthetic or rehabilitation system with potential real-life application. Because the earlier the intention state of any human subject can be recognized, the earlier the prosthetic system parameters can be adapted and prepared according to the subject‘s needs.

In this chapter, ICA was used along with other algorithms to clean the EEG data. However, the computational complexity involved in EEG source analysis by combining ICA and blind source localization is quite significant. That is why most of the ICA based EEG analysis tools offers offline processing. However, recently there has been an introduction and demonstration of Real-time EEG source mapping toolboxes, e.g. REST [81], Online Recursive ICA (ORICA) [82] which use recursive independent component analysis [83] to estimate a solution to the source separation problem in near real-time, allowing low latency access to source information. Thus, the recent technologies have shown promise to make possible innovations in experimental designs for a lot of BCI systems. In addition to that, traditional spatial filtering techniques including Laplacian filtering and common average referencing are also available as alternative [49, 50, 77]. These filters aim to minimize the contribution of the rest of the EEG electrodes to each channel thus better isolating the information from each of the electrodes. Such spatial filtering technologies can be useful alternatives until an enhanced and robust online ICA algorithm is

developed for real-time application. Moreover, the window equidistant between the 'start' and 'stop' windows were taken as 'walking' and 'resting' windows in this study. The lengths of 'walk' and 'rest' periods were bigger than those of 'start' and 'stop' periods by a great margin. Usage of the whole chunk of data corresponding to 'walk' and 'rest' period for classification would have led to imbalanced classes making the classification result highly biased. To ensure the formation of balanced classes, 'walk', 'rest', 'starting' and 'stopping' data windows were selected so that they were of the same length. Additionally, we wanted to measure the separability of intention of 'starting' and 'stopping' data from steady state 'walking' and 'resting' data in this study. Due to subjective variability and data non-stationarity, the initial changes corresponding to gait starting and stopping might cause interference to the walking and stopping data if those windows were chosen immediately before the gait windows. Such condition would have significantly affected the outcome of the study. Therefore, we ensured that the 'walking' and 'resting' data were not corrupted by neural waves caused by intention of gait by choosing data windows far from the 'start' and 'stop' data windows. In an online scenario the data would be accessed asynchronously and each data window would be assessed independently which would be included in the future work related to the study.

The two-sample t-test with Bonferroni-Holm correction suggests that for both 'Rest' vs. 'Start' and 'walk' vs. 'Stop' classification, it was possible to yield similar classification performances using either trans-event or only pre-event EEG signals. This, in turns, shows that the addition of post-event data windows does not always add much statistical value to the intention detection methodology. This outcome is a very significant one because being able to predict human gait intention using the data before the movement only gives much more preparation time for prosthetic system preparation and proper operation which is a key to successful prosthesis and

neuro-rehabilitation. It is to be noted that significance in t-test does not guarantee a similar performance in real life, rather an online study should be operated to evaluate the validity of the outcome of this offline study. However, t-test is a widely used inferential statistic used to calculate and evaluate the probability of difference between two sets of data. In this study, the t-test was used to determine whether, statistically speaking, the distribution of accuracies obtained from the "pre-movement" data windows and combined "pre-movement" and "post-movement" data windows are statistically different or not. The use of t-test is significant in the scope of this study to quantify the statistical significance of difference in performance obtained using the two types of intention detection models. For instance, even if the accuracy resulting from either of cases is greater than the other by a very small margin it can simply arise from modeling bias and thus no conclusion about superiority or similarity of performance can be drawn from mere visual inspection. Therefore, there must be some statistical measure to evaluate the significance of the obtained results and t-test serves that purpose in this study. Probabilistically, the results of the t-tests at 5% significance level implies that there is at least 95% probability that the two sets of results in contention come from different distributions thus have statistical difference from each other.

In this study, the instantaneous time-frequency information was used for gait intention detection. Now, neurological studies regarding voluntary human movement suggest that gait-related changes in human brain waves may start 1.5-2 seconds before the movement and may sustain till 2 seconds after the movement. The initial change in neural waves originates from motor preparation in the motor cortex which is strengthened by sensory feedback immediately after the movement. Due to the subject dependent variability in motor preparation and execution, the time of initial changes related to gait preparation may vary. Nevertheless, such physiolog-

ical changes are very strongly present close to the moment of movement initiation and termination which diminish with time. Therefore, the intention of gait initiation and termination is expected to be detected more successfully from the data windows close to the time of event. In our study, the EEG information originating from data windows closest to the event, namely the [-1,0] and [-1,1] second windows resulted in the best results. The results comply with the neurological facts established by previous neurological studies. The overall statistics show that for both 'walk' vs. 'stop' and 'stand' vs. 'start' classification problems, the [-1,1] and [-1,0] windows achieved a comparatively more balanced performance in terms of sensitivity and specificity. This is a very significant outcome as this suggests that these two windows contained comparatively more distinguishable features. This result further shows the potential of these data windows in real time application. The other data windows, namely [-2,0], [-1.5,0.5] and [-1.5,0] included more data from before the event of gait which might be responsible for corrupting the classification models by introducing randomness and thus skewing the obtained classification hyper-plane.

For all the detection models, the average specificity was higher than the average sensitivity values. These values mean that the system was able to detect the 'walking' and 'resting' windows much more successfully than the 'start' and 'stop' windows. The highest sensitivity was obtained from [-1 0] data window for 'Rest' vs. 'Start' and the highest sensitivity for 'Walk' vs. 'Stop' was reported from [-1 1] window. However, achieving only higher sensitivity does not ensure safe operation of a prosthetic system. Instead, a low specificity results in higher FPR, which can be very hazardous to the person using the prosthetic system. That is why while training the classification models, a higher cost was assigned to the wrong detection of intention. This precautionary action was taken to prevent a high false positive detection rate which can lead to high risk for a user of prosthetic system. On top of that, the

subjective heterogeneity in results might arise from the innate randomness and non-stationary nature involved in the gait related EEG data. The huge disparity between sensitivity and specificity in some cases originated from the extra cost put on false positive detection which made the intention detection criterion much stricter. This also suggests that in those cases the features corresponding to the 'start' and 'stop' classes did not hold enough distinguishable information to separate them from the 'rest' and 'walk' classes and thus could lead to erroneous detection in the daunting task of online gait intention detection. This resulted in slightly random labels for the testing samples leading to higher disparities in specificity and sensitivity values. Therefore, the average sensitivity is slightly lower than the average specificity. This limitation can be overcome by advanced machine learning techniques like ensemble learning or majority voting. For both the classification problems, the [-1 0] data window yielded the most balanced average sensitivity and specificity values, which shows the potential of this data window in real time application.

The average classification performance obtained for the amputated subjects were higher than those of the healthy subjects. Although the number of amputated subjects was low, the classification performances were consistently higher than the average performance for the healthy subjects. This occurrence might be due to the fact that, as the amputated persons were asked to start and stop their gait cycle on their prosthetic leg, it required more effort and concentration on their part. That is why it might result in easier detection of the intention of gait initiation or termination. Moreover, for the amputees, the best window for intention detection was found to be the [-1.5 0] window compared to the [-1 0] window for the healthy subjects. That points to the possibility that those amputated subjects appear to prepare for the upcoming change in gait state slightly earlier than their non-amputated counterparts. These are interesting questions which can be looked further into for insight

about gait preparation and execution of the amputees for a better experimental design. On another note, neurological studies regarding voluntary human movement suggest that gait-related changes in human brain waves may start 1.5-2 seconds before the movement and may sustain till 2 seconds after the movement. The initial change in neural waves originates from motor preparation in the motor cortex which is strengthened by sensory feedback immediately after the movement. Due to the subject dependent variability in motor preparation, the time of initial gait related changes may vary. Nevertheless, such physiological changes are very strongly present close to the moment of movement initiation and termination which diminish with time. Therefore, the intention of gait initiation and termination is expected to be detected more successfully from the data windows close to the time of event.

Although there are very few studies with the same experimental design, a similar offline classification was reported in [49] with a True Positive Rate (TPR) of 54.8% and 2.66 FP/min. Another study reported in [50] achieved an accuracy of 72.91% with 71.81±11.48 % true positive rate and 4.56 ± 1.84 FP/ min for start detection and accuracy, TPR and FP/min of 80.65±11.49 %, 57.38 ± 12.03 % and 2.10 ± 1.20 for stop detection. In a more recent study [77], the accuracy, sensitivity and FP/min were reported as 78.61±11.20 %, 76.90±11.75 % and 3.52±1.82 for start detection and 84.36±10.19 %, 68.68±14.69 % and 2.06±1.12 for stop detection. It is to be noted though that these studies used a very large detection window of 4- seconds containing data from two seconds before the starting and stopping event to two seconds after the occurrence of the event. The results suggest that the proposed method resulted in better or competitive accuracy, sensitivity with an enhanced specificity for start detection using a smaller pre-movement data window. For stop detection, the existing studies showed better accuracy, however the true positive rates were inferior to the ones achieved in this study. Thus the proposed

study provides a balanced start and stop detection methodology without accessing the post event data windows. This enhanced accuracy with higher TPR and lower FP/ min show the prospect of the proposed method in successfully classifying gait starting or stopping intention vs. steady state walking or stopping trials.

2.6 Conclusion

This paper proposes a wavelet transform-based methodology using Hjorth parameters as features for predicting human intention for gait starting and stopping. A combination of ASR and ICA was carried out to clean the data off any non-brain artifacts or noises. As the results suggest, it was possible to generate statistically similar intention detection performance using only the pre-movement time windows. As a result, the obtained results show a promising ability to predict movement intention, even if the intentions are relatively sudden. The proposed methodology can be a good starting point for future studies to implement a real-time BMI system for assistive devices. However, the study simply evaluates how separable the 'walking' or 'resting' periods' data windows are from 'start' or 'stop' walking data windows using the proposed methodology. Due to the extremely noisy and non-stationary nature of EEG signals accompanied by the subjective variability of gait preparation, the uncertainty involved in solving such detection problem is very high. This causes the classification performance to degrade significantly. For safe and robust control, asynchronous intention detection schemes need to be carried out and the performances need to be evaluated in terms of critical parameters necessary for real-time BCI application. Advanced signal processing techniques in addition to enhanced machine learning methodologies like threshold regulation, combination of decisions from multiple consecutive windows, neural networks can be applied to

further increase the classification accuracy. Future works can be done in the scope of decreasing the false positive rates, increasing the accuracy, sensitivity, and specificity of the system, asynchronous prediction of movement intention and application of an enhanced methodology in real-time studies.

CHAPTER 3

EXPLORING THRESHOLD RESGULATION AND MAJORITY VOTING FOR ASYNCHRONOUS INTENTION DETECTION

3.1 Background

This chapter is an edited version of the author's previous work published in [84] ©2019 IEEE. The significant steps in EEG-based BCI systems for gait rehabilitation are threefold: extraction of brain waves, signal processing, and translation of the information to control a prosthesis or orthosis system. For effective operation, early detection of intention is essential. Although higher sensitivity is expected, a lower FP/min is critical for safe operation as higher false-positives would lead to frequent accident compromising the security of the user. Therefore, designing a safe and reliable BCI system for people with motor disabilities with early and high intention detection accuracy, sensitivity with low false-positive activation is the most daunting challenge in the field of BCI for gait rehabilitation research.

3.2 Current Work

This chapter introduces a methodology for asynchronous pseudo-online movement intention detection, which utilizes discrete wavelet transform for signal processing and Hjorth parameters as features. The study uses EEG data from 1.5 before to 0.5 seconds after the actual onset of the event for training a Support Vector Machine classification model with Radial Basis Kernel. The classification problem is designed as a two-class problem, where the classes are 'intention' or 'active' class and 'non-intention' or 'inactive' class. In this paper, a threshold regulation method has been implied to reduce the number of false positives per minute. To reduce the false-

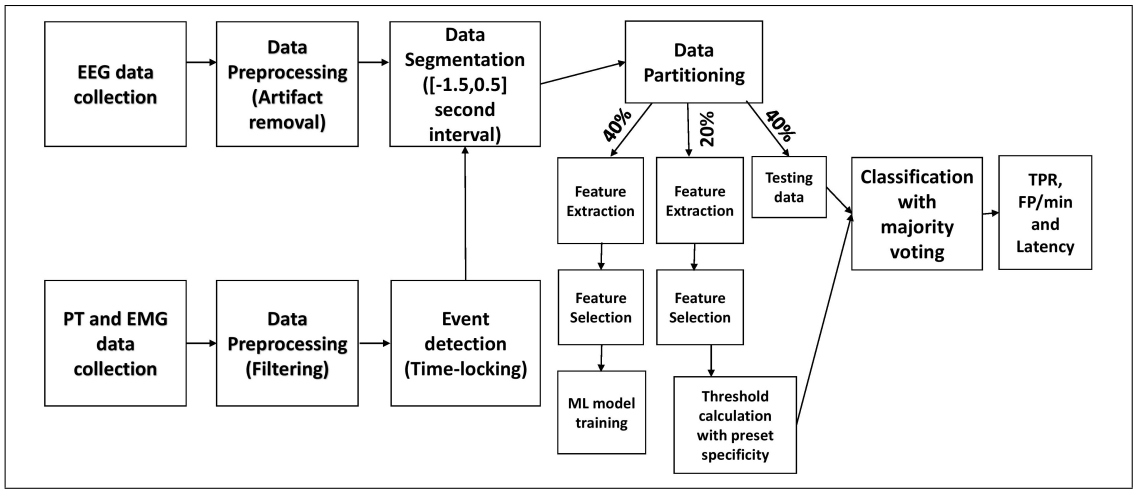

Figure 3.1: Block diagram of the proposed methodology.

positive activation, a majority voting algorithm was applied. The results show that the combination of threshold regulation and majority voting algorithm results into a higher sensitivity, and lower false-positive activations per minute with relatively smaller latency.

3.3 Methods

This section discusses about the proposed methodology and its different steps. The details of subjects, experimental protocol, data acquisition, segmentation and preprocessing have already been provided in the previous chapter. The proposed methodology is presented in Figure 3.1.

3.3.1 Data Segmentation

The goal of this study was to evaluate the performance of the BCI system in an online environment. However, as the data were collected before the processing they were accessed and processed as if they were being collected online real-time. For this

purpose, the EEG data was divided into three segments. The first 40% of data was used for training, the next 20% for threshold calculation and the remaining 40% for testing. The training and threshold calculation portion of the data was segmented using the time points extracted in the previous section. The gait initiation and gait termination time points were marked as 'intention' time points. After that from 1.5 seconds before the 'intention' time points to 0.5 seconds after the said time points were marked as intention time windows. The rest of the data were marked as 'non-intention' data. No cross validation was performed because in a pseudo-online scenario, it was simulated that epochs are processed as they are acquired.

3.3.2 Feature Extraction and Selection

In the proposed method, Hjorth parameters- activity, mobility and complexity were extracted as features to capture the frequency information in time domain signal. The Hjorth parameters were calculated using Discrete Wavelet Transform (DWT) as described in the previous section. For training the classification model, the 2-second data windows were further subdivided into 1-second epochs in steps of 0.2 second. Features were calculated for each 1-second window to create the feature vector corresponding to one 'intention' or 'non-intention' events. A two-sample unpaired Wilcoxon test was used to select 20 out of the initial 48 features per epoch.

3.3.3 Asynchronous Detection

The walking and resting cycles which were less than 5 seconds in duration were removed from the dataset before asynchronous detection. The procedure was com-

posed of three major steps: training classification model, threshold selection for testing, and Evaluating the model on unseen test data.

The classification model was trained for classifying between 'intention' and 'non-intention' classes. The feature set was standardized to have values between 0 and 1. The standardizing parameters were also recorded to be used in the following steps. An SVM classifier was trained to classify between 'intention' and 'non-intention' classes with a Gaussian or Radial Basis kernel.

To achieve a proper threshold or working point, the 'intention' and 'non-intention' epochs in the validation set were segmented and labeled. The corresponding features were standardized by using the parameters obtained from the previous step. After that, the obtained unlabelled data were classified by the classification model. Different thresholds were calculated for specificity values ranging from 75% to 90% in a step of 5% to avoid a high number of false-positive detection.

3.3.4 Evaluation of the model and thresholds

The validation on the testing set was conducted using sliding windows, shifted every 200 ms with the window length of 1 s. After obtaining the predicted scores of the test set data, the thresholds obtained in the preceding step were used to determine the class label of any particular data window. The output at any time was determined by only the data window before that particular time. To further reduce the risk of false-positive detection, a 3-window majority voting technique was applied. If the detected time was in the [-1.5,0.5] limit corresponding to the actual moment of event onset, then the decision was marked as correct detection. However, False Positive was detected only when an active detection was decided more than 1.5 seconds before or more than two seconds after the actual onset of the event.

Table 3.1: Classification performance for different subjects with threshold regulation

Preset Specificity	Subject	Threshold	TPR(%)	FP/min	Latency (ms)[1]
70%	S1	-4.5927	78.95	21.85	-584 ± 771
	S2	-2.2857	72.88	14.58	-602 ± 669
	S3	-1.3638	69.44	27.29	-721 ± 656
	S4	-2.1371	71.84	21.91	-660 ± 649
	S5	-2.8344	55.56	8.35	-363 ± 665
	S6	-2.0828	64.81	15.44	-669 ± 709
	S7	-4.0404	67.24	17.24	-285 ± 803
75%	S1	-3.7573	72.81	17.59	-556 ± 757
	S2	-2.1493	65.25	12.62	-497 ± 738
	S3	-1.3167	62.96	23.68	-703 ± 667
	S4	-1.9540	61.17	18.24	-611 ± 699
	S5	-2.6366	50	6.56	-340 ± 711
	S6	-1.9521	57.41	12.05	-510 ± 749
	S7	-3.6459	62.07	12.99	-245 ± 825
80%	S1	-3.7573	62.28	15.15	-514 ± 751
	S2	-1.9792	50.85	10.20	-483 ± 766
	S3	-1.2732	52.78	20.5	-729 ± 690
	S4	-1.7834	53.4	14.91	-534 ± 716
	S5	-2.3622	41.67	4.77	-395 ± 666
	S6	-1.8079	46.3	8.88	-436 ± 751
	S7	-3.2365	53.45	9.15	-322 ± 815
85%	S1	-3.2946	51.75	10.83	-393 ± 775
	S2	-1.8194	40.68	7.91	-433 ± 778
	S3	-1.2329	49.07	17.77	-617 ± 706
	S4	-1.5823	41.75	12.52	-443 ± 700
	S5	-2.1133	37.5	3.87	-475 ± 612
	S6	-1.6792	37.04	6.85	-435 ± 754
	S7	-2.8877	43.10	5.96	-218 ± 713
90%	S1	-2.6478	34.21	6.32	-447 ± 725
	S2	-1.5588	30.51	5.23	-455 ± 751
	S3	-1.1728	43.52	14.59	-596 ± 751
	S4	-1.3361	26.21	9.05	-552 ± 611
	S5	-2.1133	37.5	3.87	-475 ± 612
	S6	-1.4734	27.78	4.98	-465 ± 702
	S7	-2.4331	22.41	2.34	-185 ± 732

3.4 Results and Discussion

For evaluating the performance of the proposed BCI, the following parameters were calculated under different conditions: true positive rate, false positive/ minute and latency. The parameters are defined as follows:

$$\text{TPR} = \frac{TP}{TP + FN} \tag{3.1}$$

$$FP/min = \frac{FP}{t_{non\ intention}} \tag{3.2}$$

Here TP, TN, FP, FN denote the true and false detection of 'intention' and 'non-intention' samples and $t_{non\ intention}$ denotes the total duration of 'non-intention' windows.

Table 3.1 represents classification performances for different subjects for different thresholds. When the preset specificity is at a comparatively conservative value like 70% or 75%, the True positive rates were quite high, but the FP/min values were higher as well. When the thresholds were increased by fixing a higher preset specificity, the True positive rate went down but with much lower false-positive activations per minute. The mean latencies of detection were constantly very small, and negative values suggested that movement intention could be detected even before the gait onset or termination.

Table 3.2 represents the cross-subject average performance metrics with standard deviation. It is evident from the table that the highest average TPR was achieved for the preset specificity of 70% and the lowest FP/min was achieved for the 90% specificity value. The average latency of detection increased consistently with the increase of preset specificity except for 90% specificity. Therefore, it can be observed that increasing preset specificity constraint decreased FP/min, but at the same time, it decreased TPR with increased latency.

Table 3.2: Cross subject average performance metrics with standard deviation.

Preset Specificity	Mean TPR(%)	Mean FP/min	Mean Overall Latency (ms)
70%	68.67 ± 7.33	18.09 ± 6.17	-554.85 ± 703.14
75%	61.67 ± 5.99	14.82 ± 5.51	-494.57 ± 735.14
80%	51.53 ± 6.45	11.93 ± 5.23	-487.57 ± 736.43
85%	42.98 ± 5.57	9.39 ± 4.71	-430.57 ± 719.71
90%	31.73 ± 7.22	6.62 ± 4.08	-439.29 ± 697.71

In order to find a proper operating point, the tradeoff between TPR, FP/min, and mean latency should be considered. Having stated that, this paper uses only a two-second window to detect movement intention, which is a much smaller compared to that of other similar studies stated in [49, 50]. These studies used a four-second detection window comprising two seconds of data from both before and after the movement onset. This could be too large in real life online implementation. Usage of a two-second window with only a 0.5 s second of the post-event EEG data gives the proposed study an edge over the state-of-the-art methods.

3.5 Conclusion

This chapter presents the application of a threshold regulation methodology to reduce the number of false-positive gait intention detection in an asynchronous pseudo-online study. The outcome of the study suggests that with adaptive threshold regulation technique a high True-positive rate is attainable with very low latency. However, to reach an overall acceptable and operable threshold point, more works are needed in the future. An adaptive thresholding technique can be investigated by utilizing other sensor features. Moreover, advanced machine learning and deep learning technologies can be applied for better results. However, the outcomes of the study show promising feasibility of the proposed approach in the application of neurorehabilitation.

CHAPTER 4

ASYNSCHRONOUS PREDICTION OF GAIT INTENTION

4.1 Background

This chapter contains an edited version of the author's work in [85] ©2020 IEEE. The ultimate goal of BCIs for gait rehabilitation is to incorporate the human brain in the system loop in such a manner that natural movement capabilities are restored. However, this endeavor requires diligent efforts in understanding human motor cognition, voluntary movement planning, and execution process. The significant challenges to be addressed in gait intention detection for effective real-life control of powered exoskeleton or prosthesis are maintaining high true positive detection rate, achieving low false-positive detections/min and detecting intention as early as possible. Although successfully detecting as many gait intention events as possible is worthwhile, maintaining lower FP/min is even more critical because false-positive detections can lead to missed steps, falling, and other accidents that are hazardous to the user. So, FP/ min has to be kept to a bare minimum while maintaining an acceptable true positive detection rate. Meanwhile, lower latency is required to give the prosthetic system enough preparation time to adapt to the neural control command for flawless prosthetic control.

An increasingly desirable feature for such BCI systems is the ability to predict the intention of natural gait execution, not only to identify movement once it has already occurred. In the BCI context, this is useful to make movement seem more natural. Neurological evidence stated above suffices that the neural activation corresponding to voluntary gait operation starts as early as 1.5–2 s before the actual execution of movement. Recently, Hasan et al. showed that it is feasible to predict human intention to start or stop walking from pre-movement EEG data only [86]. Therefore,

there is a possibility to predict movement intention earlier than the actual movement through reliable extraction and selection of features from EEG signals corresponding to ERD or MRCP and by applying proper machine learning algorithms.

4.2 Current Work

The goal of this study was to investigate whether it is possible to predict human voluntary self-paced gait intention reliably before it takes place from scalp EEG signal with a low false-positive rate and a reasonable sensitivity. Furthermore, another goal of the study was to determine when a reliable prediction could be made. Ideally, the expected detection time should be as early as possible before the movement onset but not so early that it leads to erroneous detection. In this study, a binary supervised classification problem was designed to differentiate between steady state resting or walking and intention to move or stop. The classification problem was approached in two ways: offline and pseudo online. In offline approach, a ten-fold cross validation scheme was implemented to evaluate the performance of the proposed methodology. However, it is necessary to test the proposed methodology in real-time scenario to properly portray the effectiveness of it. As the data were already collected at the time of the testing, a pseudo online testing paradigm was also implemented in the study. This means that the data were collected and preprocessed beforehand, but the preprocessed data were handled and processed as if they were being collected in real-time while decision making. Further details on this approach will be presented in the following sections. When it came to feature extraction, ERD features were chosen over MRCP because mu and beta ERDs can be observed in single-trial EEG-signals. In contrast, MRCP has a very low DC amplitude of about 8-10 µV and is generally only evident after averaging multiple trials of repeated voluntary move-

ments. This fact makes ERD features more suitable for real-time online prediction of self-paced gait intention compared to MRCP despite being more prominent on and after the movement onset. As ERD feature extraction requires time-frequency analysis of the EEG signals, wavelet transform was used for signal processing as wavelet transform retains information in both time and frequency domain and provides better time frequency-resolution compared to traditional methods like Fourier transform. For prediction in offline scenario, the classification accuracy, sensitivity and specificity were calculated. Whereas in pseudo online scenario, a threshold regulation method was proposed to decide a working point keeping in mind the trade-off between sensitivity and specificity. A majority voting algorithm was implemented later to decrease the number of false-positive detections even more. By reporting a high true positive rate, low false-positive rate, and early detection time, this study is expected to extend the capacity of state-of-the-art BCIs.

4.3 Materials and Methods

This section provides detailed information about the experimental protocol, data acquisition, and signal processing. The details of subjects, experimental protocol, EEG and EMG data collection and preprocessing of EEG data have been provided in chapter 2 of this dissertation. However, instead of visual inspection, IClabel [87] was used for selecting brain components from the extracted independent components. Moreover, only the data obtained from six healthy subjects are used in this section.

4.4 Computational Methods for Prediction

4.4.1 Data segmentation and epoching

The neurological changes caused by self-paced gait intention can start up to 1.5 - 2 seconds before the actual onset of movement and can exist up to 2 seconds after the movement. That is why after getting the times of the starting and stopping events, windows comprising data from 1.5 seconds before the event to 1.5 seconds after the event occurrence times were marked as intention windows. The rest of the data were labeled as non-intention data, which consisted of data from both walking and resting periods. The intention and non-intention data windows were further subdivided into 1-second long epochs by sliding the windows every 0.2 seconds to obtain a finer time-frequency resolution. For pseudo online testing, however, a different windowing technique was applied. These will be described in detail in the following sections. The windowing methods for offline training and validation as well as pseudo online testing are shown in figure 4.1.

4.5 Signal Processing for Time-frequency Analysis

Three different signal processing tools were tested in this study to extract gait-related information from the cleaned EEG signal. The methods are discrete wavelet transform, empirical wavelet transform, and wavelet synchrosqueezed transform.

4.5.1 Discrete wavelet transform

DWT acts as a filter bank to investigate the signal in the time-frequency domain [88]. It provides an excellent temporal resolution because it is discrete in scale

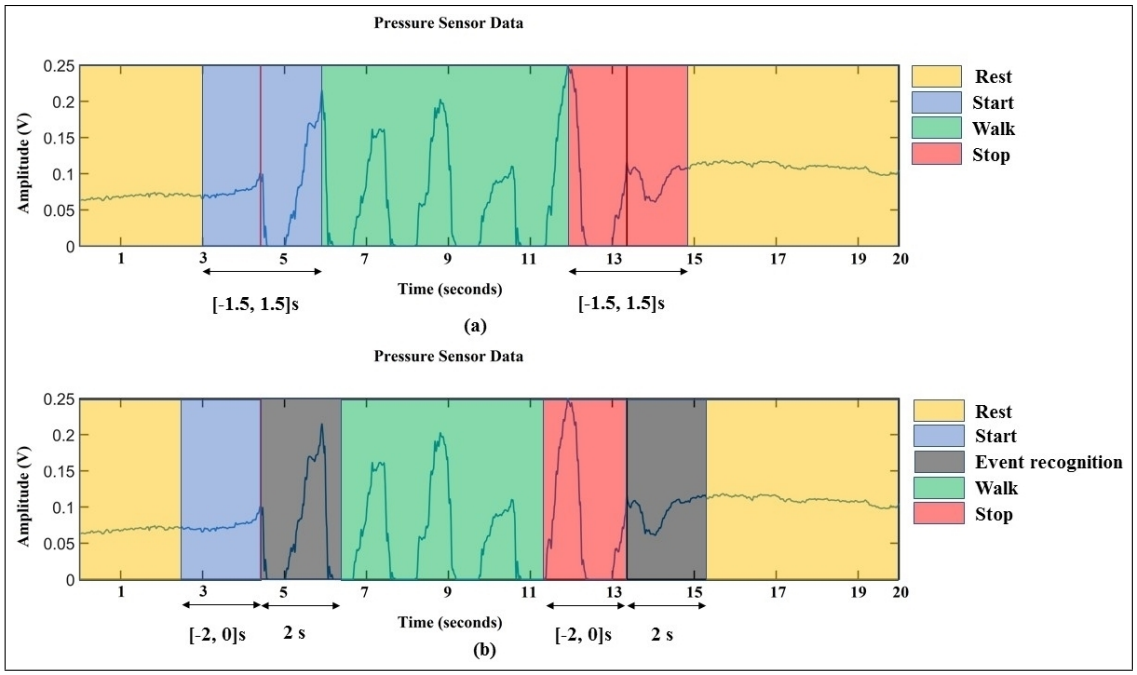

Figure 4.1: Data windows used for offline classifier training and validation, and pseudo-online testing. (a) Data windows used for offline classifier training and validation. Two separate classifiers were trained to distinguish 'rest' and 'start', and 'walk' and 'stop'. [-1.5,1.5] s data window corresponding to the time of event were used for this purpose. (b) Data windows used for testing in pseudo online paradigm. The pseudo online paradigm uses only 2 seconds of data before the event. After every event, 2 seconds of data were used to recognize the current state of gait and select the appropriate classifier between 'rest' vs. 'start' and 'walk' vs. 'stop'
.

and shift but continuous in time. By choosing a proper mother wavelet and level of decomposition, it is possible to investigate a specific frequency range over time. The details of discrete wavelet transform are included in chapter 2.

4.5.2 Empirical Wavelet Transform

Empirical Wavelet Transform (EWT) is an empirical and data-driven approach for wavelet decomposition [89]. This algorithm aims to decompose a signal where wavelet frames are built adaptively. This process removes the complexity in choos-

ing a proper mother wavelet for other wavelet transform approaches like DWT. For one dimensional signals, EWT tries to detect some modes in the Fourier spectrum and then uses those Fourier supports to build Littlewood-Paley type wavelets. Reportedly, EWT has shown more consistent decomposition than other data-driven decomposition approaches like Empirical Mode Decomposition (EMD) with a lesser number of modes. In this study, we used EWT to analyze the epoched EEG signals from all the channels. The number of intrinsic mode functions returned by the algorithms was limited to 3 because higher-order IMFs contain an increasingly higher frequency portion of the data, which did not hold any information concerning the study. The corresponding IMFs were then utilized to compute power features to use in the later sections. For each data epoch, the number of resulting power values was 3 per channel.

4.5.3 Wavelet synchrosqueezed transform

The Wavelet Synchrosqueezed Transform (WSST) is a time-frequency analysis method that is useful for analyzing multicomponent signals with oscillating modes [90]. The wavelet transform uses a mother wavelet as its time-frequency atom, which is translated and scaled to represent the signal. This representation is accompanied by some time-frequency spreading affecting the sharpness of the signal analysis in the process. The wavelet synchrosqueezed transform compensates for the spreading effects caused by the mother wavelet by reassigning the signal energy in frequency. Synchrosqueezing reassigns the energy only in the frequency direction while preserving the time resolution of the signal. By preserving the time, the inverse synchrosqueezing algorithm can reconstruct an accurate representation of the original signal. The beta and alpha band brain signals were extracted, and the power of those two bands

was extracted. Like the DWT, the number of features per epoch was 2 for each of the channels.

4.6 Feature extraction and prediction

In this study, the intention of self-paced voluntary movement initiation and termination were predicted using separate classification models. One classifier was trained to distinguish the intention to move from rest state data, and another one was modeled to predict the intention to stop from walking state data. The modeling of both classifiers was done in similar ways but using data from different states of the experimental protocol. Hereon after the overall process will be generally described without stating walking or stopping intention detection model unless otherwise stated for simplicity of description. The classes will be stated as 'active' and 'inactive' classes where 'active' class represents both walking intention and stopping intention windows, and 'inactive' classes represent both resting state and walking state.

The preprocessed dataset was divided into three parts for evaluation in a pseudo-online manner: training set, validation set, and test set. As the paradigm of the evaluation was pseudo online, which means the data were accessed as if they were being acquired real-time, 60% of the data was used for training the classifier, 20% were used as validation set for model tuning and the last 20% of the data were used for testing. This approach is inspired by and enhancement of a previous exploratory study which has been summarized in chapter 3. It is important to note that EEG data are often shown to have large variations in decoding performance with different training, validation and test sets. In order to account for this and to test the robustness and promise of the proposed methods, an offline testing was also carried

out on the combined training and validation test which consisted of 80% of the total data for all the subjects. Later, for testing the robustness of the method in the pseudo online paradigm, the training and validation sets were chosen ten times randomly from the first 80% data and thus ten different classifiers were trained and tuned by applying the following techniques. The obtained classifiers were then tested on the last 20% of the data in an asynchronous fashion.

4.6.1 Feature extraction

From the training and validation dataset, all the epochs were processed using the signal processing techniques stated in the previous subsection, and features were extracted accordingly. Each 1-second data epoch was labeled as a sample belonging to the corresponding active or inactive class. For DWT operation, the number of power values per epoch was 2 frequency bands $\times$ 8 channels = 16. Similarly, the number of power values for EWT was 24, and in the case of wavelet synchrosqueezing transform, it was 16. After the calculation of the power of corresponding bands, the first four data frames of each trial were taken as baseline to calculate ERD features. The ERD features were calculated for each channel in the following manner:

$$P_{i,j} = \frac{1}{N} \sum_{k=1}^{N} x_{i,j,k}^2 \tag{4.1}$$

$$P_{ref_i} = \frac{1}{l} \sum_{j=1}^{l} P_{i,j} \tag{4.2}$$

$$ERD_{i,j} = \frac{P_{i,j} - P_{ref_i}}{P_{ref_i}} \times 100\% \tag{4.3}$$

Here equation (1) represents the calculation of average power for each 1-second long epoch. Equation (2) shows the process of calculating baseline power for each

trial. While, equation (3) shows the calculation of ERD for each 1-second long epoch each trial. $x_{i,j,k}$ is the kth sample of the jth 1- second epoch of the ith trial of preprocessed single channel EEG data. $P_{i,j}$ is the averaged power of the jth 1-second epoch of the ith trial and N is the number of samples in the corresponding 1-second epoch. P_{ref_i} is the average power in the reference interval of the ith trial. The reference interval included the first l number of 1-second epochs of the corresponding trial[91]. $ERD_{i,j}$ denotes the ERD in percentage corresponding to the jth epoch of the ith trial.

4.6.2 Modeling

The classification problem was addressed by support vector machine, i.e., SVM [92, 93] classifiers with Radial Basis Function. Separate classifiers were trained for offline and pseudo online prediction. The offline modeling was tested by a 10-fold cross validation scheme. In each fold of the cross-validation, one-fold was used as test set and all the other folds were used as training set. MATLAB function 'fitcsvm' was used for modeling offline classifiers. The input 'OptimizeHyperparameters' was set to 'auto' which by default performed a five-fold cross validation within the training dataset of that loop and optimized the hyperparameters by minimizing the classification loss function. The optimization option was chosen to be Bayesian Optimization. The hyperparameters obtained by this method were used to train the model and classify the corresponding testing samples.

On the other hand, for pseudo online paradigm the working point or threshold of the classifier was determined from the validation set to obtain a minimal false positive rate while maintaining an acceptable true positive detection rate. This methodology is inspired by the outcomes of the previous chapter.

4.6.3 Determining a working threshold

The validation set was used for the threshold setting for asynchronous testing of the test set data. For this purpose, the epochs in the validation dataset were classified using the classifier model obtained in the previous section. The threshold was chosen by setting a limit on the specificity obtained by classifying the validation set samples. Here, the specificity is defined as:

$$Specificity = \frac{True\ Negative}{True\ Negative + False\ Positive} \tag{4.4}$$

The lower limit was set at 50% specificity. A stricter lower limit might lead to very low true positive detection, which is not a very desirable outcome. That is why a moderate constraint was selected for proper working point detection. However, additional measures were taken to ensure very low false positive detection, which is described in the following subsection.

4.6.4 Majority voting

EEG data is highly noisy and nonstationary. The uncertainty involved in EEG might still lead to false positive detection. That is why to reduce the number of false-positive detections even further, a 10- window majority voting scheme was applied as an extra caution. In the majority voting algorithm, if more than five positive detections were made in a 10- window interval, then the overall 10-window period was marked as true positive detection. Otherwise, the detection was discarded. The same procedure was repeated to produce all detection results. As the samples were collected by sliding data windows by 200 ms, a decision was made every 2 seconds.

Figure 4.2 shows the pseudo online testing procedure for one testing trial. The threshold chosen from the validation dataset is marked as a horizontal line, while the scores assigned to each 1-s data sub epoch are shown in blue. The testing

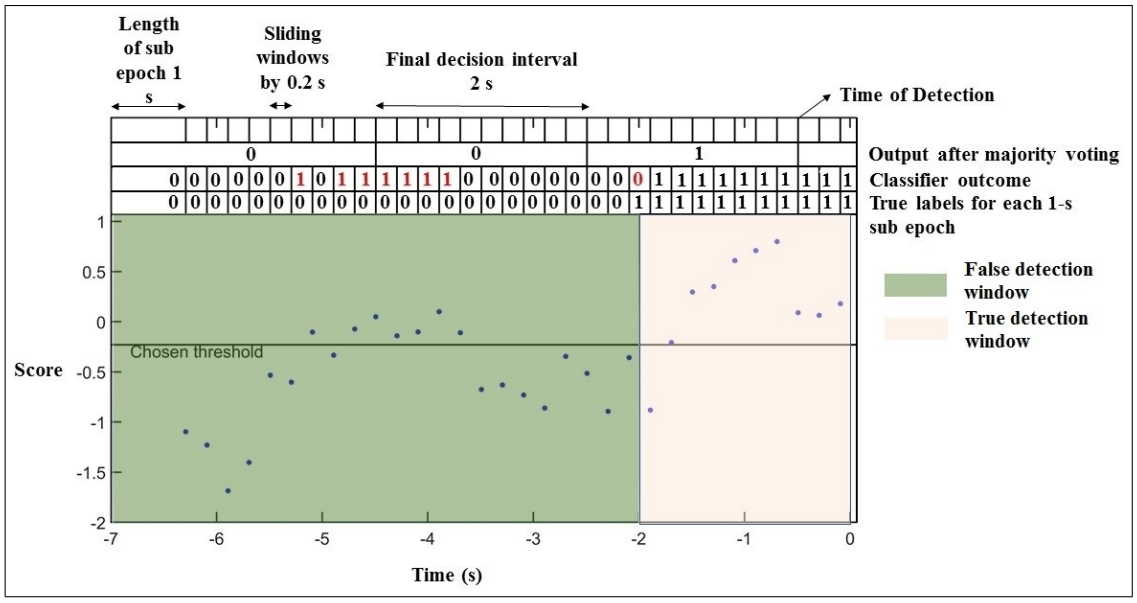

Figure 4.2: Pseudo Online testing procedure. The figure shows the execution of the testing procedure for one testing trial.

.

outcome of the model for each sub epoch and their true labels obtained from the motion capture system are also shown. Without the application of majority voting, there are several false outcomes which are marked in red. Finally, by applying a 10-window majority voting algorithm, the false positive detections are removed in exchange of decision bit rate. The time of detection is marked as the final time frame of the majority voting window which resulted in true positive outcome. After that, a 2-second buffer data window was used to recognize the current stage of gait to select the proper classifier to predict the next intention event.

4.6.5 Neurophysiological Data Analysis

The collected data were examined and analyzed offline to investigate the neurophysiology following human voluntary gain intention. The data analysis was done using the EEGlab processing tool. Epoching was done with windows of -4 to 2

seconds with respect to the detected event onset times. The epochs were cleaned off artifacts using the pre-mentioned data preprocessing pipeline beforehand. The obtained epochs were then used to perform a time-frequency analysis to investigate the ERD. For ERD calculation, -4 to -2 s data were used as the baseline. A 400-sample smoothing window was used to smooth the ERD representation. The ERD for subject 2 is presented in figure 4.3 and figure 4.4. Figure 4.3 shows ERD corresponding to 'stopping' of gait, while figure 4.4 shows ERD corresponding to 'start' of gait. As can be seen from the figure, significant ERD activity was found in the beta and alpha frequency bands, which is marked in blue. The Event Related Synchronization (ERS) was observed after the event onset.

4.7 Results

4.7.1 Evaluation indices

In this study, the offline performance was evaluated by reporting the classification accuracy, sensitivity and specificity. The classification was carried out in a 10-fold cross validation scheme and the performance metrics thus obtained were averaged across all the fold and all the subjects to obtain the average accuracy, sensitivity and specificity.

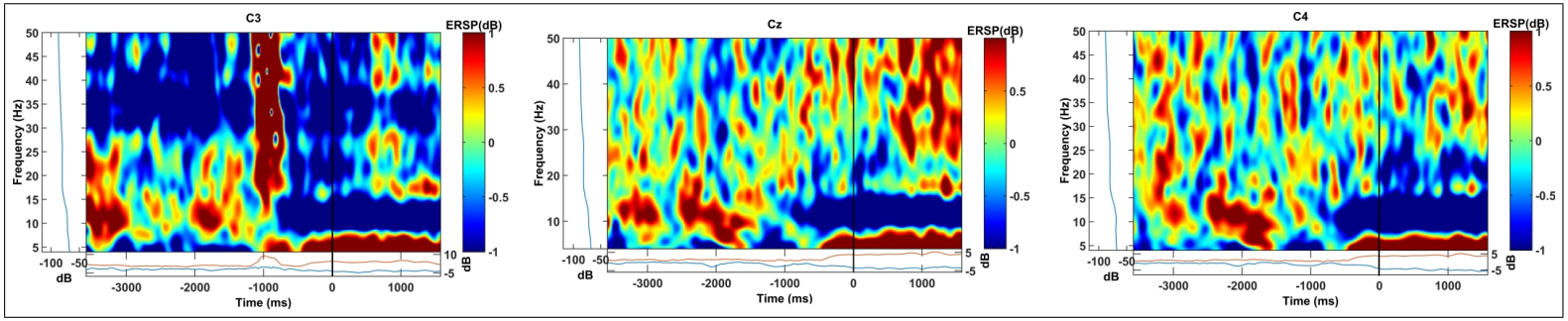

Figure 4.3: ERD activity from C3, Cz and C4 channels corresponding to 'stop' of gait.

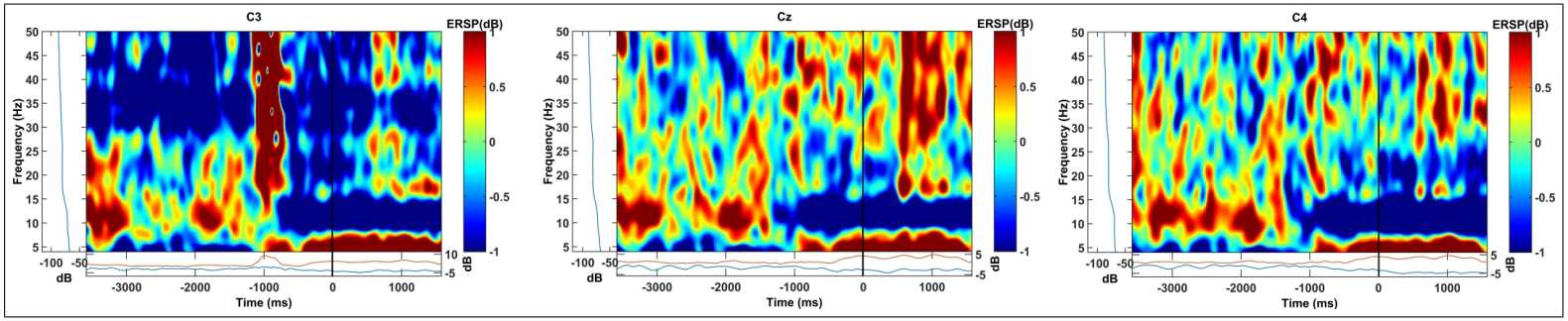

Figure 4.4: ERD activity from C3, Cz and C4 channels corresponding to 'start' of gait.

On the other hand, the performance metrics used for evaluation in pseudo online analysis were: True Positive Rate (TPR), False Positive per Minute (FP/min) and latency. In a pseudo online scenario, the window of true positive detection was set as [-2, 0] second corresponding to the movement onset times. That means if any positive detection was made inside that time window, it was marked as an accurate detection. Otherwise, it was marked as a false positive detection. After the occurrence of every gait event, a 2- second buffer time was employed to avoid confusing outcomes due to Event Related Synchronization following the corresponding event but preceding the next event. The 2-second window was also used to determine the current stage of gait. TPR and FP/min was determined as:

$$\text{TPR} = (Number\ of\ True\ Positive\ Detection)/(Number\ of\ True\ Positive\ events) \tag{4.5}$$

$$FP/min = \frac{Number\ of\ false\ positive\ detection}{Duration\ of\ total\ inactive\ windows\ in\ minutes} \tag{4.6}$$

4.7.2 Offline Analysis

Table 4.1 and table 4.2 show the results for obtained in offline classification. The evaluation of results was done by presenting accuracy, sensitivity and specificity. A two-sample t-test with Bonferroni correction was also performed to look for statistical significance of the results obtained by different methods.

Table 4.1 shows that in case of start of walking intention detection, DWT resulted in 78.28±3.45% accuracy with 76.08±5.67% sensitivity and 79.78±8.28% specificity. While EWT resulted in 76.72±2.50% accuracy with 73.67±5.98% sensitivity and 76.54±6.33% specificity. Lastly, WSST provided a detection accuracy of 88.23±1.59% with 85.42±4.03% sensitivity and 90.24±2.78% specificity. The results

Table 4.1: Offline 'Start' of Gait Prediction Results (Mean±Standard Deviation)

S. N.	Accuracy (%)			Sensitivity (%)			Specificity (%)		
	DWT	EWT	WSST	DWT	EWT	WSST	DWT	EWT	WSST
S1	83.64±2.04	72.56±2.75	92.99±1.26	79.6±2.14	68.21±8.78	90.39±2.66	87.04±3.66	76.26±9.74	95.22±0.69
S2	82.12±2.68	81.65±2.20	89.27±1.73	79.57±6.09	78.12±3.72	86.15±7.50	83.70±6.20	83.83±4.09	91.19±5.14
S3	67.44±7.57	76.51±2.15	76.53±2.38	70.27±10.8	69.63±6.02	77.32±5.04	65.83±17.7	74.16±3.96	76.07±4.76
S4	80.54±2.12	78.05±1.96	87.83±1.25	7±3.580.50	72.22±5.68	82.03±3.24	8±3.007.26	79.94±4.70	91.70±2.30
S5	81.27±1.58	79.18±2.65	90.71±1.78	82.23±6.00	84.20±5.02	88.21±3.23	79.97±9.87	70.80±8.62	94.11±2.12
S6	74.67±4.72	72.37±3.30	92.07±1.13	74.29±5.38	69.63±6.67	90.81±2.52	74.86±9.20	74.22±6.87	93.17±1.69
Overall	78.28±3.45	76.72±2.50	88.23±1.59	76.08±5.67	73.67±5.98	85.42±4.03	79.78±8.28	76.54±6.33	90.24±2.78

Table 4.2: Offline 'Stop' of Gait Prediction Results (Mean±Standard Deviation)

S. N.	Accuracy (%)			Sensitivity (%)			Specificity (%)		
	DWT	EWT	WSST	DWT	EWT	WSST	DWT	EWT	WSST
S1	84.47±1.63	75.30±2.67	92.92±1.29	75.66±3.81	76.85±3.92	88.78±2.94	88.54±2.16	74.50±4.51	95.04±1.11
S2	73.16±4.56	76.85±1.91	87.43±2.85	80.12±8.49	74.08±4.40	87.12±4.90	68.12±12.86	78.85±3.89	87.64±6.83
S3	68.84±2.67	69.31±1.78	77.22±1.39	63.48±10.47	65.33±7.89	73.78±6.21	73.42±10.52	72.72±7.77	80.17±4.23
S4	74.26±2.66	76.67±2.87	83.02±1.97	65.01±6.32	71.33±5.82	72.53±4.54	79.01±4.84	77.87±7.25	89.30±2.80
S5	75.14±6.17	74.15±3.75	90.84±1.45	75.28±7.36	68.12±11.6	84.37±3.75	75.05±13.64	76.12±11.4	94.66±1.52
S6	65.96±7.37	70.08±3.79	90.79±1.34	72.52±20.3	68.30±6.58	89.58±2.43	61.65±24.86	71.58±7.78	90.56±1.73
Overall	73.64±4.18	73.73±2.80	87.04±1.72	72.23±9.23	70.67±6.70	82.69±4.13	74.30±11.40	75.27±7.10	89.59±3.04

obtained by WSST showed statistical significance over those obtained by DWT and EWT at 5% significance level.

Table 4.2 presents the results of intention detection in the case of stop of walking. By using DWT, EWT and WSST, accuracies of 73.64±4.18%, 73.73±2.80%, and 87.04±1.72%, sensitivities of 72.23±9.23%, 70.67±6.70%, and 82.69±4.13% and specificities of 74.30±11.40%, 75.27±7.10% and 89.59±3.04% were achieved respectively. The results obtained by using WSST showed statistical significance over the results of DWT and EWT in the case of stopping intention prediction as well at 5% significance level. The initial offline evaluation of performances of different methods hinted that the synchrosqueezing approach might be a more suitable signal processing technique for online prediction of starting and stopping intention detection.

4.7.3 Pseudo-Online Analysis

The real purpose of this study was to investigate the performance of a BCI in an online environment. In an online scenario, the subject would try to activate an assistive device with the output of the BCI. As the trials were acquired before the signal processing techniques were applied, the performances were instead evaluated in a simulated online environment. In the pseudo online scenario, the data were accessed, and epochs were processed as they were acquired, which is more realistic than offline analysis.

Table 4.3 provides the TPR, FP/min, and detection latency for different methods and subjects for the start of walking detection, where Table 4.4 provides the same information for the stop of walking intention detection. A two-sample t-test with Bonferroni correction was also performed to look for statistical significance of the results obtained by different methods.

Table 4.3: Pseudo-online 'Start' of Gait Prediction Results (Mean±Standard Deviation).

S. N.	TPR (%)			FP/min			Latency (ms) (Mean ± std)		
	DWT	EWT	WSST	DWT	EWT	WSST	DWT	EWT	WSST
S1	71.4±6.2	75.6±8.6	82.5±2.2	5.0±1.8	5.4±1.0	5.8±2.2	-845±607	-1000±114	-866±584
S2	84.0±2.7	83.7±5.9	87.7±1.0	6.6±0.4	6.2±0.6	6.7±0.3	-898±647	-914±656	-887±649
S3	76.9±4.1	75.2±2.5	80.5±5.5	6.2±0.5	6.3±0.5	6.7±0.4	-1089±619	-1187±577	-1036±609
S4	77.4±3.9	75.7±1.8	82.8±2.6	7.5±0.4	8.1±0.7	7.9±0.3	-1178±565	-1070±638	-1160±591
S5	91.8±2.0	90.5±0.1	94.5±0.1	6.8±0.1	6.3±1.0	6.7±0.3	-993±593	-981±590	-981±589
S6	68.2±4.4	80.0±5.0	85.0±3.1	6.8±0.4	6.4±0.7	6.7±0.3	-1139±585	-1144±637	-1082±595
Overall	78.3±8.6	80.1±6.1	85.5±5.0	6.5±0.8	6.5±0.9	6.8±0.7	-1024±602	-1049±535	-1002±603

Table 4.4: Pseudo-online 'Stop' of Gait Prediction Results (Mean±Standard Deviation).

S. N.	TPR (%)			FP/min			Latency (ms) (Mean ± std)		
	DWT	EWT	WSST	DWT	EWT	WSST	DWT	EWT	WSST
S1	75.5±5.0	78.3±9.3	82.4±4.1	9.2±0.4	9.3±0.5	9.8±0.6	-1074±686	-1074±676	-1054±670
S2	85.0±2.4	84.7±3.2	82.3±1.6	7.0±0.5	7.4±0.3	8.3±0.3	-850±619	-770±601	-730±550
S3	77.4±2.7	92.9±4.8	83.7±3.1	8.3±0.6	7.2±0.4	8.6±0.5	-1007±734	-1055±730	-1012±733
S4	64.0±4.1	73.8±5.7	75.4±5.1	9.1±0.4	8.5±0.7	9.2±0.4	-843±491	-782±600	-828±609
S5	79.7±6.1	75.0±4.5	79.3±4.4	9.7±0.5	11.8±0.6	9.6±1.3	-1096±473	-1141±434	-1117±414
S6	67.4±4.6	83.7±5.8	84.0±1.6	12.7±0.5	10.8±1.4	11.04±0.5	-993±675	-923±634	-917±640
Overall	75.3±7.9	81.4±7.2	81.2±3.3	9.3±1.9	9.2±1.8	9.4±1.0	-977±613	-957±612	-943±603

Table 4.3 shows that an average TPR of 78.3% with a standard deviation of 8.6% was achieved using DWT, whereas using EWT and WSST, the prediction TPR was 80.1 ± 6.1 % and 85.5 ± 5.0 % respectively. The best TPR was achieved for S5, which was 94.5% using WSST, while the lowest TPR achieved was 71.4% for subject 1 using DWT. The FP/min achieved by the methods were 6.5±0.8, 6.5±0.9, and 6.8± 0.7, respectively. All the methods resulted in these TPR and FP/min while predicting the intention to start walking almost 1 second before the actual onset in an average. The two-sample t-test with Bonferroni correction showed that WSST performed significantly better in True Positive Detection compared to DWT and EWT at a 5% significance level. The FP/min and latency of detection did not show any statistical significance at 5% significance level.

Table 4.4 shows that the average TPRs obtained by DWT, EWT, and WSST were 75.3±7.9%, 81.4±7.2%, and 81.2±3.3%, respectively. These values, however, did not have any statistical difference at 5% significance level. The average FP/min achieved by the methods was 9.3±1.9, 9.2±1.8, and 9.4± 1.0. And finally -977±613, -957±612 and -943±603 ms detection latencies were obtained. Here, again, the prediction was achieved almost 1 second before the actual termination of movement, which is a significant outcome for a BCI for real-life control. None of the parameters obtained for stop prediction yielded any statistical difference at 5% significance level.

4.8 Discussion

In this paper, a purely predictive BCI technology utilizing traditional discrete wavelet transform, data-driven empirical wavelet transform, and wavelet synchrosqueezed transform was implemented to predict human voluntary gait initiation and termi-

nation intention in a pseudo online environment. Six healthy subjects' data were collected and tested for this purpose.

As a part of the experimental protocol, the subjects were requested to keep unnecessary movements, like eye movements, body movements to a minimum level. They were asked to do so in order to keep the unnecessary artifacts as low as possible. However, in a real-time scenario this condition would not be applicable because the duration of application of the corresponding BCI would be much longer. And it would be impossible to control the unrelated movements throughout the duration of operation. Despite the instructions, however, the artifactual components were very strongly present in the data. The preprocessing tools ASR and ICA performed very well to remove whatever eye artifacts and movement induced artifacts there were in the data. But, the data and memory requirement of these algorithms make these a poor choice for real-time application. For real time application, therefore, a robust, computationally efficient, effective online movement artifact system must be implemented. Also, the subjects should be allowed to carry out the tasks in a less controlled and more natural manner. These issues will be addressed in a future extension of the current study.

It is to be noted here that the preprocessing was done only once offline before the execution of pseudo online decision making. For all further signal processing, feature extraction and classification in both offline and pseudo online paradigm, this preprocessed EEG dataset was utilized. The major preprocessing tools that were implemented in this study, ASR and AMICA requires a large chunk of data to work properly. ASR needs a significant amount of data to determine artifact free clean EEG data for estimating and removing artifact from the artifact laden EEG data. On the other hand, ICA requires a lot of data as well to properly localize all the contributing independent sources inside the brain. Because of the requirement

of a large amount of data, these preprocessing tools are generally used in offline processing pipelines. Recently, advanced real-time versions of ICA namely Online Recursive ICA [82], Real-time EEG Source-mapping Toolbox (REST) [81] are coming into being. However, more advanced and computationally efficient algorithmic developments are necessary to accommodate these tools in online environments. Because of the shortcomings of these methods, in this study they were only implemented in offline preprocessing. Once the data were preprocessed, the dataset was used to perform pseudo online signal processing, classifier modeling and testing. In future real-time study, viable preprocessing technologies and filters, for example, Laplacian filters[49, 77], will be explored to ensure that all the steps can be carried out in real-time.

The EEG data were initially recorded at 500 samples per second which was intrinsic to the system. However, the data were down sampled to 250 Hz at the first step of preprocessing for reducing the size and increasing efficiency. For online implementation of BCI, higher sampling rate would result in huge amount of data to transmitted across wireless signal, processed multiple times and stored for application. Therefore, down sampling can help reduce the memory requirement and speed of operation of the corresponding BCI. However, down sampling is accompanied by aliasing which could always introduce additional noise to the data if implemented carelessly. Only the lower frequency ranges, namely the alpha (8-16 Hz) and beta (16-32 Hz) band brain waves were necessary for the purpose of this study. As the chosen sampling frequency of 250 Hz was much higher than the Nyquist frequency to obtain those frequency ranges, the effect of aliasing noise would be minimal. Even so, an anti-aliasing FIR filter was applied to the data and the delay introduced by the filter was properly compensated as precaution.

This study compares the performance of DWT, EWT and WSST produced features in predicting human intention to start or stop walking. For DWT, the mother wavelet was chosen to be 'db4'. The choice of mother wavelet was based on literature review and available state of the art methodologies [94, 95]. Daubechies wavelets are very commonly used in numerous applications which involve the processing of EEG signals. Among various orders of Daubechies wavelets, Daubechies 4 or 'db4' has been used very extensively. Because db4 mother wavelet is renowned for its orthogonality property, smoothness and its suitability to detect changes in EEG activity [94]. Studies have also suggested that db4 mother wavelet has shown good cross correlation between original and reconstructed signal, thus ensuring low reconstruction error. This suitability has led to the use of db4 mother wavelet in various EEG-based applications, for example seizure detection [96, 97], sentiment recognition [98], movement intention detection [84]. That being said, the choice of mother wavelet is always an application dependent task and more mother wavelets like Symlets, Haar wavelets or Morlet wavelets should be examined in future studies.

The offline results show that WSST outperformed both DWT and EWT in terms of accuracy, sensitivity and specificity for both intention of 'start' and 'stop' prediction. The statistical test performed to differentiate between the performances of the three methods showed significance enhancement across all evaluation metrics when WSST was used. The preliminary offline analysis presented a promising outcome which inspired the pseudo online testing procedure applied in this study. As the goal of the study was to evaluate the effectiveness of the BCI in a real-time scenario, the result of pseudo online analysis held more importance to validate the hypothesis of the study.

The statistical test performed on the pseudo online start prediction result showed that the WSST performed better than the traditional DWT and EWT in terms of

TPR. This result suggests that the data-driven approach of EWT might result in distinguishing feature extraction in the time-frequency domain, however, to optimize the outcome of this signal processing technique selection of appropriate empirical modes holds utmost importance. Therefore, the choice of proper modes for gait related neural information extraction should be investigated in future study. The synchrosqueezing approach provided promising TPR with low FP/ min. This approach retains the sharpness of time-frequency analysis, which contributes to features with better resolution. These results showed the potential of advanced wavelet transform techniques to successfully predict the start of voluntary human gait.

The methods did not show any statistical difference in the stop of gait detection although the results obtained by synchrosqueezing approach was better than those of DWT and EWT. Moreover, the TPR was lower, and FP/min was higher compared to start prediction. The main reason behind this phenomenon might be the artifact corrupted baseline EEG of walking windows. Although extensive movement artifact removal pipeline was employed, the baseline for ERD calculation for 'stop' prediction was still not as clear as the baseline for the 'start' prediction. The low SNR and noisy nature of EEG accompanied by the movement artifacts resulted in declined performance compared to the 'start' of gait prediction. Further work is needed to predict stopping intention with higher TPR and lower FP/min.

Both starting and stopping events were predicted quite successfully almost 1 second before the events. This outcome is significant because this would allow the assistive device enough preparation time to adapt to user intention. Such a transition period will, in turn, result in a more natural and smoother transition in real- life prosthesis systems.

The results obtained for the various methods look promising and those for stopping of gait are even more intriguing. However, whether there is any way to tell that

the methods used can differentiate the intention to stop gait from a change in gait itself for the purpose of stopping is an interesting question. In more strict terms, how one can know that the neural signatures used to predict stopping of gait, in the window preceding the actual termination of gait, are indicative of strictly a higher order mental intention to stop and not a sensorimotor correlate of change in gait itself for stopping is worth investigating. The answer to the question can be discussed in terms of the neurophysiological background involved with walking. Automaticity is a special feature of walking of healthy people which refers to the fact that the nervous system can successfully control steady state walking with minimal use of executive control. This in turns means that during steady walking the nervous system is seldom, if ever, in automatic control. Rather, the sensorimotor cortex takes over control only in the event of intention to change the current state of gait [99]. Even though a person is walking steadily, the lack of activity in the sensorimotor cortex, therefore, creates a suitable baseline just like in the standing condition. Moreover, the investigation of ERD corresponding to both starting and stopping intention show similar pattern which only originates from intention to change state of gait (figure 4.3, figure 4.4). These facts confirm that the neural correlates namely ERD corresponds to the intention to change state of gait itself. Moreover, human walking is controlled by volition [100]. Before the execution of change in gait state, changes corresponding to the intention appear in the sensorimotor cortex which facilitate the volitional control of movement. In fact, studies suggest that "cerebral initiation of a spontaneous, freely voluntary act can begin unconsciously, that is, before there is any subjective awareness that a 'decision' to act has already been initiated cerebrally"[101]. So, in summary, the change in gait stages can generate a responsive neural change, but the intention to start or stop is more likely to appear first (sometimes unconsciously) which creates neural changes to accommodate the

change in gait. However, it is indeed a difficult question to answer and supportive data from a denser grid of EEG or fMRI with a better temporal resolution could help isolate and distinguish the effect of intention to stop and response to change in sensorimotor correlates. This question should be addressed in the future extension of this study.

The comparison of the present task with previous work is quite tricky. This study presents an entirely predictive BCI system to predict human voluntary gait intention. Other studies have used information from either before and after the movement initiation and termination or have used a long baseline period for extracting neural information. On the other hand, the current study used data from healthy subjects only while other studies might have collected data from stroke patients or amputees as well. Moreover, to find studies which had similar experimental protocol was also quite challenging. So, the comparison of results is quite complex. Table 4.5 shows the comparison of the current study to the state-of-the-art studies. Ortiz et al. [77] used a four-second detection window for pseudo-online start and stop detection, which employed data from two seconds before the movement to two seconds after the movement. They achieved an average of 80.47±14.63% TPR with 4.43±3.67 FP/min in 'start' detection and 84.06±14.63% TPR with 4.73±5.34 FP/min in 'stop' detection. The current study achieved competitive TPR with a higher FP/min with a comparatively smaller detection window. Moreover, the proposed BMI is predictive, whereas the study mentioned above employed more of a detection approach. Lin et. al [102] achieved 75.5±12.0% true positive detection rate with 2.2±0.8 FP/min for detecting intention of Ballistic dorsiflexion using a [-2,1] s detection window. Bai et al. [60] used a fully predictive [-1.5,0] s window for detecting intention of wrist movement but the achieved TPR was lower than the current study and the detection time was also later than that of the current study.

Table 4.5: Comparison of Results with Existing Works.

Study	Task	Intention window	TPR	FP/min	Detection Times (ms)
Ortiz et. al [25]	Start of gait	[-2, 2] s	80.47±14.63	4.43±3.67	-
Ortiz et. al [25]	Stop of gait	[-2, 2] s	84.06±14.63	4.73±5.34	-
Lin et. al [26]	Ballistic dorsiflexion	[-2,1] s	75.5±12.0	2.2±0.8	-
Bai et. al [27]	Wrist movement	[-1.5,0] s	40 ± 7	-	-620
Sburlea et al. [28]	Initiation of gait	[-1.5,0] s	67.2 ± 5.9	0.79 ± 0.17	-350±170
Sburlea et al. [29]	Initiation of gait	[-1.5,0] s	66 (Median)	-	-
Present Study	Start of gait	[-2,0] s	85.5 ± 5.0	6.8 ± 0.7	-1002 ± 603
Present Study	Stop of gait	[-2,0] s	81.2 ± 3.3	9.4 ± 1.0	-943 ± 603

Sburlea et al. [55, 56] used a smaller prediction window of [-1.5, 0] s to achieve lower TPR and later detection time for predicting intention of gait initiation. However, they reported an impressive FP/min of 0.79 $\pm$ 0.17 which was the best FP/min that was found in literature. In summary, the current study shows promise in early prediction of gait intention, however, specially the FP/min achieved by this study needs improvement to be applied in real time study. It is to be noted though that the lower FP/min resulted from the use a fully predictive window where a detection made slightly after the event would also be counted as a false positive detection. Nevertheless, incorporation of other sensors' data to aid the prediction performance of the BCI might be an interesting solution approach which will be addressed in the future study.

4.9 Conclusion

In this study, it has been demonstrated that it is possible to predict 'start' and 'stop' of human voluntary gait intention using EEG data from before the event only. Advanced wavelet transform technologies equipped with threshold regulation and majority voting algorithm for adaptive prediction of gait intention is a promising approach for real-life application. More efforts are necessary to improve the TPR and FP/min, especially for predicting the intention of gait termination. However, the current promising results show the feasibility of the proposed approach in the context of real-life lower limb rehabilitation.

CHAPTER 5

VMD-WSST: A COMBINED BCI FOR MOVEMENT INTENTION DETECTION

5.1 Background

The work presented in this chpater has been reprinted from the author's work published in [103], ©2021 IEEE. Prediction of movement intention is of paramount importance to enable volitional control of assistive devices. The performances of current Brain-Computer Interfaces (BCI) are yet to reach the desired degree of accuracy necessary for real-life assistive technologies. Therefore, the prediction of gait intention remains a critical topic of research. Over the recent years, various signal processing and machine learning technologies have been applied to detect human intention to initiate and terminate movement.Over the recent years, various signal processing and machine learning technologies have been applied to detect human intention to initiate and terminate movement.Although the results of these studies have been encouraging, the accuracies of such models are not sufficient to incorporate these methodologies in real-life scenarios yet. Therefore, further works are necessary to ensure high-quality time-frequency decomposition to acquire the most discriminative EEG features.

This paper proposes a methodology to detect human gait intention from gait-related EEG signals leveraging the ERD phenomenon. Extraction of useful ERD-related features requires time-frequency analysis with very little to no spectral leakage, preservation of the sharpness of decomposition, and a good time-frequency resolution. In this study, the incorporation of two practical, data-driven empirical time-frequency analysis tools, namely Variational Mode Decomposition (VMD) and WSST, has been proposed to design a BCI algorithm. Gait-related EEG data from

six healthy individuals described in the previous chapter were analyzed, and two binary classification problems were formulated to detect human intention to start or stop walking. The classification problems were approached with SVM classifiers with radial basis kernel. The performance of the BCI algorithm was evaluated by the accuracy, sensitivity, and specificity achieved by the classifiers.

5.2 Materials and Methods

This chapter uses the EEG, GRF, and EMG data used in the previous chapter. Data acquisition and preprocessing was done using the same procedure. The [-1.5, 1.5] second window was used as the intention window for creating the classification model while the rest of the epoch was marked as non-intention data. The epoched data were then further subdivided into 1-second long sliding windows with 80% overlap. This step resulted in a finer time-frequency resolution.

5.2.1 Variational Mode Decomposition

VMD [104] is a data-driven approach that decomposes a temporal signal into K number of narrowband amplitude and frequency modulated Intrinsic Mode Function (IMF)s. The variational mode decomposition method simultaneously calculates all the mode waveforms, $u_k(t)$ and their central frequencies, $f_k(t)$, that minimize the constrained variational problem. The optimization problem is solved using the Alternating Direction Method of Multipliers (ADMM).

In this study, the EEG data were analyzed by the VMD algorithm, and each 1-second data window yielded 10 IMFs. As the ERD phenomenon is present in the Mu (8-16 Hz) and Beta (16-35 Hz) frequency bands of the brain signal, the central frequencies of the obtained IMFs were monitored, and only the IMFS with central

frequencies in the range of 10-32 Hz were retained. The rest of the IMFs were removed from the data to reduce redundancy. Thus, the use of VMD enabled us to remove the irrelevant and redundant portion of the EEG data and thus enhance the quality of subsequent time-frequency decomposition. Moreover, as the IMFs are well separable in the time-frequency plane, removal of IMFs outside the range of interest retains the sharpness of the time-frequency features of the frequency range of interest, which traditional signal processing techniques cannot achieve. As the VMD algorithm is entirely data-driven, the number of retained IMFs could vary from frame to frame. This nonuniformity could make the task of feature extraction much harder. That is why, instead of taking the IMFs as intermediary features, they were reconstructed back into 1-second-long data windows. The data were then ready for time-frequency decomposition using the WSST algorithm. The overall VMD process has been summarized in figure 5.1. The equations for calculating ERD can be found in the previous chapter.

5.3 Wavelet Synchrosqueezing Transform

The VMD-reconstructed EEG data were then analyzed using the WSST algorithm. Using WSST, the Mu and Beta band EEG signals were extracted, then used for ERD calculation. Figure 5.2 compares the ERD in Mu and Beta bands of 'start' related EEG obtained by VMD+WSST and a 4th order Butterworth bandpass filter. The analysis included all the trials from channel Cz of subject 1. The analysis was performed on [-4,3] s data window with reference to the onset of the gait event. The first two seconds of the window were taken as the baseline for ERD calculation. Figure 5.3 shows the same for 'stop' related EEG. The proposed method resulted in an observably higher negative peak in ERD for both 'start' and 'stop' of gait. How-

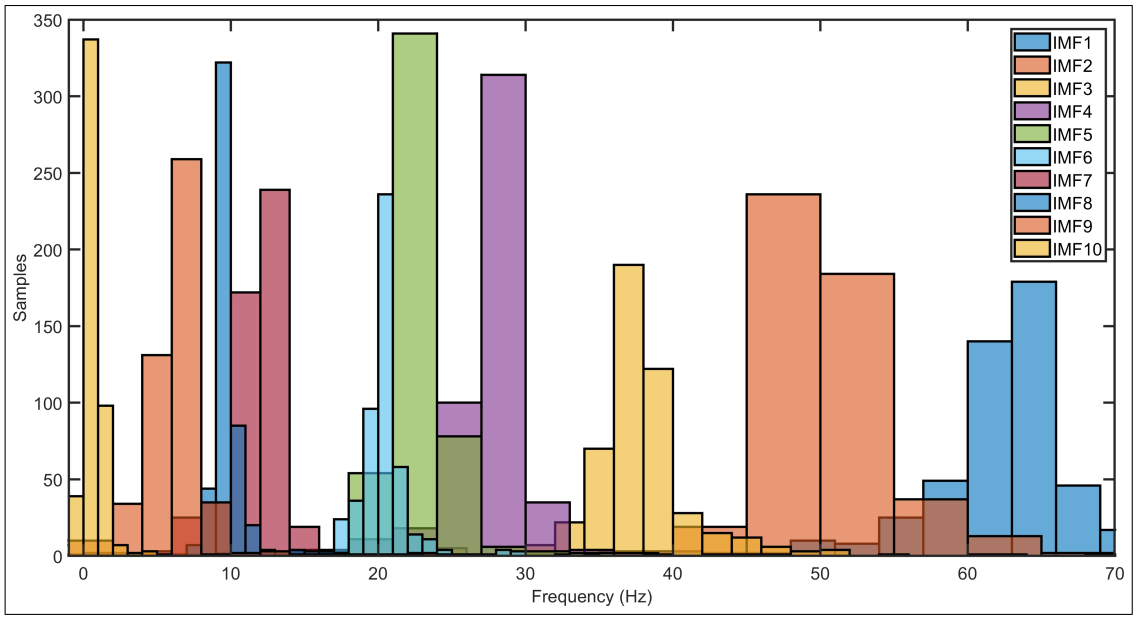

Figure 5.1: The instantaneous frequencies of the IMFs obtained from a 10-second window. Only the central frequencies of IMFs 4,5,6,7 were in the range of interest (10-32 Hz). Therefore, only those IMFs were retained
.

ever, no visible difference could be recognized between the time-frequency analysis obtained for the 'stop' of gait. Future works should include statistical analysis on a larger scale to validate the enhancement in time-frequency analysis.

5.4 Feature extraction and Classification

The Mu and Beta band EEG signals obtained in the previous step were then used to compute ERD features for classification. In this study, two binary classification problems were formulated, and two classifiers were designed to address the problems. The two classification problems were "Rest" vs. "Start" and "Walk" vs. "Stop". Due to the movement artifacts, the baseline EEG activity under resting and walking states would be significantly different. The two classification problems helped address the difference in baseline and, in turn, the difference in feature distribu-

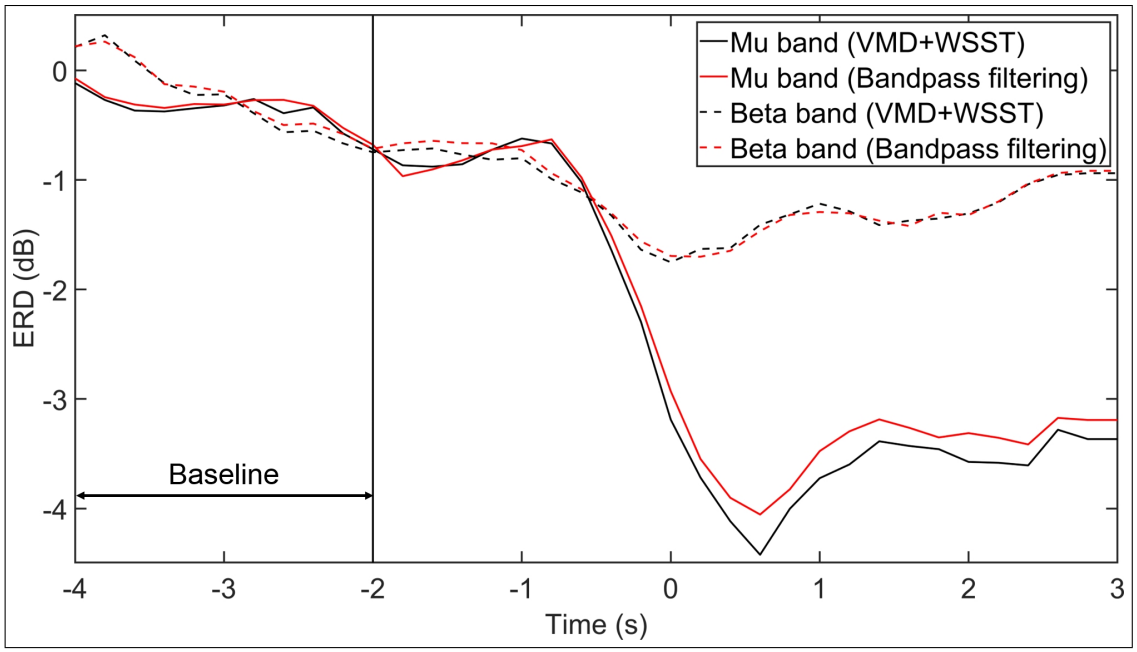

Figure 5.2: Comparison of ERD activity obtained by the proposed method and a 4th order Butterworth bandpass filtering correspoding to start of gait. The EEG data were acquired from Subject 1 channel Cz. Time 0 indicates the onset of gait.
.

tion. For both classification problems, Mu and Beta ERDs were used as features. As there were 8 channels, each 1- second data window yielded 16 features. Both classification problems were approached with an SVM classifier with a radial basis kernel. The classification was done in a 10-fold cross-validation scheme where one-fold were used as a test set, and all the other folds constituted the training set at each step of validation. However, the data were imbalanced (70% vs. 30% in favor of the non-intention class). That is why it was necessary to balance the classifier models so that they did not favor the majority class and subsequently result in enhanced classification accuracies. It was ensured by maximizing the F1-score in each step of training. As a result, the threshold or working point of classification was appropriately regulated.

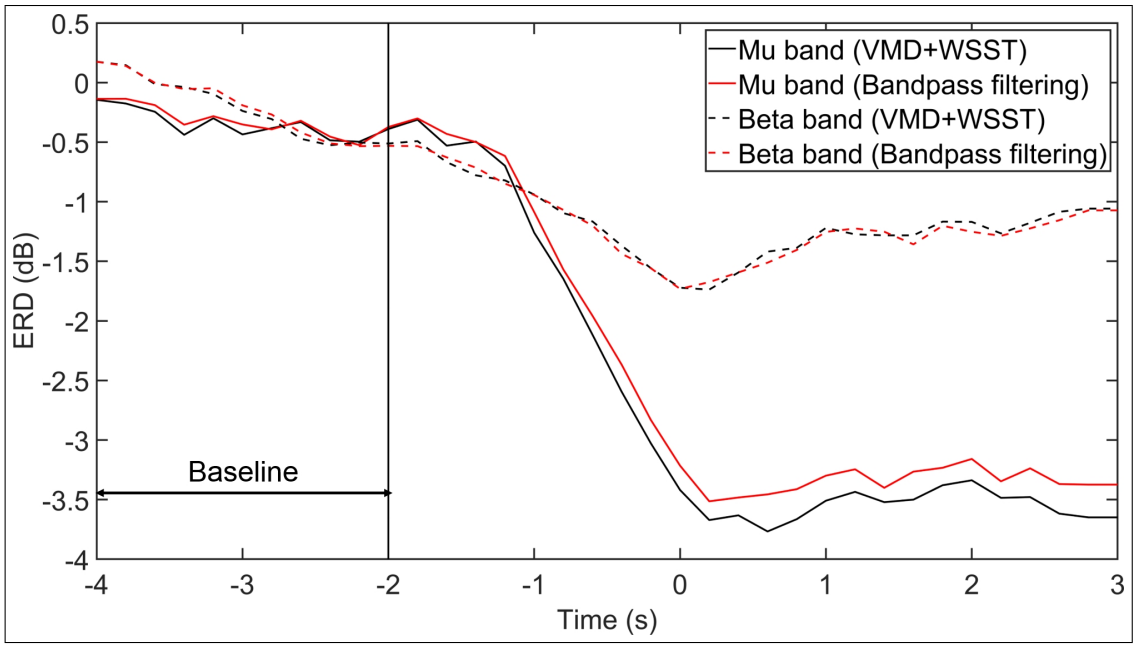

Figure 5.3: Comparison of ERD activity obtained by the proposed method and a 4th order Butterworth bandpass filtering correspoding to stop of gait. The EEG data were acquired from Subject 1 channel Cz. Time 0 indicates the onset of gait.
.

5.5 Results and Discussion

5.5.1 Classification Results

Table 5.1 and table 5.2 show the results of classification. The evaluation of the performance of the proposed approach is done by reporting accuracy, sensitivity, specificity. In the case of "Rest" vs. "Start" classification, the proposed approach resulted in an accuracy of 83.36±1.75% accuracy with 82.83±2.99% sensitivity and 83.45±3.59% specificity. On the other hand, in the case of "walk" vs. "stop" classification, the classification accuracy, sensitivity, and specificity were 81.57±1.70%, 81.14±3.06%, and 82.06±3.28%, respectively.

Comparison with similar works is tricky because different studies used classification windows of different lengths and time ranges from the movement onset.

Table 5.1: 'Rest' vs. 'Start' Classification Results using VMD+WSST

S.N.	Classification Performance		
	Accuracy	Sensitivity	Specificity
S1	87.13 ± 1.82	88.47± 2.44	85.98 ± 3.66
S2	85.72 ±1.61	85.85± 1.77	85.63± 2.66
S3	85.49± 1.32	86.2± 1.94	84.5± 2.91
S4	71.99± 3.27	70.2± 4.11	73.02± 6.12
S5	82.15± 1.38	82.04± 4.62	82.22± 4.80
S6	87.67± 1.08	84.27± 3.07	89.38± 1.37
S7	83.36± 1.75	82.83± 2.99	83.45± 3.59

Ortiz et al. [77] achieved 78.61±11.20% accuracy in start intention detection and 84.36±10.19% accuracy in stop intention prediction using a [-2,2] s detection window. Hortal et al. detected starting and stopping during a gait cycle with 54.8% and 56.1% true positive rates with 2.66 and 1.90 false positives/min in offline and real-time scenarios, respectively [49]. Our previous study [85] on the same dataset yielded an accuracy of 73.64±4.18%, 73.73±2.80% in stop intention prediction using DWT and EWT. While, in the case of start prediction, accuracies of 78.28±3.45% and 76.72±2.50% were achieved using DWT and EWT. The current approach resulted in better classification accuracies with balanced sensitivity and specificity than DWT and EWT. Although Ortiz et al. [77] reported a slightly higher classification accuracy in stop detection, their intention detection windows were 1 second larger than used in this study.

Interestingly, our previous work yielded slightly better classification performance using WSST only [85]. This result indicates that VMD provides a means to perform datadriven signal processing and filtering. However, for proper VMD operation, it is critical to reduce inter IMF spectral leakage while limiting the loss of signal

Table 5.2: 'Walk' vs. 'Stop' Classification Results using VMD+WSST

S.N.	Classification Performance		
	Accuracy	Sensitivity	Specificity
S1	87.52 ± 1.05	87.01± 2.45	87.83 ± 1.25
S2	83.97 ±2.53	84.42± 3.24	83.65± 4.15
S3	84.08± 1.14	84.62± 1.96	83.76± 1.99
S4	71.51± 2.07	72.80± 2.74	70.39± 4.93
S5	76.00± 2.02	74.04± 4.86	77.15± 4.76
S6	86.34± 1.39	83.92± 3.12	87.58± 2.57
S7	81.57± 1.70	81.14± 3.06	82.06± 3.28

information. In this study, we used a stationary number of IMFs, which does not ensure the above conditions. Therefore, the number of IMFs for each data frame should also be selected in an empirical manner keeping the above goals in mind. This critical limitation should be extensively addressed in future extensions of this study. Overall, the classification results show promising outcomes in predicting human intention to start or stop walking from movement-related EEG.

5.6 Conclusion

The paper presents a novel algorithm for time-frequency analysis using a combination of VMD and WSST. VMD was used to extract the desired IMFs in the Mu and Beta frequency bands, which were then reconstructed to obtain the desired brain signal—after that WSST based time-frequency analysis yielded Mu and Beta band ERD, which were used to detect the human intention to start and stop walking. The classification results show promise; however, some critical challenges need to be addressed. First, the success of VMD largely depends on estimating the number of modes in the data, which is a difficult task. Further studies are necessary to address this issue. Moreover, advanced machine learning and deep learning algorithms

should be deployed to enhance the performances even further. Additionally, offline classification results do not always guarantee similar success in real-time scenarios. Therefore, pseudo online and real-time testing should be implemented in the future to test the efficacy and robustness of the approach.

CHAPTER 6

REAL-TIME PREDICTION OF GAIT ACCELERATION INTENTION

6.1 Background

Volitional control of prosthetic devices can potentially provide the user with a more natural movement experience. Currently, there is no feasible volitional triggering method to adapt the prosthetic device to user's intention to accelerate during walking. Therefore, real-time prediction of human acceleration intention from the pre-acceleration electroencephalogram (EEG), and subsequent adaptation of the prosthetic device's control parameters for seamless transition remains a daunting research area. In that aspect, this study investigates the neural changes responsive to human intention to accelerate during walking. Furthermore, this study also explores whether the acceleration intention can be predicted from real-time EEG to subsequently enable parametric adaptation for an external prosthetic device.

6.2 Related Work

Most of the current studies have investigated neural changes related to gait initiation and termination [105, 59, 106]. In addition to that, seamless transition between different gait speeds is a very important and desirable feature of an effective assistive device. It is therefore very critical to reliably and accurately predict human intention to change gait speed to facilitate the user with a natural rehabilitative experience. As previous studies have shown promising results in identifying neural changes related to gait initiation and termination from EEG, scalp EEG can be a very convenient tool to identify appropriate neural biomarkers of intention to

change gait speeds and subsequently enable parameter adaptation according to the desired speed. However, the neural changes corresponding to intention of speed change while walking has not been addressed extensively and further investigations are necessary to understand and utilize the neural changes that occur in response to acceleration intention. Lisi et al reported suppression in mu and beta rhythms while speed changes in treadmill walking [105]. A more recent study has reported a reduction in alpha and beta spectral power in sensorimotor cortex in response to faster speeds in treadmill walking [107]. But no study has investigated neural changes related to gait acceleration intention during self-paced walking according to the authors' knowledge. If the gait acceleration intention can be predicted from pre-acceleration EEG features, the predicted information can be transformed into control commands for enabling adaptive control of an external prosthetic device. Such adaptive control can pave the way to a natural and realistic control of assistive devices resulting in regaining of motor ability.

In this study, the gap in current studies have been addressed by investigating the neural changes corresponding to the intention of acceleration during self-paced walking. The mu and beta band activity were monitored to look for suppression in power before the acceleration onset. An SVM classifier with radial basis kernel was trained to distinguish between the constant speed and accelerated speed condition using processed pre-acceleration EEG. The classifier was evaluated offline using a 10-fold cross validation scheme. Another classifier was designed for the same classification task in a pseudo-online scenario where the samples were accessed as if they had just been just acquired. For 10-fold offline classification scheme, performance was evaluated in terms of accuracy, sensitivity and specificity. While, in pseudo-online paradigm the performance was evaluated in terms of true positive rate, false positives per minute and intention detection latency. Furthermore, a real

time experiment was also carried out to test the efficacy of the proposed methodology in real-time scenario. In real-time test, an online SVM classifier was trained to detect intention to speed up while self-paced walking. In addition to EEG, IMU and GRF signals were used to optimize the system performance by minimizing the false positive detection rate. The proposed methodology provided promising results which would encourage future investigative studies regarding prediction of human gait acceleration intention and subsequent adaptative control of associated assistive device.

6.3 Current Work

In this study, the gap in current studies have been addressed by investigating the neural changes corresponding to the intention of acceleration during self-paced walking. The mu and beta band activity were monitored to look for suppression in power before the acceleration onset. An SVM classifier with radial basis kernel was trained to distinguish between the constant speed and accelerated speed condition using processed pre-acceleration EEG. The classifier was evaluated offline using a 10-fold cross validation scheme. Another classifier was designed for the same classification task in a pseudo online scenario where the samples were accessed as if they had just been just acquired. For 10-fold offline classification scheme, performance was evaluated in terms of accuracy, sensitivity and specificity. While, in pseudo online paradigm the performance was evaluated in terms of true positive rate, false positives/ minute and intention detection latency. Furthermore, a real time experiment was also carried out to test the efficacy of the proposed methodology in real-time scenario. In real-time test, an online SVM classifier was trained to detect intention to speed up while self-paced walking. In addition to EEG, IMU and GRF signals were used to

optimize the system performance by minimizing the false positive detection rate. The proposed methodology provided promising results which would encourage future investigative studies regarding prediction of human gait acceleration intention and subsequent adaptative control of associated assistive device.

6.4 Materials and Methods

6.4.1 Subject

One healthy right-handed male subject participated in the study (26 years, 150 lbs, 172 cm). According to the knowledge of the authors, the subject did not have any preexisting neurological disorder. The experimental protocol was approved by the institutional review board (IRB) and signed consent was collected from the subject before the execution of the experiment.

6.4.2 Experimental Procedure

The experimental procedure was carried out in a laboratory setting. The experimental protocol was designed to detect intention to speed up during self-paced walking. For the purpose of this study, two different experimental sessions were carried out. One session of data collection was done for offline and pseudo online testing, while the other session of data collection was carried out for real-time testing.

In the first session, the subject was asked to speed up during self-paced walking in multiple trials. Each trial started with a constant speed walking leading to an acceleration in speed and then continuing to walk with that same accelerated speed for a few more gait cycles. No audio or visual cues were offered to the participant because of probable corruptive effect on acceleration related neurophysiological sig-

nals. The subject sped up according to his own will at any moment he wanted. However, it was made sure that he was completing at least three full gait cycles before speeding up. That was done to make sure proper baseline EEG activity could be registered for successful subsequent intention detection.

For the real-time testing session, data collected in the previous session was used to train an online classifier to detect intention to speed up in real-time scenario. In this second session, the subject continued the same task, only this time continuous detection of his intention to speed up was carried out and the decisions were saved online. In this session, the subject carried out 12 trials of the same task.

After each trial, the subject could rest for as long as he needed. Each trial lasted for approximately 10 seconds. And in each trial, the following tasks were repeated periodically: start, walk in constant speed, accelerate and continue walking in the same speed. The subject executed 60 repetitions of the task in the first session and 12 repetitions in the real-time testing session. Overall, the experimental procedure took 50 minutes to complete. Figure 6.1 shows the experimental protocols briefly.

6.4.3 EEG Data Acquisition

An active electrode system (actiCAP, Brainproduct GmbH) was used to collect 16-channel EEG from Cz, C1, C2, C3, C4, C5, C6, CP3, CP4, CPz, FC3, FC4, FCz, Fz, Pz and Oz channels according to international 10/20 system. The reference and ground electrodes were placed at Fpz and AFz consecutively. The EEG data acquisition board was equipped with two on board ADS1299 amplifiers (Texas Instruments) for online data amplification and recording. The data was recorded at 250 samples per second.

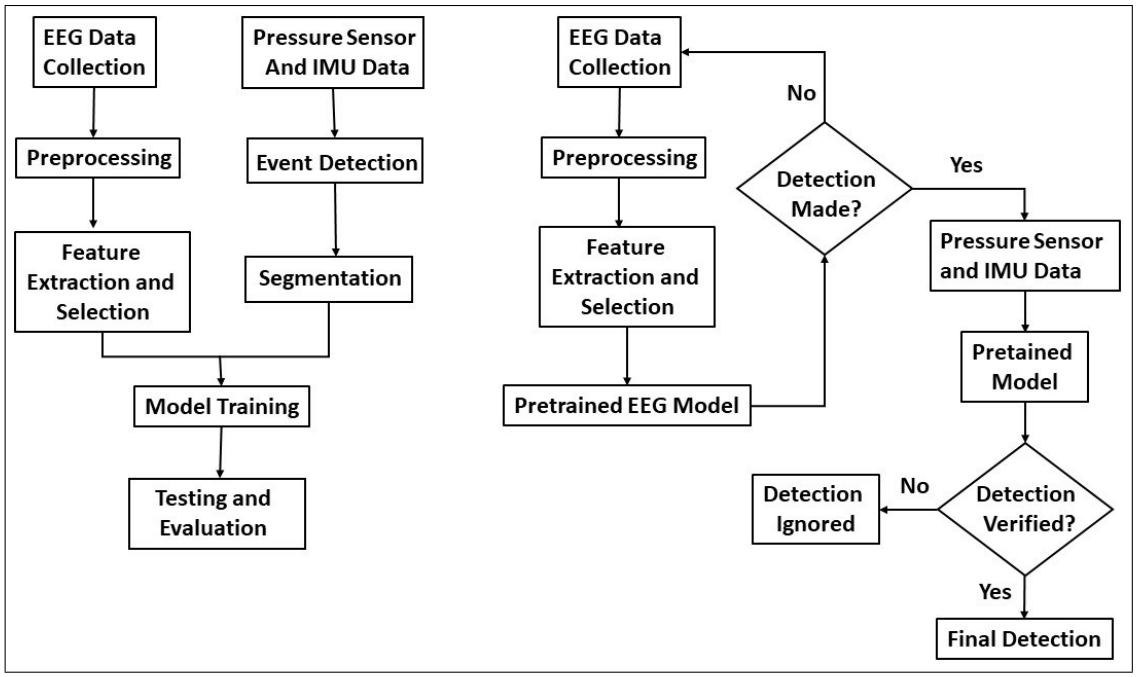

Figure 6.1: Left: The offline protocol of the study, right: the real-time protocol of the study.

.

6.4.4 Event Detection

For acceleration event detection and time locking the events, two custom-made in-sole pressure sensors were placed inside the shoe of the participant. The specially designed sole contained three pressure sensors which could detect heel, mid foot and toe contact. In addition to that two IMU sensors were also placed on the spine of the subject to monitor the relative transfer in balance to accommodate change of speed. The IMU sensors could also sense the minute motions using multiple sensors such as accelerometer, gyroscope and magnetometer [108]. One IMU was placed on the top part of the spine close to the neck along the vertebra. While the other one was placed on the bottom part of the vertebra near the waistline. The IMU sensors had a sampling rate of 1000 samples per second while the in sole pressure sensors recorded data at 100 samples per second rate.

6.4.5 Data Preprocessing

In this study, two different kinds of data preprocessing techniques were implemented. For the data obtained for offline evaluation, an EEGLAB [70] based data cleansing procedure was implemented which has been discussed in previous sections in details whereas for online testing dataset, a computationally less complex and more time efficient procedure was employed to facilitate the feasibility of real-time evaluation.

In pseudo online and real time testing purposes, however, the EEGLAB based cleansing protocol proved to be computationally too heavy to be implemented online [85]. Additionally, in real-time scenario a very small window of data was accessed at a time and all the preprocessing was carried out on that small window of data. Both ASR and ICA needs a big length of data to work properly. That is why, an alternative preprocessing technique was employed for pseudo online and online testing. For these sessions, the data were first high pass filtered using a 6th order Butterworth filter at 1 Hz cutoff frequency for DC drift removal. A notch filter was then applied at 60 Hz to remove line noise. To remove the nonstationary and abrupt large amplitude artifacts, PCA was applied and the principal components which contributed to 90% of the variance of the data were removed. The application of PCA was inspired by the definition of ASR which uses sliding window PCA to remove big artifacts from continuous EEG. The cleaned data were then common average referenced. Afterward, a Laplacian filter method was applied to remove the effects of surrounding channels from the EEG data [9]. This was inspired by the source localization aspect of ICA. The Laplacian Filtering method can be expressed by the following equations:

$$s_i^{LP} = s_i - \sum_{j \neq i} c_{ij} s_j \tag{6.1}$$

$$c_{ij} = \frac{\frac{1}{l_{ij}}}{\sum_{i \neq j} \frac{1}{l_{ij}}} \tag{6.2}$$

Here i denotes the EEG electrode to be filtered whereas j denotes all the other electrodes. s_i^{LP} denotes the outcome of the Laplacian filter. The algorithm penalized the EEG electrode's signals by subtracting a weighted sum of all the other electrode's data. The weights c_{ij} were defined by the distance between the corresponding electrodes, where the distances l_{ij} were measured following the three-dimensional Euclidean method [9].

6.4.6 Data Segmentation

As stated earlier, the insole pressure sensors were used to detect acceleration in walking state. The acceleration action was accompanied by a larger pressure value detected on the pressure sensors. That was because of the stronger impact on the foot to facilitate the larger swing of the other foot resulting in increased speed. The IMU signals on the back were used to verify the correct detection of acceleration as well. The overall segmentation procedure has been portrayed in figure 6.2. In the offline session, the data were recorded, segmented and visually inspected to make sure that the data segmentation was done properly. Moreover, it was also made sure that all the sensors were synchronized to ensure proper segmentation and epoching.

6.4.7 Neurophysiological Data Analysis

The collected data were then analyzed offline to investigate the neurophysiology involved with human gait acceleration intention. The data was analyzed using the EEGLAB toolbox. Epoching was done from -4 to 2 seconds corresponding to the event of acceleration. The obtained artifact-free epochs were then used to perform

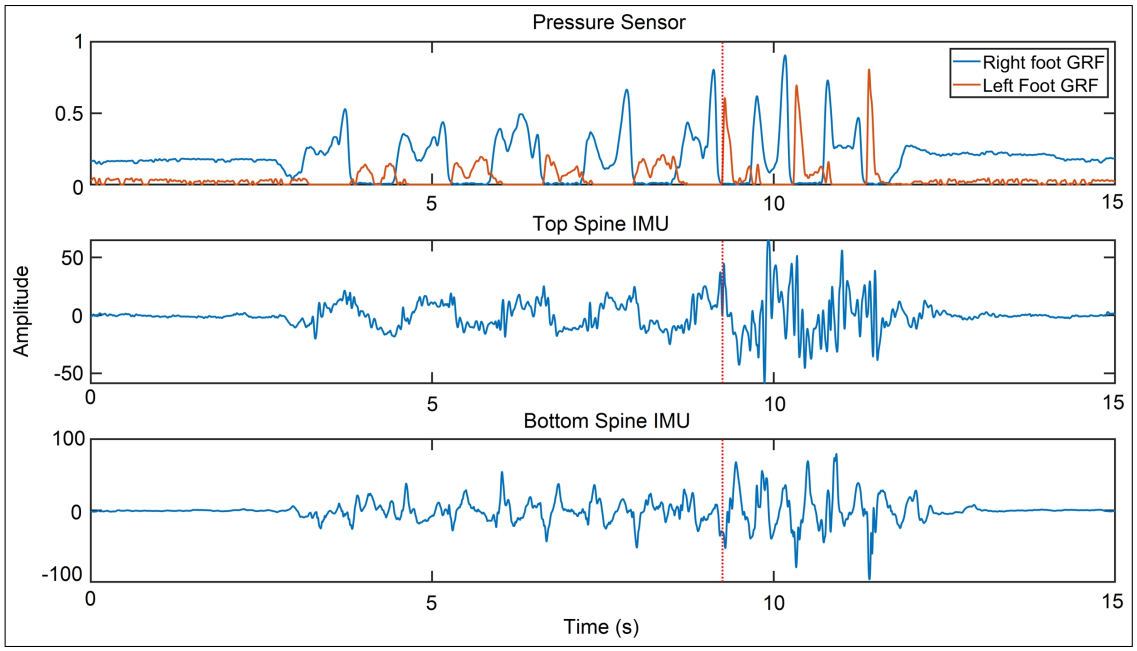

Figure 6.2: A 15-second segment of pressure sensor, top and bottom spine IMU sensor data respectively. The red line corresponds to an acceleration event characterized by the large peak on the pressure sensor compared to the previous steps. The IMU sensors showed increase variance with increased speed.

.

a time-frequency analysis to look for suppression in mu and beta bands (8-32 Hz). For ERD calculation, -4 to -2 seconds data were used as baseline. A 400-sample smoothing window and a frequency padding ratio of 4 was used for smoother and cleaner representation. Moreover, a permutation test was also performed to highlight the statistically significant ERD activity at $p<0.05$. The statistical significance was obtained by calculating all possible values of the test statistic under 200 rearrangements of the data points obtained in time-frequency analysis. In addition to ERD, the presence of MRCP were also investigated. A low-pass filter with a cutoff frequency at 5 Hz was implemented to capture the slow change in amplitude near DC level. A significant ERD activity was found in both mu and beta bands corresponding to the intention of speeding up while walking between -2 to 1.5 s data window with the onset of acceleration as reference. Also, a clear increase of negative

amplitude was observed in both the channels and the trend was consistent across almost all the trials in the same time frame. Further discussion about the results will be presented in the results section of the article. In the following sections the ERD activity will be used for classification between constant speed and accelerated classes.

6.5 Binary Classification and continuous decoding

After the data segmentation, a binary classification problem was formulated to distinguish between constant speed and acceleration state. The goal of this study required continuous monitoring and decoding of neural signals. As a result, a specialized classification scheme had to be applied. A small window of data from 2 seconds before the acceleration to 1.5 seconds after the acceleration were marked as acceleration state. While the rest of the trial was marked as constant speed. This was inspired by the neurophysiological data analysis which showed the presence of significant ERD activity in both Mu and Beta bands from 2 seconds before the acceleration to 1.5 seconds after the acceleration.

6.5.1 Feature Extraction and Selection

For ERD calculation, both the accelerated walking state and constant speed state data were further divided into 1-s long epochs with 80% overlap. A wavelet synchro squeezed transform (WSST) was performed on the data epochs to extract mu (8-16 Hz) and beta (16-32 Hz) band power. In each trial, the first 10 windows were taken as baseline and the average baseline mu and beta power was used to calculate the ERD in the subsequent windows. Here, ERD is computed in the simple manner

stated below:

$$ERD_{i,j} = \frac{P_{i,j} - P_{baseline}}{P_{baseline}} \times 100\% \tag{6.3}$$

Here i and j denote the i-th data window of j-th channel where $P_{baseline}$ denotes the baseline power of the corresponding trial and $P_{i,j}$ denotes the power of the i-th data window of the j-th channel. For evaluating the offline intention detection, the mu and beta band ERDs were extracted as features. Thus, for each 1-second long data epoch, 16 channels $\times$ 2 features = 32 features were extracted. To enhance the distinguishability of the extracted features, a two-sample unpaired Wilcoxon test was carried out and the absolute value of the resulting u-statistic was used for feature selection. Moreover, the cross-correlation coefficients between an existing feature and the next incoming feature was calculated and a threshold of 0.9 was set to exclude highly correlated features. This procedure reduced the number of features down to 20 for each 1-second epoch.

6.5.2 Offline Evaluation

In total, the offline dataset contained 3719 1-second long epochs. As the number of subjects was limited, as many data samples as possible were collected from the subject in order to ensure reliable and interpretable classification results. These epochs were labelled according to data segmentation procedure described above. For offline evaluation, a 10-fold cross validation was performed on the epoched dataset using an SVM classifier with radial basis kernel. SVM classifier has been used quite successfully in EEG-related classification tasks in various applications, like emotion recognition [93], gait intention prediction [84, 85, 86]. That is why SVM was chosen to classify the neural signals obtained from EEG.

6.5.3 Pseudo-Online Evaluation

To test the real-time detectability of intention to accelerate during walking, a pseudo online testing paradigm was also experimented for continuous decoding. In the pseudo online paradigm, the data were subdivided into three parts. 60% of the data were used as training dataset, 20% were used for validation or model tuning and 20% were used for testing. For the sake of unbiased testing, the test set were kept untouched but the rest of the data which amounted to 80% of the whole dataset were utilized to randomly select 10 different train-validation splits. This testing protocol is inspired by a previous study carried out by the authors [85].

In each train-validation split, the training procedure was the same as the offline training procedure. However, in the validation set a specialized classification rule was applied. The validation set was used to find a suitable working point or threshold such that the model could reach a maximum of 95% specificity while maintaining a minimum sensitivity of 75% while classifying the validation dataset. The constraint on specificity was put so that the working point does not bias the classifier into predicting only the majority steady state class. The minimum sensitivity was also set so that the classifier would maintain a decent success in positive prediction. However, this could result into too many predictions of intention leading to an increased false-positive detection. In a real-time scenario, false positive activation might trigger the prosthetic device in an unwanted time, thus leading to accidents or falling. So, further precaution was necessary to reduce the number of false positive prediction of acceleration intention in the test set. To further reduce the chance of false positive detections, a 10-window majority voting algorithm was applied while classifying the test set which took the decisions of 10 consecutive windows and returned the decision which was mostly reported in that 10-window period. This meant that in the pseudo online protocol, decisions were processed every 2

seconds. If any detection was made between 2 seconds before the acceleration and the acceleration onset, then it was marked as true positive detection. Otherwise, it was marked as false positive detection.

6.5.4 Real-time testing

Lastly, a real-time testing procedure was implemented. In this part, an SVM classifier was trained based on the epoched and labelled offline dataset. The offline dataset was split into an 80-20 split as train and validation sets. The first 80% of the data constructed the training set which was used to train the real-time classifier while the validation set was used to satisfy the same classification rule as described in the pseudo online evaluation section. The threshold thus obtained was stored and used for decision making in real-time testing.

To reduce the number of false positive detections, an SVM classifier with Radial Basis Function (RBF) kernel was trained based on the GRF sensor and IMU sensor data which would be termed as motion sensor classifier. For training this classifier, the mean and variance of the sensor data were used as features and working points were determined using the same classification rule described above. All the sensors were accessed every 500 milliseconds and a 2-second long data window were extracted. All the preprocessing and feature extraction procedures were done real-time and decisions were made. Whenever a detection was made by the EEG classifier, the corresponding pressure sensor and IMU sensor data were accessed and classified using the motion sensor classifier. If the decision of the EEG-classifier was supported by the motion sensor classifier, only then the detection was considered. Otherwise, the decision by EEG classifier was ignored.

6.6 Results

6.6.1 Result of Neurophysiological Data Analysis

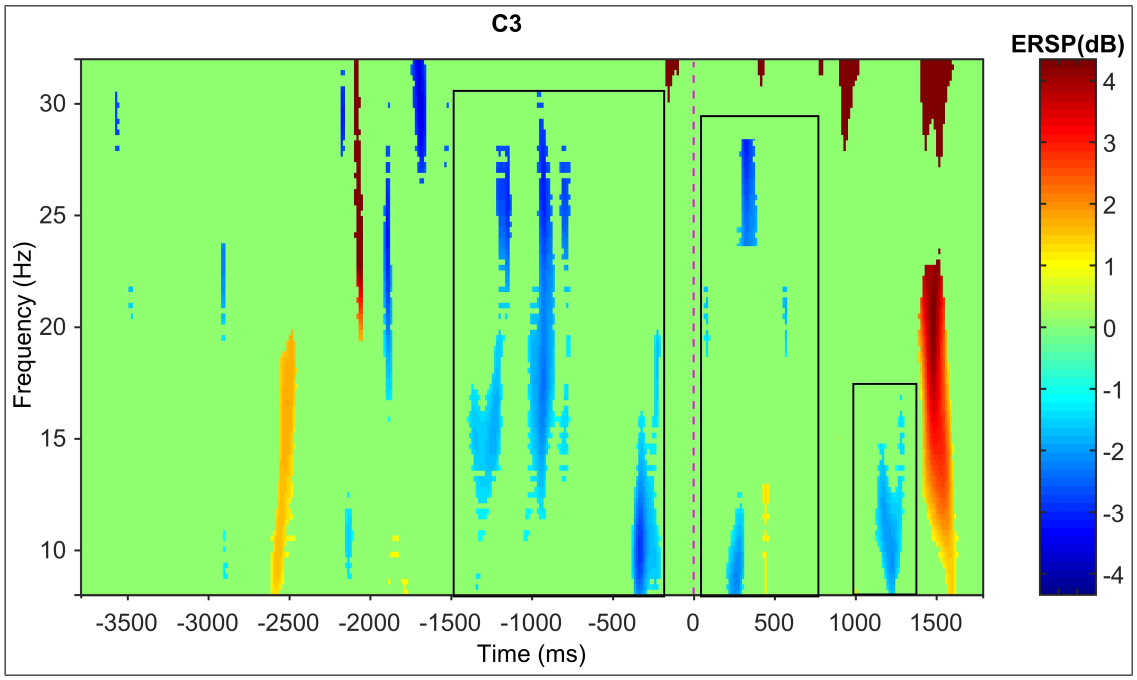

Figure 6.3: Time-frequency analysis of EEG signals obtained from C3. Significant ERD activity at $p<0.05$ has been marked by black rectangles. The significant ERD activities were found between -2 to 1.5 s data window corresponding to the onset of acceleration.

.

The results of neurophysiological data analysis are shown in figure 6.3, figure 6.5, figure 6.4 and figure 6.6. Figure 6.3 and figure 6.4 show the time-frequency analysis plot of C3 and C4 channels situated over the sensorimotor cortex. While, figure 6.5 and figure 6.4 show the low frequency amplitude plots obtained from the EEG signals of the same channels. Figure 6.3 and figure 6.4 show clear blocks of significant ERD in both the channels between -2 to 1.5 second data window of the acceleration onset. The significant ERD activities in Mu and Beta bands are marked in black rectangles in the figure. Meanwhile, figure 6.5 and figure 6.4 show clearly visible increase in

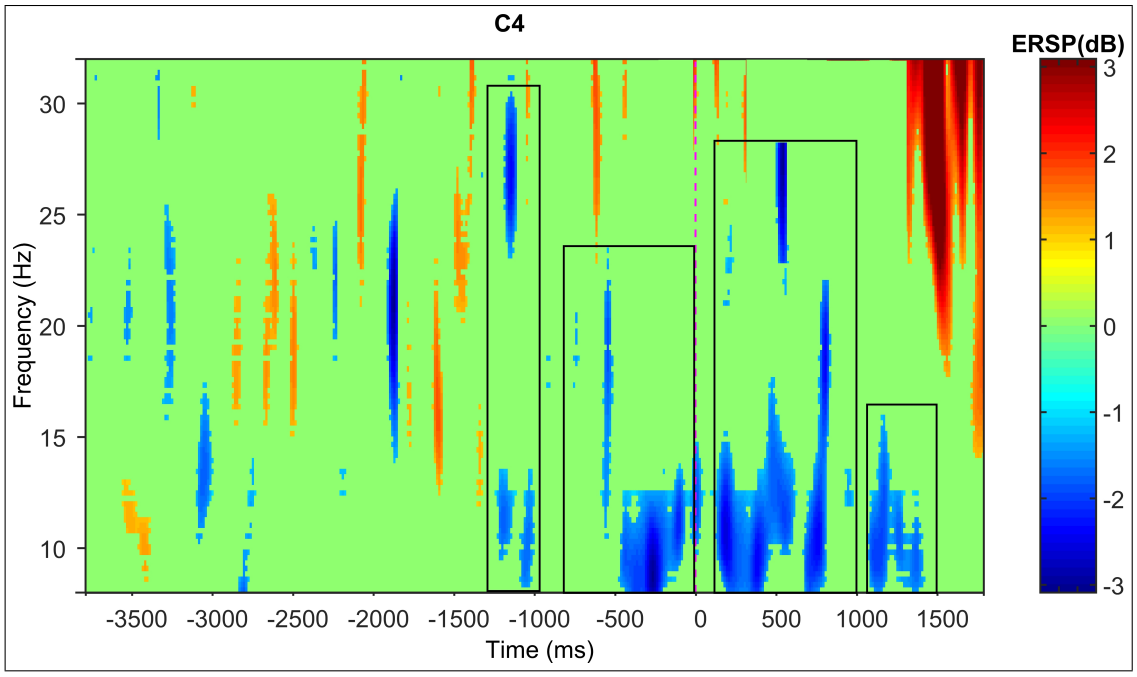

Figure 6.4: Time-frequency analysis of EEG signals obtained from C3. Significant ERD activity at $p<0.05$ has been marked by black rectangles. The significant ERD activities were found between -2 to 1.5 s data window corresponding to the onset of acceleration.

.

negative amplitude between -2 to 1.5 s windows of acceleration. The onset and end of MRCP has been marked in red in the figure. Additionally, it is visible from the figure that the negative increase in low frequency EEG amplitude was consistent among almost all the trials which confirms the robust presence of MRCP in the sensorimotor cortex corresponding to the intention to speed up during self-paced walking.

6.6.2 Performance Metrics

The offline classification procedure was evaluated using the following performance metrics: accuracy, sensitivity, specificity and F1-score. For pseudo online evaluation, the performance metrics were: True Positive Rate, False Positives/ minute and

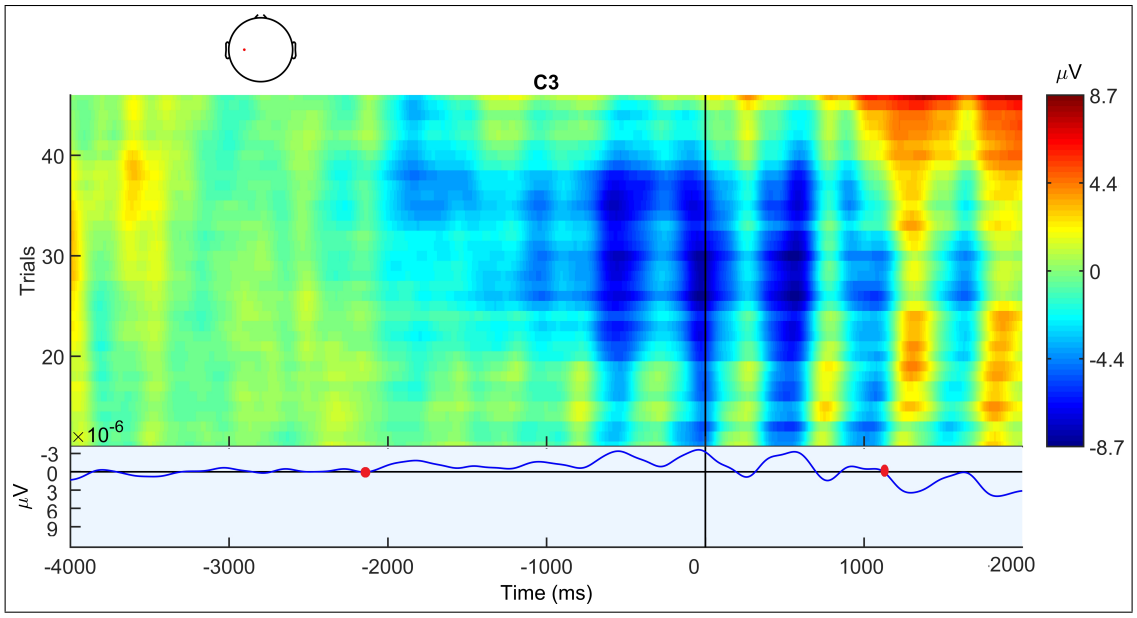

Figure 6.5: MRCP plots obtained from C3. The initiation and termination of MRCP has been marked by red dots. The increase in negative activity is mostly noticed between -2 to 1.5 second window with respect to the onset of acceleration.

.

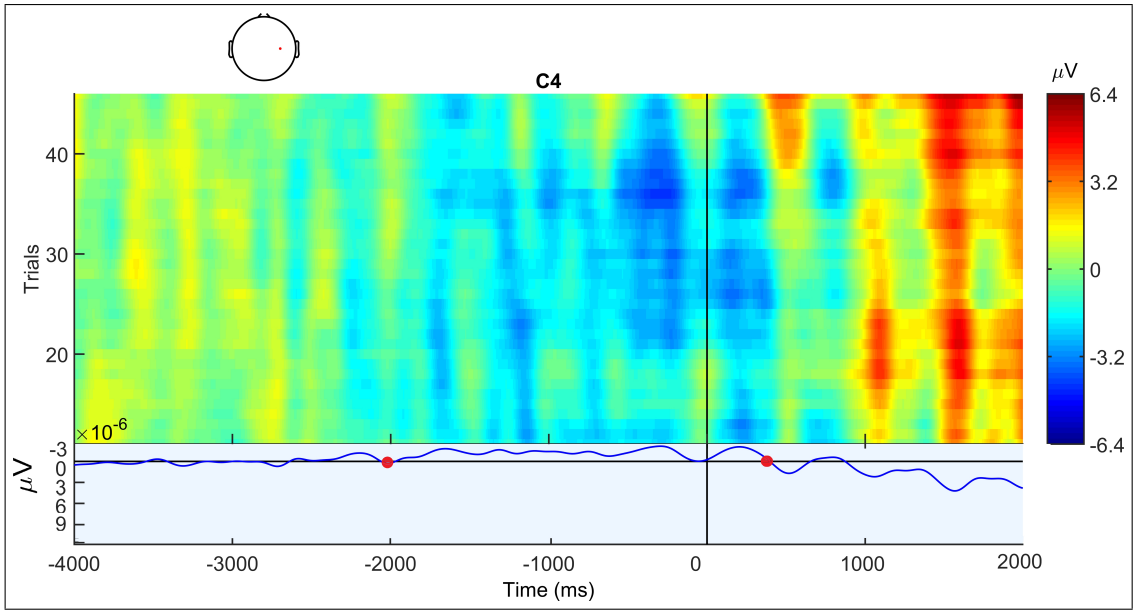

Figure 6.6: MRCP plots obtained from C4. The initiation and termination of MRCP has been marked by red dots. The increase in negative activity is mostly noticed between -2 to 1.5 second window with respect to the onset of acceleration.

.

detection latency. For real time testing, the detection times, true detection and number of false detections have been reported. In future studies, the decisions of the classifiers would be passed to a physical prosthetic leg to change its parameters adaptively.

6.6.3 Offline Classification Results

Table 6.1: Offline Performance Metrics.

Accuracy	Sensitivity	Specificity	F1-score
85.9±2.9%	86.1±5.9%	85.7±4.7%	80.1±3.6%

Table 6.1 shows the classification performance in offline scenario. The classification results showed good detection performance well beyond the chance level. The average specificity was slightly better than the average sensitivity. But the classification results were balanced despite the classes being imbalanced, i.e. samples belonging to the negative class or the constant speed class were greater in number compared to the samples in the positive class or acceleration intention class.

6.6.4 Pseudo-online Classification Results

The pseudo-online performance metrics are represented in table 6.2. In pseudo online testing, the system showed good classification results with 81.9±7.4% true positive detection rate with 7.7±0.8 false positive detections per minute.

Table 6.2: Pseudo-online Performance Metrics.

TPR(%)	FP/min	Latency (ms)
81.9±7.4%	7.7±0.8%	-844±572

6.6.5 Real-time classification results

Table 6.3: Real-time Testing results.

Detected events (total events)	False positive detections	Latency (ms)
9(12)	3	-741

The results obtained in real-time prediction of acceleration intention has been reported in table 6.3. Out of 12 real time testing trials, 9 intentions to accelerate could be detected. The rest were undetected. The average detection latency was found to be -741 ms.

6.7 Discussion

This goal of this study was to investigate the neural changes corresponding to the intention to speed up during self-paced walking on level ground. It was also investigated whether the neural biomarkers corresponding to speeding up gait could be used to predict intention to speed up so that the information could be used to adapt the control parameters of a prosthetic device accordingly. To achieve these goals, EEG signals were collected from one healthy subject with no prior neurological condition while the subject performed multiple trials of acceleration while walking. The EEG signals thus obtained were then cleaned and various signal processing techniques were applied to identify neural markers that could distinguish and help predict intention to increase walking speed. Significant presence of ERD and MRCP were noticed in the sensorimotor cortex in the -2 to 1.5 s window corresponding to the onset of acceleration. According to this information, ERD was used in this study to predict intention to speed up during walking. The evaluation was done in offline, pseudo-online and real-time scenario. The results were promising

and could potentially be applied in real-time assistive systems to facilitate the users with seamless transition between differing gait speeds using their volition.

The neurophysiological analysis showed significant evidence that neural changes occur due to the intention to speed up. The obtained time-frequency map was a result of multiple repetition of statistical testing on permutated dataset which ensured that only the most significant ERD activities were highlighted in the plot. This action also enforced that the appearance of ERD was not an outcome of noise in the EEG data rather was related to the neural changes corresponding to the intention to speed up. Similarly, the MRCP plots showed consistent presence of increased negative low frequency amplitude over almost all the trials. This suggests that the MRCP thus obtained was also a marker of significant neural change related to acceleration intention. Moreover, the appearance of ERD and MRCP before the onset of acceleration inspired the authors to inspect the feasibility of predicting the intention to speed up rather than simply detecting it after the acceleration has already occurred. That is why, predictions made before the onset of acceleration was marked as true prediction during pseudo online and real time testing.

In pseudo-online classification, the negative value of latency showed promise because it suggested that the intentions were predicted before the acceleration onset. However, it should be noticed that the number of false positive detection was quite high. This was due to the non-stationarity of EEG data coupled with the added interference contributed by the acceleration of gait. It suggests that the incorporation multiple sensors' data with EEG can prove to be vital for real-life continuous decoding and decision making to compensate for irregular false positive detections.

In real-time testing, the negative sign of the latency proves that intention of acceleration could be detected before the actual incidence of acceleration. Another very important is that the verification classifier added to the real-time system de-

creased the number of false positive detections to just 3 in approximately 2 minutes. This suggests that the incorporation of IMU and GRF data greatly improved the prediction of acceleration intention by removing false positive detections made by the EEG classifier. This is a very promising outcome which signifies that it could be possible to detect the intention and adapt the corresponding prosthetic device before the onset of acceleration using a cascaded EEG-IMU-GRF continuous decoding system.

Close observation of results also suggests that the offline classification results were slightly better than pseudo online and real time results. But it is to be noticed that offline classification system used ICA and ASR for preprocessing of EEG which are computationally heavy and are not usable online or in real-time. The use of computationally inexpensive and efficient algorithms like PCA and Laplacian filter resulted in comparable performances which is a promising outcome. In future, however, advanced signal processing and learning techniques should be investigated to improve the prediction performance to further improve the performances of the system in real-time.

Overall, the study shows that there is significant evidence of neural changes related to speed up during self-paced walking on level ground without any audio or visual cue. However, data acquisition from a larger population and analysis is necessary to further validate and strengthen the outcome of the study. Nevertheless, a large quantity of data was collected from a single subject and neurological data analysis was accompanied by a random permutation test to prove that the neural markers are robust and consistent rather than being noisy. The promising outcome of the preliminary study would inspire the authors to expand the scope of the investigation in future studies. In future, data from multiple subjects would be collected and analyzed. Moreover, sensor fusion or cascaded classification utilizing

multi sensor data would be implemented for better classification. Another interesting addition would be attempting to tune the parameters of a prosthetic device in real-time according to the intention of the user to increase the walking speed.

6.8 Conclusions

In this study, the pre-acceleration EEG signals were investigated to find out gait acceleration related neurophysiological changes. Initial results suggest that, a significant mu and beta suppression was detected corresponding to the acceleration intention. Furthermore, difference classification schemes were carried out to explore whether such physiological changes could be detected in order to control an external prosthetic device. Offline, pseudo online and real-time testing results suggest that it could be possible to detect the intention to accelerate during self-paced walking to adaptively control an assistive device Moreover, the integration of multisensory data was found to be useful to minimize the false positive detection and therefore to improve the overall performance of the real time system. Due to the present situation involving COVID-19, it was challenging to find human subjects to participate in the study. The future studies of this would include a greater number of subjects including amputees. Additionally, more advanced computational methods could be applied to enhance the detection performance even further. The results of the proposed methodology showed promising results which could be investigated extensively to add more realistic volitional features to the existing assistive BCI devices.

CHAPTER 7

ENHANCEMENT OF MOVEMENT INTENTION DETECTION BY AFFECTIVE STIMULI

7.1 Background

A portion of this current chapter has been reprinted from the author's previous work in [109], copyright2020 IEEE. Recent psychological and neurological studies suggest that human motor preparation and execution are largely affected by the subjective emotional state. Thus, external emotion stimuli can be a potential tool to enhance the detectability of movement intention from pre-movement neural signals. This study investigated whether emotion-evoking music stimulus could improve the performances of a fully predictive BCI system for movement intention detection. For this purpose, EEG signals were recorded from twelve healthy subjects under three emotional conditions: happy, sad, and neutral. The emotions were elicited using external music stimuli while they performed a wrist extension action.

State-of-the-art endeavors to understand the neurophysiological changes related to both upper and lower limb movement intention, preparation and execution have utilized both ERD and MRCP. Pfurtscheller et al utilized ERD/ERS during upper limb movement for BCI application [44]. Blankertz et al used the Bereitschaftspotential (BP) to predict finger movement in a study reported in [110]. Liao et al combined spatial features to classify single trial EEG signals in a finger movement task in [111]. Lu et al proposed an adaptive spatio temporal filtering method to detect movement related potentials in [112]. Zeid et al. proposed a pipeline of spatio-temporal filtering to predict the laterality of self-initiated movements using readiness potentials [113]. Wang et al. used ERD and MRCP to decode pre-movement EEG patterns for BCI application [114]. Jeong et al proposed a subject dependent and

section wise spectral filtering to decode movement related cortical potentials [115]. Ortiz et al applied Stockwell transform to EEG signal obtained during active gait to detect intention to start or stop walking using ERD [77, 50]. Sburlea et al used gait related EEG signals to decode EEG phase patterns for intention detection [55]. Similarly, several studies have focused on understanding EEG patterns corresponding to various upper body [116, 117, 118, 119] and lower body [120, 121, 122, 86, 85] movements and implementing them in BCI application. Additionally, efforts have also been put in to realize the underlying neural phenomena related to both movement imagery [123, 124] and execution [125, 126]. In addition to that various signal processing, advanced filtering and modified classification technologies have also been investigated in order to improve volitional self-paced movement intention detection performance.

Despite the efforts discussed above, the current state of the art BCIs are still far from being applicable and reliable in real-time situation. Early and accurate movement intention detection is the most significant feature of assistive BCI systems. The most critical properties of a viable assistive BCI are low false positive detection, high true positive detection and early detection time [84]. Most of the studies use movement-related neural corelates to detect the intention to move after it has already happened rather than being able to predict the intention before the occurrence [77, 50, 49]. On one hand, non-stationarity and randomness of EEG signals makes it difficult to make a reliable and early decision about movement intention. In addition to that interference of movement-related potentials from other limbs of the body as well as possible imagined movements hinder the detection of movement intention from pre-movement EEG signal. Additionally, various psychological, behavioral, environmental or even emotional factors continuously affect the performance of movement intention detection. Being unable to incorporate the emo-

tional attachment to human motor intention, preparation and execution is one of the shortcomings of current state of the art BCIs.

Psychological and neurological studies suggest that human movement intention and preparation are greatly affected by the subject's emotional state [127, 128]. A variety of studies have investigated the effect of individual emotional states on motor preparation and execution [127, 128, 129]. It is reported in a study carried out by Naugle et al [127] that highly arousing unpleasant emotional states accelerate the initial motor response. While, pleasant emotional states generally facilitate the initiation of forward movement due to the approach-oriented directional salience of the movement. Moreover, it is reported in several studies that under pleasant emotional stimuli flexion movements are facilitated while under unpleasant stimuli extension movements are enforced [130, 131, 132, 133]. Although there are conflicting doctrines about the specific effect of an affective state on movement intention, these studies unanimously conclude that upper and lower body motor intention and execution are highly affected by the emotional state of the subject as well as emotional impact of the environment on the subject. As a result, there is no denying the fact that "human emotion and motor actions are largely intertwined and reciprocally interrelated" [132, 134]. Understanding the complex relationship between emotion and movement intention is therefore very crucial in order to develop an accurate and reliable BCI for movement intention detection.

To enhance movement intention detection accuracy, all the internal and external factors affecting movement-related neural signals are to be studied and addressed. One way of doing this could be to enhance the motor control circuitry of human brain during the movement preparation stage by including external stimulus, so that the movement-related neural correlates become easily detectable despite the non-stationary nature of brain waves. Emotion is one of the most prominent factors that

may affect motor intention. Neurological studies suggest that information from the limbic pathways can reach the motor pathways via the midbrain dopamine neurons, where a high degree of integration exists between emotion and motor control circuits [135]. Moreover, successful initiation of movement relies on nigrostriatal dopamine in the basal ganglia circuits [136]. Therefore, activating dopamine in emotion circuits may be a complimentary method to facilitate the basal ganglia motor circuits, in effect facilitating enhanced motor control. Therefore, an external emotional stimulus can enhance the detectability of neural changes during motor preparation. The external emotion stimulus can be provided through images, videos or music. As music is one of the most powerful emotion conveyors [137], a music stimulus can be used to affect a person's affective state.

In this study, we investigate whether it is possible to enhance prediction of movement intention significantly from EEG during a wrist extension by associating proper emotion-evoking musical stimulus. To investigate this question, we use sad, happy and neutral music stimuli in order to evoke various emotions in the subject while performing a wrist extension action. A 16-channel EEG system along with 2-channel EMG system were used to collect data from twelve healthy subjects. The EMG data were used to time lock the wrist extension events while EEG data were used to capture the mu and beta band ERD and MRCP. An SVM classifier with threshold regulation was utilized to use the obtained MRCP and ERD information to predict motor intention under the influence of three different emotional stimuli. The corresponding intention prediction performances were analyzed in terms of false positives/min, true positive rate and latency. To closely replicate an online scenario, the data were handled, processed and classified in a pseudo online arrangement. Moreover, a statistical analysis was also performed to exhibit the difference between the MRCP and ERD activities in the sensorimotor cortex under different stimuli.

7.2 Materials and Methods

7.2.1 Subjects

Twelve healthy individuals (eight male and four female, age 28.4±4.3) participated in the study. All the subjects were right-handed except for one. None of the subjects had any history of neurological disorder. The study was approved by the institutional review board of Florida International University. Before participating in the study, all the participants were properly trained about the task and they were required to sign a consent form before proceeding.

7.2.2 Emotion Stimulus Database

The database used in this article was established in a music and emotion study by Eerola et al [137]. The study produced a well-defined set of stimuli for music mediated emotions. The database consists of a set of 360 film music excerpts. Film music were chosen for the purpose of mediating powerful emotional cues and at the same time maintaining neutrality in terms of preferences and familiarity. All the excerpts were between 10 and 30 seconds in length. Half of the excerpts were moderately and highly representative examples of five discrete emotions namely anger, fear, sadness, happiness and tenderness while the other half were moderate and high examples of the six extremes of three bipolar dimensions (valence, energy arousal and tension arousal). In this study, the sad and happy labelled music excerpts were used for eliciting targeted emotion in the subjects. There were 30 music excerpts in each of these two categories. The music samples were rated by a group of 12 expert musicologists in a scale of 1 to 10 according to the perceived emotion in each audio clip.

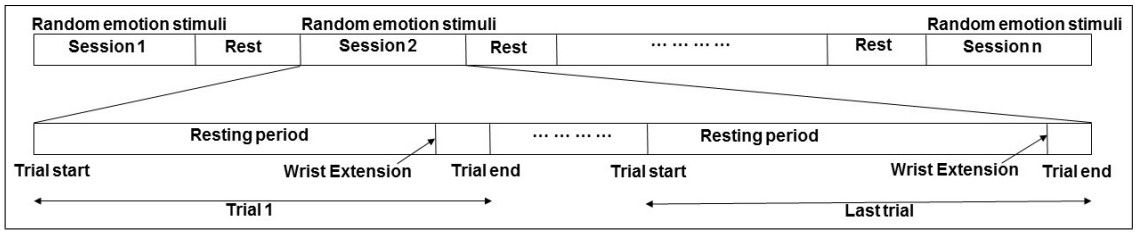

Figure 7.1: Experimental protocol of the study in summary. Each session contained sad, happy or neutral emotional states at random. Four sessions of each affective state were recorded. Each session consisted of three minutes of non-cued self-paced wrist extension action.

7.2.3 Experimental Protocol

The experiments were carried out in the Human Cyber-Physical Systems lab at Florida International University. During the experiment, the subjects were seated in a comfortable chair in front of a monitor. They put their hands flat on a desk in front of them and were asked to keep their hands, forearms and elbows as relaxed as possible to minimize any contaminating muscle activity. The height and position of the chair was adjusted properly so that the participants could be comfortable to begin the experimental process.

Before the beginning of the study, the subjects listened to all the 60 music clips and selected one happy and one sad audio clip which elicited the targeted emotions most successfully in them. This was done to correctly address the subject dependent variability in perceived affective state from the audio clip. After the selection of proper emotional stimuli, the participants moved into the wrist extension task. Figure 7.1 shows the experimental protocol in summary. At the beginning of each trial a countdown of 10 seconds appeared in the monitor in front of the participants. All the subjects were required to perform a simple wrist extension as soon as the countdown timer showed zero. That made sure that all the participants extended their wrists approximately every 10 seconds.

The experiment consisted of a total of 12 sessions. Out of those 12 sessions, four sessions were termed as neutral sessions because those sessions were free of any musical stimulus. The rest of the sessions involved the inclusion of either sad or happy emotional stimuli which were preselected by the subjects. In these sessions, the affective audio clips were played in a loop while the subjects carried out the wrist extension task. Each of the sessions were 3 minutes long with a break of 2-5 minutes between two consecutive sessions. Moreover, consecutive sessions were randomized in order to remove any additional affective bias resulting from the order of the sessions. In each session, the subjects completed approximately 18 repetitions of wrist extension which aggregated to 65 to 75 wrist extension events under each affective state namely happy, sad and neutral.

7.2.4 Analysis of Subjective Emotional Stimuli

Although the emotion evoking music stimuli were rated beforehand, emotion itself is a subjective experience. That is why the task of selecting proper music stimulus was given to the individual participant. Table 7.1 shows each participant's chosen music stimulus for happy and sad emotion and their corresponding sad and happy rating provided in the database. It is to be noted that the participants chose different music stimuli, however the overall average rating for happy and sad stimuli were quite distinguishable and abided by the range of original ratings in the database. This suggested the selection of proper emotion stimuli for evoking targeted emotions according to the database standards.

Table 7.1: Subjective Emotion Stimuli.

Subject	Happy music stimulus		Sad music stimulus	
	Happy rating	Sad Rating	Happy Rating	Sad Rating
S1	7.17	1.17	1.00	7.00
S2	7.33	1.00	1.00	7.00
S3	6.20	1.00	1.00	7.17
S4	6.17	1.00	1.00	7.17
S5	6.20	1.00	1.00	7.00
S6	5.67	2.50	1.00	5.67
S7	7.17	1.00	1.00	5.83
S8	6.20	1.00	1.00	5.67
S9	6.20	1.00	1.00	4.60
S10	7.17	1.00	1.00	7.67
S11	7.00	1.00	1.17	7.50
S12	6.20	1.00	1.17	7.50
Overall	6.56±0.56	1.14±0.43	1.03±0.07	6.65±0.96

7.2.5 Data Collection and Event Detection

For the purpose of this study EEG signal was recorded from the subjects' brain while performing the task. An active electrode system (actiCAP, Brainproducts GmbH) was used for collecting EEG data from 16 channels. The board contains two on board ADS1299 (Texas Instruments) amplifiers. The EEG electrodes were placed at Cz, C1, C2, C3, C4, C5, C6, CP3, CP4, CPz, FC3, FC4, FCz, Fz, Pz, Oz. The placement of the electrodes has been shown in figure 7.2. The ground and reference electrodes were placed at AFz and FPz respectively. The EEG data were recorded at a sampling rate of 500 samples per second. For event detection and time locking, two electromyography sensors were placed on the forearm of the subjects. The electrodes were placed at Extensor Digitorum and Extensor Carpi Ulnaris muscles with the ground electrode on the bony surface of the wrist (Figure 7.2).

The EMG data were recorded at 1000 samples per second which was then band pass filtered with a FIR filter with cutoff frequencies at 20 Hz and 400 Hz. The initiation of spikes in EMG data provided the time instances of the wrist extension action and that time information were used later for EEG feature extraction and

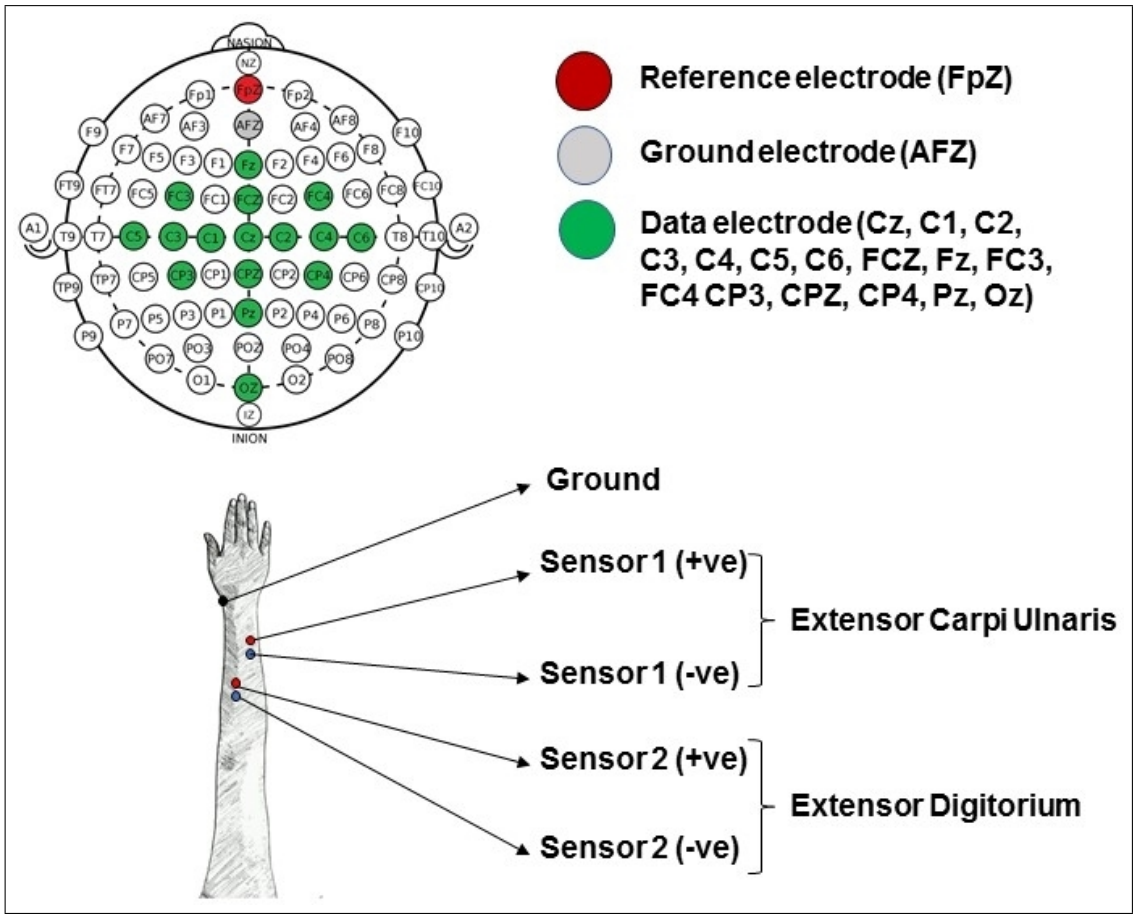

Figure 7.2: EEG and EMG sensor locations. EEG sensors were placed ac-cording to the international 10/20 system. EMG sensors were placed according to a bipolar montage with ground placed at the bony surface of the wrist.

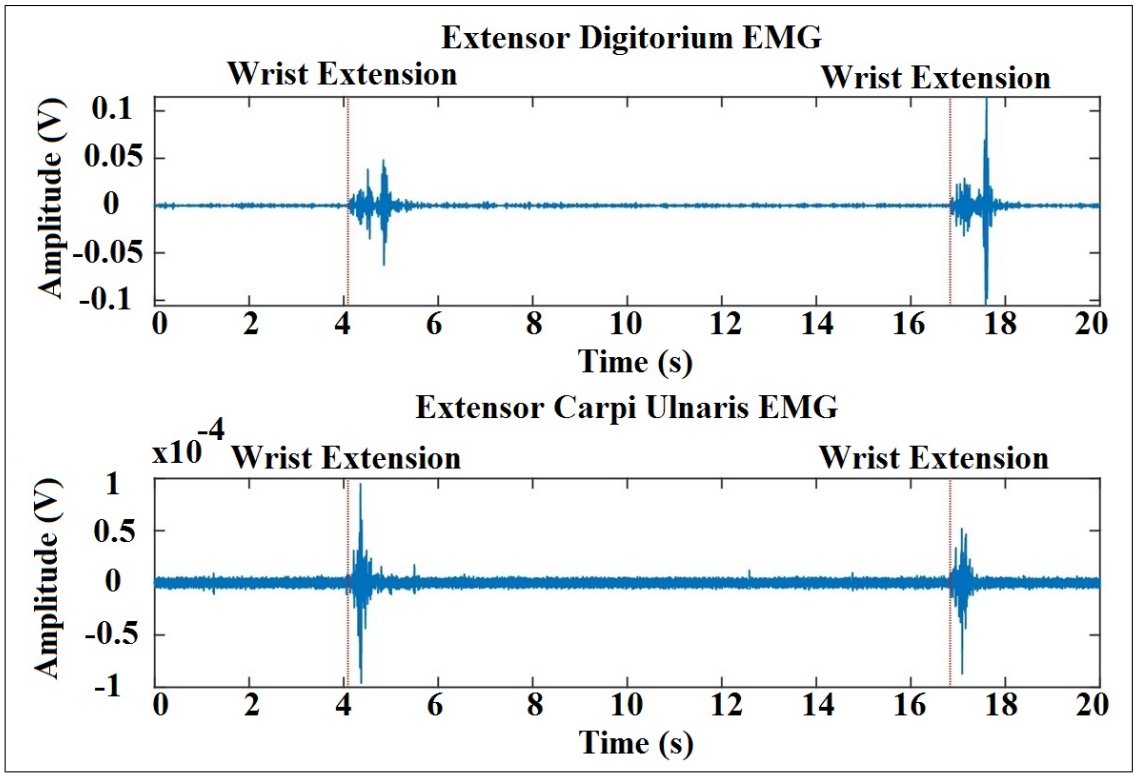

Figure 7.3: Wrist extension event detection. EMG data from Extensor Digitorium and Extensor Carpi Ulnaris muscles were used for event detection. Spikes in the EMG corresponded to onset of wrist extension.

formulation of a binary classification problem. The event detection procedure has been shown in figure 7.3.

7.2.6 Data Preprocessing

Information retrieval from EEG signal is accompanied with some critical challenges. Few of those challenges are the non-stationarity and randomness of the EEG signals, low signal to noise ratio and susceptibility to external artifacts. Therefore, proper filtering and cleansing of the collected EEG data is necessary for extracting valuable movement related information. The details of EEG preprocessing have been provided in previous chapters.

However, ASR and ICA are not suitable methods to be used in real-time application because these are computationally heavy and need a lot of data to work properly. That is why, an alternative and computationally more efficient methodology was applied for pseudo online testing. To comply with the offline sessions, data of one second long were accessed every 200 ms. A 4th order Butterworth high pass filter at 1 Hz cutoff frequency was used to remove DC drift. A notch filter at 60 Hz removed the line noise. After that a common average reference filter was used to reference the data to the grand mean of all the channels. Lastly, a Laplacian filter method was implemented to remove the effects of neighboring channels from any individual channel [77]. The Laplacian filtering method penalized each channel subtracting a weighted sum of the contributions coming from all the neighboring channels, where the weights are derived from channel to channel Euclidean distance. The Laplacian filtering method can be expressed as:

$$x_i^{LP} = x_i - \sum_{j \neq i} w_{ij} x_j \tag{7.1}$$

$$w_{ij} = \frac{\frac{1}{l_{ij}}}{\sum_{i \neq j} \frac{1}{l_{ij}}} \tag{7.2}$$

Here, i represents the index of the channel being filtered and j represents the indices of all other channels. x_i^{LP} is the output of the Laplacian filter. The weights w_{ij} were calculated from the distances between neighboring channels l_{ij}. The distances were calculated using the three-dimensional Euclidean method [77].

7.2.7 Data Segmentation

As stated in one of the previous subsections, two EMG sensors were used for wrist extension detection. A spike in the EMG sensor data represented the occurrence of a wrist extension event. After the data were collected, the data were visually

examined, and the times of events were extracted manually by visual inspection. It was also made sure that all the sensors in the network were synchronized so that there was no delay between the data of any pair of sensors. The extracted time points were saved for use in further processing.

7.2.8 Binary Classification Problem

After the data segmentation was completed, a binary classification problem was formulated to test the hypothesis of the study. The two classes in the problem were steady state and active intention state. The steady state corresponded to the period of each trial when the subjects were seated at a relaxed state without any intention to move their wrist. On the other hand, a small window of data close to the initiation of wrist extension were taken as active intention class. The classification problem was addressed in two different settings: offline and pseudo online. For the purpose of this, the first 80% of the data were used for offline testing as well as training and tuning the pseudo online classifiers. The last 20% of the data were excluded from this operation and were kept aside as unseen data for asynchronous testing to replicate the real time performance of the proposed methodology in a pseudo online environment.

For training the offline and pseudo online classifiers, data from 2 seconds before the movement to 2 seconds after the movement were marked as active intention state. This window selection was inspired by neurological background which suggests that mu and alpha (mu) band ERD can originate 1.5-2 seconds before the movement starts and can elongate till 2 seconds after the event [60].

However, this 4 second window was used as active intention state only for offline cross validation and for modeling and tuning the pseudo online classifiers. While

testing any unseen sample using the trained classifiers, the intention to move was required to be detected before the occurrence of the movement. This was to ensure that the BCI is allowed enough time to trigger the associated assistive device before the initiation of the movement. For pseudo online testing, therefore the detection window was set to 2 seconds before the movement up to the onset of movement. If any intention was detected outside this intention detection window, it was marked false positive detection. The overall windowing methods, window lengths, and necessary details have been summarized in figure 7.4.

The goal of the study was to investigate the effect of external emotion stimuli on the movement intention detection performance of the BCI. To evaluate the difference in detection performance, three different classifiers were trained for the three emotion stimulus conditions in both offline and pseudo online paradigms. The metrics for performance evaluation however remained the same. At the end, the results of the classification process were compared and analyzed. The binary classification process consisted of signal processing for feature extraction, feature selection and pseudo online classification. These steps have been discussed in the next few paragraphs.

7.2.9 Signal Processing for Feature Extraction

In the study, the event related desynchronization phenomenon was used for movement intention detection. ERD was chosen because of its ease of detection from single trial EEG. To calculate ERD, the first two seconds of each trial were extracted as the baseline. Afterwards, the ERD features were calculated according to the equations stated in the previous chapters.

In order to obtain ERD features with high resolution, both the steady state and active intention state EEG data were further subdivided into 1 second long epochs

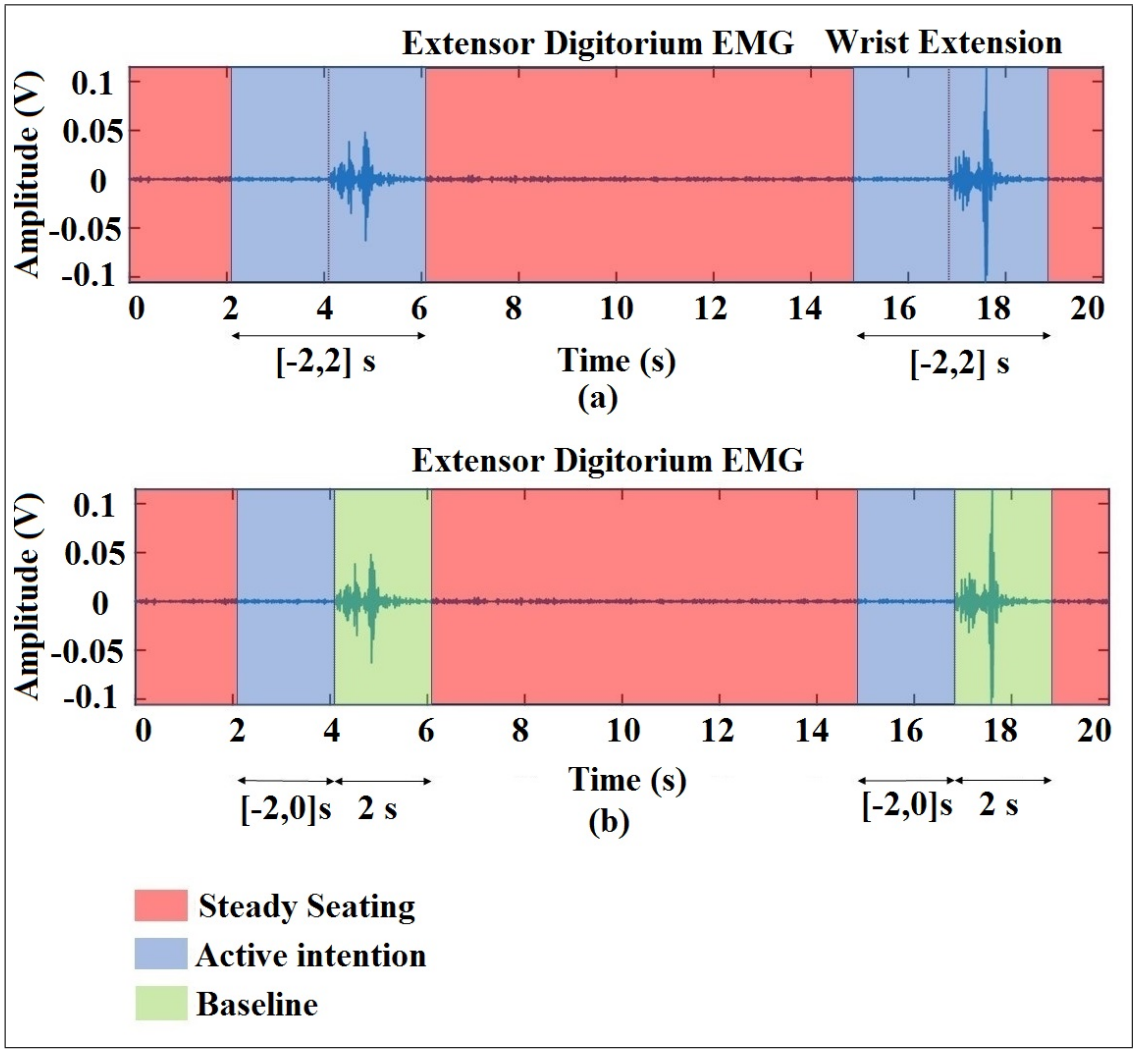

Figure 7.4: Windowing and segmentation method for offline and pseudo-online paradigm.(a) shows the windowing and segmentation method for offline cross validation, and training and tuning pseudo online classifier. (b) shows the windowing method for pseudo online testing procedure.

with 200 millisecond overlap. Each epoch was then processed for ERD extraction. Because of its ability to retain the sharpness of decomposition to a great extent, wavelet synchro squeezed transform was utilized for calculating alpha (mu) (8-16 Hz) and beta (16-32 Hz) band power in this study. After the calculation of the band powers, ERD features were calculated for each 1-second epoch. The number of ERD features were therefore 2 per channel for each epoch. Although data were collected from 16 channels, the EEG data from Oz was discarded from ERD calculation as the occipital region does not hold useful information about movement preparation and execution. More emphasis is put on the channel in the central area of the brain where the sensorimotor cortex is located. As a result, for each 1-second epoch 30 ERD features were extracted for further processing.

7.2.10 Offline and Pseudo-online Training

The set of features were ready to train classifiers for solving the binary classification problem between steady state and active intention state. As stated before, both offline and pseudo online classification schemes were employed to test the current hypothesis. Pseudo online approach is defined as an approach where the data in the test set are accessed as if they are acquired real-time.

For this purpose, the whole dataset was divided into three parts. The last 20% of the data were accessed in a pseudo online arrangement to test the efficacy of the model in a simulated real-life scenario. Among the rest of the data, 60% were used for training the classifier for pseudo online testing, and 20% of the data were used for validating and tuning the classifier. To test the robustness of the pseudo online results, the training and validation sets were chosen at random and this process was repeated ten times to obtain average performances along with standard deviation.

This randomization was done to account for any bias in the trained model. The offline classification was carried out using the combined training and validation dataset which comprised of 80% of the whole dataset. The testing was carried out in a 10-fold cross validation scheme to obtain average classification performance with standard deviation.

All the classification problems were addressed by training support vector machines with radial basis kernel [93]. While training the models, [-2,2] second window corresponding to the onset of wrist extension was used as active intention state and the rest of the trial was used as steady state. The hyperparameters of the classifiers were optimized using a grid search method at each step. Further details of the testing processes have been added in the following paragraphs.

7.2.11 Parameter Tuning

After training the classifier using 60% of the data, the next 20% were used for tuning the parameter so that the classifier maintains a reasonable true positive detection rate while ensuring a minimal false positive detection. The 1-s epochs in the validation set were classified using the trained classifier. The working point or the threshold was tuned so that the validation set could be classified with no more than 95% specificity while maintaining at least a sensitivity of 75%. Here sensitivity and specificity are defined as:

$$Specificity = \frac{True\ Negative}{True\ Negative + False\ Positive} \tag{7.3}$$

$$Sensitivity = \frac{True\ Positive}{True\ Positive + False\ Negative} \tag{7.4}$$

Here positive and negative classes represent the active intention and steady state class respectively. It is to be noted that the working point could be selected to

achieve a higher specificity to ensure low false positive detections in the testing section. But that would lead to lower true positive detection rate which would result the intention to move to be totally ignored at times. That is why a comparatively less strict condition was imposed on the preset specificity value. However, for proper operation a real-time BCI for an assistive device the false positive detection per minute must be well controlled and be kept to as low as possible. To ensure that further protective measure was taken in the pseudo online testing paradigm.

7.2.12 Pseudo-online Testing

The testing process was carried out in a pseudo online arrangement in an asynchronous fashion. For the purpose of testing, the data was accessed one 1-second epoch at a time. It is to be noted that all the data preprocessing was done offline and the preprocessed data were used for pseudo online testing. After the classifier returned a decision about an epoch, the decision was stored, and the next 1-second epoch was passed to the classifier after 0.2 second. Thus, the pseudo online asynchronous testing was performed.

To further reduce the chance of false positive detections due to the nonstationary nature of EEG signal, a protective scheme was applied. The protective algorithm took in the decisions of 10 consecutive epochs and returned one uniform label for all of them. If all 10 consecutive epochs were labeled as intention class, a detection was reported. If even one of the epochs were labelled as steady state class, any detected intention was discarded. Once a decision was made, the next 10 epochs were taken, and their labels were processed in the same way. As the windows were moved 0.2 second at each step, the final decision was made every 2 second about the previous 10 windows. The overall pseudo online testing procedure has been

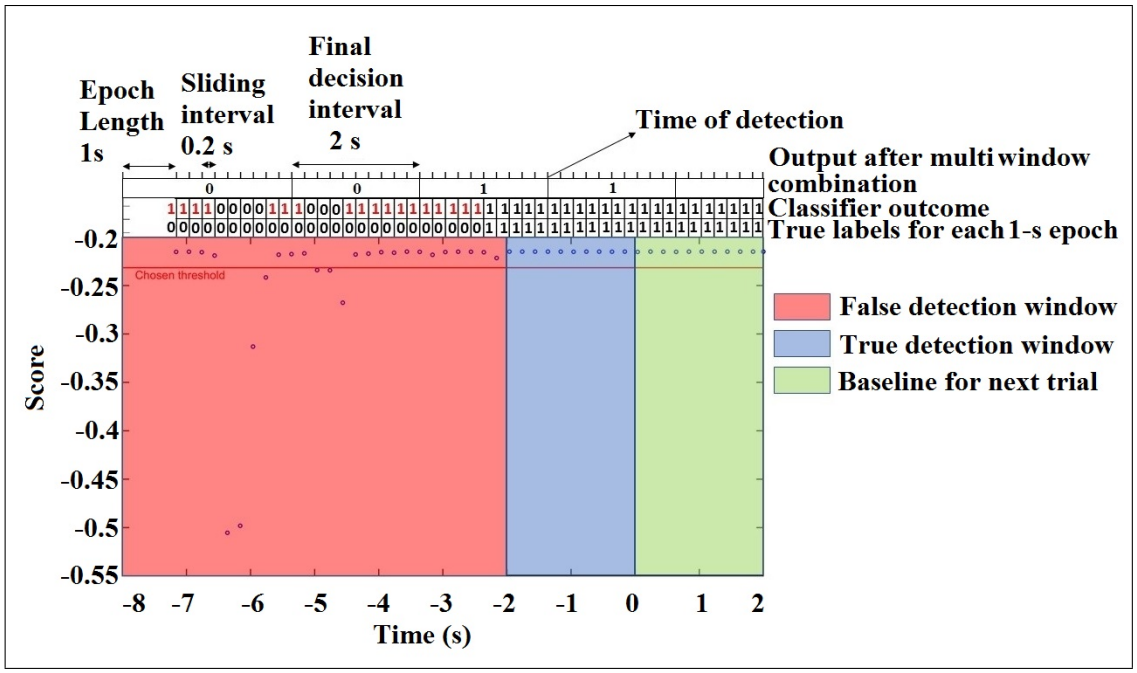

Figure 7.5: Pseudo online testing procedure. Data were classified one 1-s epoch at a time. The blue dots represent the classifier assigned score to the 1-s epoch and the red horizontal line indicates the threshold deter-mined by the validation set. The intermediate decisions made about each 1-s epoch contained a lot of false positive detections which are marked in red. A multi-window combination approach was employed to minimize the false positive rate in exchange for lower decision bit rate. A decision was made after every 10 windows which amounted to 2 seconds.

pictorially explained in figure 7.5.

7.2.13 Performance Metrics

To quantify the performance of the proposed pseudo online methodology, the TPR, FP/min and latency were calculated similar to the previous chapter. It is to be noted that a detection was termed as true positive only if the decision was made in a [-2,0] second interval corresponding to the onset of the wrist extension event. If the decision was made outside that window, then the detection was marked as false positive detection. Moreover, after every movement a 2-second buffer time was introduced, when all the decisions were disregarded. This was done to avoid the false

positive detections that might arise from the Event Related Synchronization phenomenon following a movement occurrence. This period was also used to calculate baseline for the next trial.

To evaluate the performance of the offline 10-fold cross validation scheme, the average and standard deviation of accuracy, sensitivity and specificity were reported for all the emotional stimuli conditions.

Additionally, the neurophysiological data corresponding to the three different affective conditions were also analyzed. The timing information related to the onset of ERD phenomena was compared and studied. The results have been presented in the results section of the article.

7.3 Results

7.3.1 Neurophysiological Data Analysis

The collected EEG data corresponding to three different emotional condition namely happy, sad and neutral were analyzed offline to study the fundamental difference in ERD phenomenon under different affective states. For this purpose, epoching was done from 10 seconds before the event to 3 seconds after the event. The epochs were preprocessed and freed from artifacts and time-frequency analysis was performed to obtain ERD. -10 seconds to -8 seconds of EEG data were selected as baseline. The obtained alpha (mu) and beta band ERD from all the channels were average to obtain an overall representation of ERD under three conditions for each subject. Figure 7.6 shows the comparison of ERD under three different emotion conditions.

The first occurrence -1 dB ERD points were selected as the point of initiation of ERD because that point referred to about 20% decrease in alpha (mu) and beta

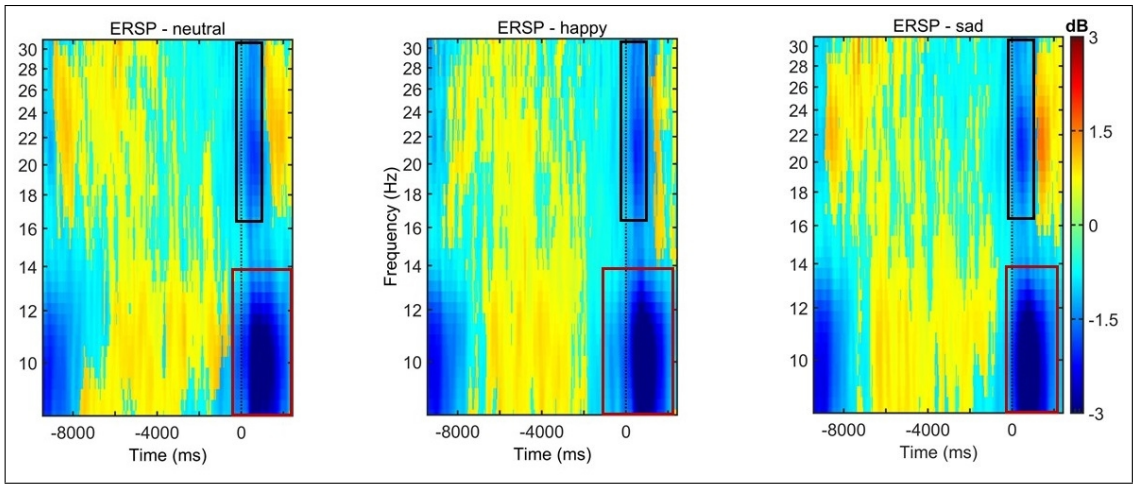

Figure 7.6: Comparison of ERD corresponding to the intention of wrist extension in three different affective states, namely neutral, happy and sad. The alpha (mu) ERDs have been marked in red boxes while the beta ERDs have been marked in black boxes. The figures suggest early occur-rence of ERD in mu band under happy music stimuli and late occurrence of ERD in sad emotion state.

band power compared to the baseline power. For neutral, happy and sad emotion states, the time of first occurrence of -1 dB alpha (mu) ERD were found to be -508.7 ms, -1045.2 ms and -419.3 ms respectively. While the first occurrence of -1 dB beta ERD were found to be at -300.2 ms for all emotion conditions in the beta band. The peak beta ERD of -1.989 dB occurred at 623.1 ms for neutral state, while for happy and sad emotions the values were -2.041 dB at 533.8 ms and -2.098 dB at 444.4 ms. Similarly, the peak alpha (mu) ERD values of neutral, happy and sad emotional states were found to be -3.781 dB at 831.6 ms, -3.996 dB at 772.1 ms and -3.993 dB at 742.3 ms.

Additionally, a permutation test was also performed to compute pairwise statistical significance of difference in ERD under three different conditions. Permutations tests were computed at a significance level of 99% and the results are presented in figure 7.7. The figure shows the result of permutation test in the range of -2 to 2 seconds corresponding to onset of movement, because this is the range where

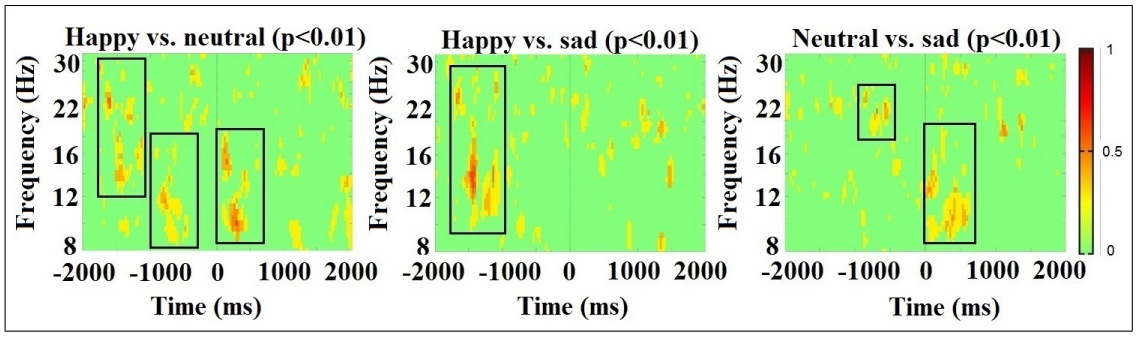

Figure 7.7: Results of a pairwise permutation test performed on ERD in the range of [-2,2] seconds in three different emotional states at 0.01 confidence level. The major significant blocks are marked in black rectangles. Happy music stimuli showed early significant differences in ERD in both mu and beta bands even before the movement onset. However, sad and neutral emotional states did not show any major significant differ-ence in ERD before the movement onset.

the appearance of desynchronization is most expected in mu and beta frequency bands. Moreover, The EEG data collected from each subject under the three affective states were analyzed in EEGlab to study the difference in MRCP. The effect of movement intention, preparation, and execution is found close to the onset of movement. Therefore, epoching was done from 4 seconds before the movement to 2 seconds after the movement. The data in the [-4, -3] second window were used as the baseline. Additionally, a permutation test was performed to compute the pairwise statistical significance of the difference in MRCP corresponding to the three different affective states. The significance level was set at 95%. A smoothing filter was used to smoothen the MRCP data to show the difference under the emotional states clearly.

The MRCP phenomena were analyzed in three-electrode groups: medial (FCz, Cz, CPz, Pz, Oz), contralateral (FC3, C1, C3, C5, CP3), and ipsilateral (FC4, C2, C4, C6, CP4). Figure 7.8 shows the three affective states' movement-related cortical potential in the brain areas. The contralateral side of the brain (left), according to the side of movement (right hand), showed the highest peak negativity under happy

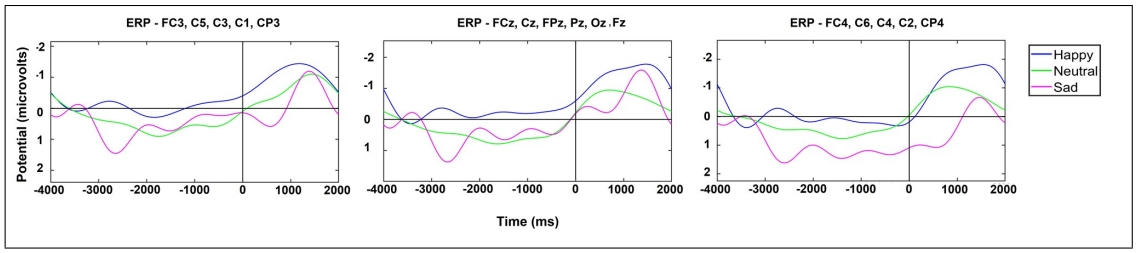

Figure 7.8: Comparison of MRCP in contralateral, medial, and ipsilateral electrodes (from left to right) under three difference affective states.

music stimulus of -1.43μV at 1011 ms after the wrist extension. Moreover, happy music stimulus resulted in the earliest appearance of negativity approximately 1105 ms before the movement. Meanwhile, sad and neutral affective states resulted in a peak negative amplitude of -1.05μV (1245 ms) and 0.98 μV (1253 ms). Negative amplitude appeared at 105 ms and 876 ms, respectively, under neutral and sad affective states. In medial EEG electrodes, negativity appeared at -2304 ms, -162 ms, and -161 ms under happy, neutral, and sad affective states. The peak negative amplitude was highest under happy state (-1.79 μV at 1572 ms) followed by sad affective state (-1.39 μV at 1561 ms) and neutral affective state (-0.83 μV at 423 ms). Happy music stimulus resulted in the highest peak negative amplitude of -1.78 μV at approximately 1571 ms on the ipsilateral side. In comparison, sad and neutral affective states caused the negative peak amplitudes of -0.68 μV (1550ms) and -0.96 μV (425ms). The first appearance of negative amplitude was located at -12 ms, 98 ms, and 1003 ms relative to the onset of wrist extension, respectively, under neutral, happy, and sad affective states.

Figure 7.9 shows the result of pairwise statistical significance testing performed to find significant differences in MRCP under different affective states. Only the [-2,2] second window relative to the moment of wrist movement was analyzed because this window was later used for classification and therefore was the window of interest. Statistical permutation testing did not show any statistical significance at

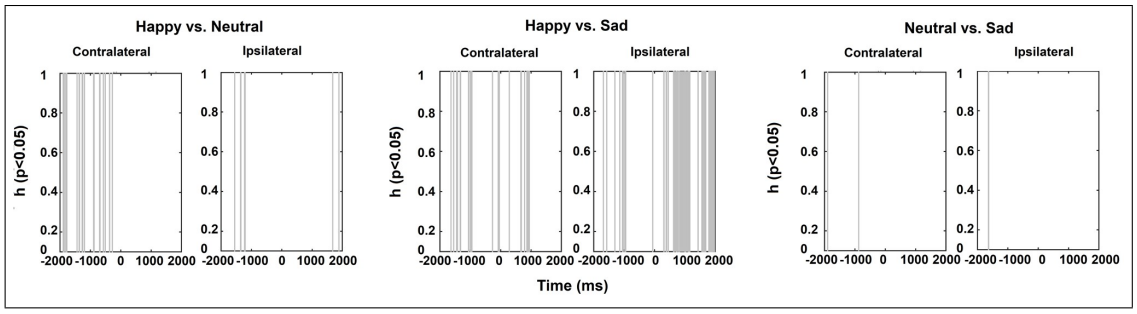

Figure 7.9: Result of statistical significance testing at $p<0.05$. Pairwise significance testing with multiple permutations was performed in ipsilateral and contralateral electrodes relative to the side of movement (right). Medial electrodes showed no statistical significance at any point of time.

any moment in the medical EEG electrodes. The comparison between the Event-Related Potential (ERP) obtained under happy and neutral emotion states suggests a statistically significant difference ($p<0.05$) mainly before the onset of the movement in the contralateral EEG electrodes. However, the statistically significant time frames are comparatively lower in number on the ipsilateral side. Therefore, it can be stated that ERP waveforms in these two conditions showed a statistically meaningful difference in the contralateral side between -1900 ms and -300 ms relative to the moment of movement onset. While comparing MRCP calculated from EEG signals corresponding to happy and sad emotional states, a substantial statistically significant difference was found before and after the movement onset. However, comparison between ERPs obtained under neutral and sad emotional states only revealed the transient presence of significance in contralateral and ipsilateral sides. In summary, happy and neutral emotion states showed significantly different MRCPs in the contralateral side and slightly weaker significance in the ipsilateral side before the movement. Happy and sad emotion states showed statistical differences over a long time before and after the movement in both ipsilateral and contralateral sides.

Moreover, to investigate how the baseline EEG was affected by the type of stimuli presented to the participant, the mu and beta band EEG powers were calculated for all the channels and users. After that, the mu and beta powers were averaged across all the channels to obtain a grand average representation for each subject. The average baseline EEG powers are summarized in table 7.2. The average alpha baseline power was much higher than beta baseline power. However, no significant difference was found between the baseline powers at a significance level of 95%. The results of t-test with Bonferroni Holm correction suggested that the baseline mu and beta powers were not affected by the type of emotional stimuli.

Table 7.2: Comparison of Baseline EEG Powers ($10^{-9}V^2$) across Subjects

Subject	Mu (Alpha)			Beta		
	Happy	Neutral	Sad	Happy	Neutral	Sad
S1	15.90±9.40	14.60±7.20	15.90±8.20	7.90±2.10	6.80±2.00	7.10±1.80
S2	3.30±1.80	5.30±7.20	2.60±1.60	1.90±0.80	3.10±3.70	1.40±0.40
S3	8.90±4.40	6.00±2.90	8.80±5.60	2.30±0.60	2.00±0.30	2.00±0.50
S4	2.00±0.90	3.20±1.30	3.40±1.80	1.10±0.20	1.60±0.40	1.60±0.40
S5	56.40±40.10	46.80±27.40	60.60±55.70	9.70±3.30	9.50±2.30	10.50±3.80
S6	6.70±3.70	6.50±2.80	6.10±2.90	3.60±0.90	4.20±1.10	3.40±0.70
S7	6.00±2.20	4.10±1.90	5.10±1.90	6.80±7.90	2.60±1.70	6.00±3.60
S8	6.10±2.00	9.40±3.00	11.20±5.60	3.70±1.20	4.10±0.90	3.80±1.10
S9	4.20±1.60	4.30±1.60	5.30±2.20	3.10±0.70	3.10±0.70	4.90±4.50
S10	2.70±0.70	2.30±0.50	2.10±0.70	2.50±1.40	1.20±0.60	2.00±0.90
S11	6.70±3.40	8.00±5.20	7.60±4.30	2.40±0.60	2.90±0.80	2.40±0.60
S12	16.80±11.50	18.20±14.10	18.30±11.20	8.30±2.20	7.30±2.10	6.70±1.30
Overall	11.31±6.81	10.73±6.26	12.25±8.48	4.44±1.83	4.03±1.38	4.32±1.63

To get further insight into the underlying factors connecting emotional stimuli and motor activity, a comparison of muscle activation under the three different emotional stimuli were also performed. The EMG powers were calculated for each trial for the subjects and finally they were averaged across trials to capture a global statistical representation of the average muscle activation energy per trial. Table 7.3 summarizes the EMG energy per trial for each subject under three different

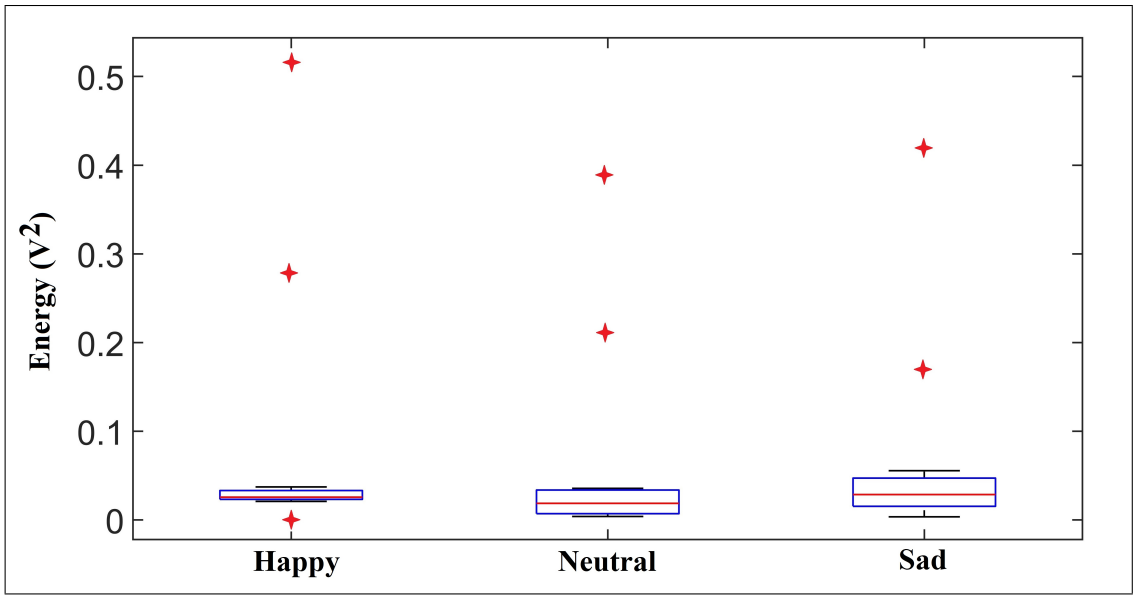

Figure 7.10: Comparison of EMG activity per trial in three different emotional states. Boxplot and t-test suggests EMG activity was not affected by emotional state.

emotional state. Initial inspection suggest that injection of emotional music stimuli resulted in a slightly higher EMG activity among the subjects on an average. However, a t-test with Bonferroni Holm correction at 95% significance level did not reject the null hypothesis. This suggests that there was no statistically significant difference in the EMG activity under difference emotional condition. Moreover, subjects 5 and 11 showed very high magnitude of EMG which could be caused by skin conductance, electrode placement, individual physiology, anatomy or biochemical properties [138]. However, the higher energy existed throughout all the emotional stimuli and did not affect any specific condition. Figure 7.10 shows a boxplot of the EMG activity across subjects which confirms that no statistical significance was found.

Table 7.3: Comparison of Average EMG Powers (V^2) across Subjects

Subject	Happy	Neutral	Sad
S1	0.0373	0.0279	0.0389
S2	0.0247	0.0074	0.0090
S3	0.0210	0.0197	0.0282
S4	0.0292	0.0179	0.0292
S5	0.5178	0.3881	0.4194
S6	0.0250	0.0357	0.0235
S7	0.0274	0.0069	0.0556
S8	0.0250	0.0083	0.0292
S9	0.0050	0.0040	0.0047
S10	0.0265	0.0319	0.0219
S11	0.2774	0.2129	0.1686
S12	0.0219	0.0065	0.0036
Average	0.08±0.15	0.06±0.12	0.07±0.12

7.3.2 Offline Classification Results

Table 7.4 shows the subject wise offline classification results under three different emotional states using mu and beta ERD. The accuracy achieved in neutral, happy and sad emotional states were 86.1 ± 2.7%, 91.3 ± 1.8%, 89.2 ± 2.1% respectively. Similarly, sensitivity and specificity achieved under neutral, happy and sad emotional conditions were 85.3 ± 9.5%, 89.0 ± 3.7%, 89.5 ± 3.5% and 86.4 ± 9.1%, 91.4 ± 3.2%, 88.5 ± 3.6% respectively.

The achieved results were also tested by a paired two tailed t-test with Bonferroni-Holm correction to investigate whether the difference in results obtained under different emotional states were statistically significant or not. The results of the t-test suggest that the accuracies obtained under happy emotional stimulus was significantly better than those obtained in neutral ($p = 0.00001$) and sad ($p = 0.0024$) emotional conditions at 95% significance level. However, no statistically significant difference was found between the results obtained in sad and neutral emotion states. These results suggested that the happy emotional music stimuli enhanced the detection accuracy and the enhancement was statistically significant at 95% significance level.

Table 7.4: Offline Classification Results in Different Emotion States (ERD)

Subject	Accuracy (%)			Sensitivity (%)			Specificity (%)		
	Neutral	Happy	Sad	Neutral	Happy	Sad	Neutral	Happy	Sad
S1	89.9±2.8	97.4±1.1	89.1±2.7	88.5±5.5	97.9±0.9	93.4±3.4	90.9±2.9	97.1±1.8	85.6±5.5
S2	89.2±2.9	93.8±1.7	88.7±1.7	88.8±11.3	90.4±2.3	86.9±2.4	89.4±8.7	96.4±2.4	89.6±2.7
S3	86.2±2.6	93.6±1.6	89.4±1.9	84.1±10.8	87.0±2.2	87.5±3.9	87.8±10.4	97.6±1.1	91.2±3.1
S4	86.4±2.9	91.2±1.7	88.1±2.2	85.4±9.6	89.1±3.8	90.7±3.5	86.5±9.2	91.6±3.3	88.8±3.5
S5	88.1±2.5	91.4±1.6	89.8±1.5	85.8±8.9	88.5±5.8	88.9±3.7	89.8±8.7	93.7±3.9	90.8±2.5
S6	82.9±4.5	93.4±1.3	89.2±1.8	85.7±13.9	92.1±1.9	88.5±3.9	80.8±16.0	92.1±1.8	91.7±3.9
S7	85.1±2.3	85.9±2.2	90.0±1.4	84.9±6.2	83.4±2.0	88.6±2.3	85.2±7.9	87.9±3.0	92.7±1.9
S8	87.0±2.9	90.3±1.8	91.2±2.0	89.5±8.3	89.1±9.5	89.9±4.4	86.2±8.9	91.2±4.2	93.6±1.7
S9	82.9±2.3	90.5±2.2	83.2±2.6	81.4±14.2	89.0±5.1	83.5±4.9	84.1±13.7	91.2±4.8	83.0±6.1
S10	82.3±2.1	90.2±1.8	84.6±2.7	81.7±6.7	88.4±3.4	83.2±2.9	82.1±7.3	91.1±3.7	85.3±3.3
S11	85.8±1.7	86.8±2.6	84.8±2.1	84.1±11.5	84.7±5.4	83.9±3.7	87.0±9.7	88.4±6.3	85.7±3.7
S12	87.0±2.3	90.5±1.8	90.4±1.9	84.7±7.8	89.9±3.3	92.4±2.9	88.6±6.9	91.0±3.4	88.0±3.8
Overall	86.1±2.7	91.3±1.8	89.2±2.1	85.3±9.5	89.0±3.7	88.2±3.5	86.4±9.1	91.4±3.2	88.5±3.6

Table 7.5: Offline Classification Results in Different Emotion States (ERD+MRCP)

Subject	Accuracy (%)			Sensitivity (%)			Specificity (%)		
	Neutral	Happy	Sad	Neutral	Happy	Sad	Neutral	Happy	Sad
S1	86.3±5.6	97.8±2.1	87.8±2.1	88.4±7.9	97.5±2.7	87.6±5.4	84.8±13.9	97.4±4.0	88.4±4.6
S2	85.5±7.6	92.7±1.1	85.6±1.7	85.9±19.5	90.9±3.2	86.6±6.7	85.1±26.5	94.2±2.4	84.8±7.2
S3	86.8±2.5	94.7±1.7	85.7±1.7	85.9±25.5	95.4±4.6	85.9±3.6	87.9±17.8	94.4±3.9	85.4±3.6
S4	86.4±2.6	92.3±2.1	82.1±2.4	87.8±16.4	91.2±7.9	84.4±5.2	85.1±13.4	93.1±6.8	81.6±6.3
S5	88.4±1.9	89.3±1.7	87.7±1.3	89.7±6.1	89.7±4.6	86.3±3.2	87.3±6.9	89.6±6.7	88.2±5.4
S6	81.6±3.7	89.8±1.6	87.9±2.2	80.1±19.6	90.0±6.1	88.9±4.2	81.9±20.1	89.6±6.7	87.2±5.4
S7	79.8±1.5	85.5±1.0	88.5±1.9	79.1±12.5	83.0±4.7	87.4±2.5	80.4±9.9	85.5±3.6	90.9±2.3
S8	83.2±4.2	87.2±1.9	86.9±2.0	81.8±16.4	87.5±1.9	86.7±5.2	84.2±14.4	87.0±2.3	88.9±2.8
S9	85.9±4.7	88.4±2.9	82.8±3.0	86.9±16.9	87.3±5.2	83.1±5.3	85.1±17.0	89.3±8.5	82.6±8.7
S10	80.1±2.4	88.9±1.1	86.7±2.4	82.3±5.8	88.1±4.2	87.1±4.6	78.4±6.7	89.5±4.2	86.4±7.4
S11	83.9±3.9	85.9±2.6	87.8±3.8	82.1±18.4	85.2±4.9	87.0±4.4	84.3±16.4	86.3±7.5	88.3±7.5
S12	82.1±1.2	96.0±2.0	88.5±1.9	82.7±12.1	94.7±5.2	88.1±5.5	81.6±8.9	97.0±5.2	89.1±5.5
Overall	84.2±3.5	90.8±1.8	86.6±2.2	84.4±14.8	90.1±9.2	86.6±4.7	84.1±14.3	91.1±5.2	86.8±5.6

Table 7.5 shows the classification results obtained under the three emotional states obtained while classifying the intention and steady-state classes. Happy music stimulus obtained the highest overall classification accuracy of 90.8±1.8%, followed by sad (86.6±2.2%) and neutral (84.2±3.5%), respectively. The highest sensitivity and specificity were achieved under happy music stimulus, which was 90.1±9.2% and 91.1±5.2%, respectively. Sad music stimuli resulted in 86.6±4.7% sensitivity and 86.8±5.6% specificity. Meanwhile, neutral emotion state yielded the lowest sensitivity and specificity of 84.4±14.8% and 84.1±14.3%, respectively. A two-tailed paired t-test with Bonferroni correction was performed to validate the classification performance difference further. The result of the t-test yielded that happy music stimulus performed significantly better than neutral and sad affective states in terms of accuracy ($p=0.000009$ and $p=0.0017$ respectively) and specificity ($p=0.000008$ and $p=0.0025$ respectively) at $p<0.05$ confidence level. Meanwhile, in terms of sensitivity, only the difference in performance between happy and neutral affective states was significantly different at $p<0.05$ confidence level ($p=0.0003$). However, no statistical significance was found between the classification accuracy, sensitivity, and specificity obtained under sad and neutral affective states ($p=0.0445$, $p=0.0901$, $p=0.0277$), respectively.

Table 7.6 shows the comparison of classification performance obtained using different feature combinations. Beta ERD resulted in the highest accuracy, sensitivity, and specificity across all the emotional states as a single feature modality, followed by Mu ERD and MRCP. MRCP yielded the lowest classification performance among single feature classification models. In the case of two feature combinations, the best performance was achieved using Beta ERD and MRCP, followed by Mu and Beta ERD and Mu ERD and MRCP. Combining all three kinds of features resulted in similar performances to the two feature combinations. However, the proposed feature

Table 7.6: Comparison of Classification Results obtained using Different Feature Combinations.

Feature	Accuracy (%)			Sensitivity (%)			Specificity (%)		
	Neutral	Happy	Sad	Neutral	Happy	Sad	Neutral	Happy	Sad
μ ERD	81.1±1.8	85.1±2.4	82.2±8.1	80.6±12.5	84.8±3.2	81.2±9.5	82.1±13.5	86.1±2.2	83.2±1.5
β ERD	82.8±2.1	87.0±2.3	84.6±8.3	81.5±7.9	86.7±1.9	85.5±8.7	83.5±9.2	87.2±2.6	84.1±3.1
MRCP	66.5±4.7	69.8±8.4	65.6±8.1	65.5±11.9	70.1±8.5	67.0±1.5	65.5±10.5	69.0±7.1	64.1±3.5
μ & β ERD	83.1±2.4	88.4±1.5	85.5±5.1	82.2±9.8	88.1±2.5	85.6±1.9	84.2±8.9	88.9±1.9	85.1±2.1
μ ERD & MRCP	82.2±1.6	86.7±2.2	84.1±2.1	83.1±8.1	85.4±2.6	83.9±1.6	81.5±9.5	87.9±2.7	84.5±2.4
β ERD & MRCP	83.5±3.1	89.1±2.1	85.9±1.5	82.9±9.5	88.1±1.9	85.1±2.6	84.5±8.2	90.2±1.2	86.8±3.5
μ,β ERD & MRCP (No FS)	83.1±1.9	88.5±1.5	85.7±2.5	83.0±11.3	88.1±4.9	84.1±2.6	83.3±10.1	89.3±2.4	87.1±5.1
μ,β ERD & MRCP (MRMR)	84.2±3.5	90.8±1.8	86.6±2.2	84.4±14.8	90.1±9.2	86.6±4.7	84.1±14.3	91.1±5.2	86.8±5.6

selection method utilizing the MRMR algorithm enhanced up to 2% in classification performance. Overall, the proposed method performed better than a single feature, double feature, and multiple feature combinations by a margin of 2-5% in terms of accuracy, sensitivity, and specificity.

7.3.3 Pseudo Online Classification Results

Although the offline classification results suggested that happy music stimulus could enhance the detection performance compared to sad and neutral emotion states, the results of pseudo online asynchronous classification held more importance to establish the fact. Because, the pseudo online scheme closely resembled the decision-making scheme in real-time scenario. Table 7.7 summarizes the pseudo online classification results under different emotional stimuli.

The true positive detection rates achieved under neutral, happy and sad emotion states were 76.9 ± 4.5%, 82.9 ±4.1%, and 74.1 ± 6.7% respectively. The proposed methodology reached the aforementioned true positive rates with 5.8 ± 0.7, 5.4 ± 0.6, 6.4 ± 0.6 false positive detections per minute respectively in neutral, happy and sad elicited emotions. Lastly, the detection latencies achieved under different emotional stimuli were respectively -1163 ± 387 ms, -1187 ± 414 ms, -1115 ± 504 ms. The negative signs of the latencies suggested that the intention to extend the wrist could be detected well before the onset of movement.

Like offline classification results, a two-tailed paired t-test with Bonferroni-Holm correction was also employed on the achieved results. The results of the t-test suggested that the average TPR achieved by the happy emotional stimuli were better than those achieved by neutral ($p = 0.0163$) and sad ($p = 0.0009$) emotional conditions at 95% significance level. The results of sad and neutral conditions did not

Table 7.7: Pseudo-online Classification Results in Different Emotion States(ERD)

Subject	TPR (%)			FP/min			Mean Latency ± std (ms)		
	Neutral	Happy	Sad	Neutral	Happy	Sad	Neutral	Happy	Sad
S1	72.7±3.4	76.4±6.4	71.8±13.1	7.9±1.4	5.6±0.2	4.6±0.3	-916±314	-1306±421	-1157±524
S2	80.0±1.4	99.3±0.4	75.3±3.4	5.4±0.3	4.9±0.1	5.9±1.6	-1144±494	-1284±306	-1132±582
S3	78.9±2.3	92.1±2.3	66.7±5.8	6.5±0.6	2.8±0.4	7.6±0.5	-1260±523	-1191±387	-994±380
S4	79.4±5.2	91.9±3.0	84.4±8.9	7.5±0.2	6.1±0.9	7.4±0.5	-954±609	-1226±382	-1156±385
S5	77.3±4.7	84.0±6.4	66.7±5.3	6.2±0.4	6.1±1.0	6.8±0.4	-970±464	-1023±584	-1025±748
S6	78.3±6.9	82.7±3.4	75.3±3.2	5.1±0.7	5.5±0.6	5.6±0.7	-1253±281	-1341±416	-1277±290
S7	72.7±3.4	77.3±3.4	69.3±7.1	5.9±0.9	6.1±0.4	8.4±0.5	-1221±305	-1047±379	-1092±663
S8	85.3±11.1	84.0±3.4	84.7±8.9	4.5±1.1	5.5±0.6	5.9±0.3	-1197±220	-1264±232	-1225±359
S9	67.3±5.1	79.3±5.8	64.0±7.2	5.9±1.5	6.0±0.8	7.1±0.9	-1192±405	-1211±486	-915±551
S10	82.3±4.2	80.0±1.1	73.3±3.1	5.4±0.6	4.5±0.6	7.1±0.8	-1270±254	-1301±317	-1067±633
S11	74.0±2.1	72.7±5.6	82.7±4.7	4.7±0.4	6.0±0.8	4.4±0.5	-1311±451	-982±548	-1241±339
S12	75.0±4.7	75.3±8.3	75.3±9.5	5.1±0.2	5.6±0.7	5.6±0.4	-1265±320	-1065±514	-1106±595
Overall	76.9±4.5	82.9±4.1	74.1±6.7	5.8±0.7	5.4±0.6	6.4±0.6	-1163±387	-1187±414	-1115±504

show any statistically significant difference at 95% significance level. The FP/min and detection latencies did not show any significant difference at 95% significance level.

7.4 Discussion

This article investigated into the effect of emotion evoking music stimuli on the performance of movement intention detection from pre-movement EEG signals. Results suggest that happy emotion stimuli could enhance the detection performance quite significantly compared to sad and neutral emotion states.

The study presented an offline as well as asynchronous pseudo online testing to test the hypothesis of the study. However, the preprocessing tools used for offline preprocessing, namely ASR and ICA was not properly applicable in online preprocessing pipeline. Because ASR and ICA need significant amount of data to work properly. ASR needs a good amount of data for estimating the clean portion of data while ICA needs the data for reliable blind source determination. For proper online application, preprocessing tools which require lesser amount of data and memory are advised to be used. That is why a computationally less expensive preprocessing methodology was also implemented for pseudo online testing which utilized common average referencing and Laplacian filtering. Recently Online Recursive ICA (ORICA) [82] has been implemented as an effort towards online ICA, but it stills needs a lot of efforts to be applicable online. For proper pseudo online or online testing, therefore proper online preprocessing tools must be used. This issue will be addressed more extensively in a future study.

The trials in this study were carried out by the subjects without any audio or visual cue. However, the presence of the timer, which motivated the participants

to initiate wrist extension in a timely manner, prevents the tasks from being called completely voluntary. The purpose of the timer was to maintain a uniform epoch size while processing the data. However, totally voluntary movement intention and the effect of emotional stimuli on that phenomenon creates a promising research area and should be carried out in an extension of this study. In future, self-paced voluntary movements and the impact of emotional stimuli on completely self-paced movement intention will be carried out to address this issue properly. However, in that case it must be made sure that a minimal length of steady state EEG activity is recorded from the participants to capture reliable and meaningful ERD. Because, if the pre movement steady state duration is too short that would hamper the extraction of proper baseline activity which is pivotal in ERD calculation.

Feasibility of external happy music stimulus in real-life situations is quite challenging. Moreover, emotion evoking musical stimuli significantly differ from person to person which makes personalization of stimuli sets a very important task. There might also be a safety hazard because listening to music while moving can be potentially dangerous. Despite all these issues, the outcome of the current study suggests that a personalized set of happy emotional music stimuli would at least help in real-life neurorehabilitation, where an injection of happy music stimulus would potentially help a person with impaired motor ability to recover the lost motor ability to some extent with lesser effort and in a shorter time. Moreover, to reduce the possibility of danger due to listening to music while movement, proper safety protocol should be designed and implemented so that the user can be alerted in the appearance of any attention demanding task while moving. This poses another very interesting research question which should be investigated in future studies.

The results of physiological data analysis revealed several interesting outcomes. As the results of the analysis was averaged across all the subjects and all the elec-

trodes of interest, the representation can be deemed as global and unbiased representation of the overall time-frequency analysis. It was found that the inclusion of happy emotional stimuli forced an early occurrence of at least -1 dB ERD compared to the neutral affective state. Moreover, it was also noticed that the introduction of sad emotional stimuli resulted in a late appearance of -1 dB ERD in alpha (mu) band. Here, first occurrence of -1 dB ERD was taken as a point of reference to compare the minimum distinguishable ERD corresponding to the intention of wrist extension.

Moreover, it was also found that the peak beta ERD was achieved before the peak alpha (mu) ERD across all the emotional conditions. However, the peak beta ERD was always smaller in magnitude compared to the peak alpha (mu) ERD. This suggested that although peak beta ERD could be an essential tool to detect movement intention, the peak alpha (mu) ERD was easier to detect.

Another interesting observation that could be made from the neurological analysis (figure 7.6) is that the initial beta ERD appeared at the same time across all emotion states. The magnitude of peak beta ERD was higher whenever any emotion stimuli were applied whether it was happy or sad. But there was no distinguishable difference in magnitude between beta ERDs of sad and happy emotion conditions. The appearance of peak beta ERD was observed slightly earlier in the sad stimuli condition followed by the happy and neutral emotional states.

In case of alpha (mu) ERD it was found out that the amplitudes of ERD became significantly different at the application of happy or sad emotional music stimuli. But the peak alpha (mu) ERDs were almost same in both happy and sad emotion states. The occurrence of peak alpha (mu) ERD was earlier in the case of sad emotion stimuli followed by happy and neutral emotional states just like beta ERD. But more interestingly, the initiation of alpha ERD was observed significantly ear-

lier under happy emotional stimuli than the other two emotional states. Happy vs. neutral ERD comparison suggested moderate to strongly significant difference from -1700 ms to -1150 ms in both mu and beta band. Approximately, -1000 ms to -250 ms showed moderately significant difference in mu ERD (figure 7.7). Immediately after the movement, from 0 ms to 700 ms approximately, a strong significance was observed in mu and lower beta bands. Happy vs. sad comparisons showed strong significant difference from -1700 ms to -980 ms across mu and beta frequency bands. But no significantly different blocks were observed after the movement onset. Comparatively, neutral vs. sad comparison showed very little significant difference prior to movement onset, however a moderate significance could be observed from 0 ms to 700 ms in mu and lower beta frequencies. Another interesting observation was that, both happy and sad music stimuli resulted in significantly different ERD after the movement onset which suggested that the degree of desynchronization was much greater in the presence of musical stimuli.

Overall analysis suggested that introduction of happy music stimuli forced significantly early detectable alpha ERD. However, sad stimuli might force early peak in alpha (mu) and beta ERD. As the peak ERDs were always found after the movement had already happened, the early occurrence of detectable ERD under happy emotion stimuli might result in better detectability and in turns better prediction of movement intention. Moreover, as there was no difference in initial appearance time of beta ERD across different emotional conditions, results suggest that the early occurrence of alpha ERD was the major contributor to the enhanced intention detection performance under happy emotional state. A recent study reported a decrease in power in the alpha and lower beta band in posterior and anterior sensor clusters responsive to arousal emotion [139]. The outcome of the current study is supported by the mentioned study, because happy emotional music stimuli also

contain high arousal rating, i.e. in the valence-arousal emotional plane, which could potentially explain the early appearance of ERD. However, further extensive studies are necessary to understand the effects of emotion on motor behavior.

The results of neurophysiological data analysis revealed that the happy music stimulus enforced statistically significant and more substantial movement-related potential before and after the movement. Compared to both sad and neutral emotional stimuli, the difference was readily evident on both ipsilateral and contralateral sides. However, the MRCP obtained under neutral and sad emotional music stimuli did not significantly differ in MRCP activities on any electrode zones. The medial electrode group did not show any statistically significant difference between the MRCP obtained under different affective states. This finding indicates that happy music stimulus can enhance the peak negativity of MRCP in specific brain areas and thus has the potential to improve the detectability of intention-related cortical potentials. As a result, this would enable accurate prediction of movement intention leading to more feasible BCI operation.

Additionally, happy music stimulus also enforced early negativity in the low-frequency brain signals in both contralateral and medial electrodes. The negative amplitude appeared almost simultaneously for all the emotional states on the ipsilateral side. The early occurrence of MRCP under happy music stimulus also suggests that the inclusion of happy emotional stimulus can enable early detectability of human movement intention. The ability to detect intention early and before the movement onset could be critical for the state-of-the-art assistive BCI systems to provide safe, reliable, on-time, and on-demand assistance. The user could benefit from using such an assistive device because it would provide an experience closer to natural human movement.

Table 7.6 shows the comparison between the classification performances obtained using different feature combinations. The lowest classification accuracy was obtained using MRCP. This event is because MRCP is a very low-frequency change in EEG amplitude, and it takes multiple trials of the same task to obtain a reliable representation of MRCP features. That is why it is challenging to classify movement-related single-trial EEG data using MRCP features only. However, the classification performance using MRCP was enhanced by applying happy music stimulus by about 4% compared to neutral and sad emotional states. This finding is consistent with the neurophysiological evidence found during the neurophysiological data analysis. Another interesting observation that can be made from the table is that combining the MRCP features with Mu and Beta ERD improved the accuracy of the classification models trained using only Mu or Beta ERDs. This finding suggests that combining MRCP to ERD features can enhance the classification performance of BCI systems which is in agreement with the findings of similar studies in the past. Additionally, the MRMR feature selection method enhanced classification performance compared to that of the three-feature combination without any feature selection. This outcome suggests that the feature selection algorithm removed some redundant features, resulting in higher classification accuracy using fewer features.

Happy music stimulus also yielded better classification performance than sad and neutral emotional states($p<0.05$). The current study reached slightly enhanced classification performance despite combining ERD and MRCP features. The MRCP features differed significantly in different emotional states, and therefore their inclusion in the classification model can improve accuracy, sensitivity, and specificity significantly. Future works should explore advanced computational methods to effectively combine the ERD and MRCP features to further enhance the proposed BCI's performance.

The t-test with Bonferroni Holm correction performed on the baseline EEG powers suggested that the baseline mu and beta powers were not affected by the type of emotional stimuli. ERD is the measure of relative change in spectral power in the basis of the baseline power. This suggests that despite having statistically similar baseline beta and mu powers, happy emotional stimuli resulted in a significantly earlier appearance of mu ERD which appeared during the movement related epochs and thus resulted in potentially easier and more accurate movement intention detection.

The classifiers were trained using the 1-second epochs and the pseudo online testing were done in the same way followed by the combination of results obtained from 10 consecutive epochs to reach a final intention prediction decision. The data before and after movement were involved in the training procedure because the suppression of mu and beta power responding to human motor intention, namely ERD starts from 1.5-2 seconds before the onset to 1.5-2 seconds after the onset of the event which has been reported by multiple studies. To capture the overall neural information, the 1-second data epochs from before and after the event were therefore used to train the classifier. Extraction of data epochs from before the movement only would rather result in partial or missed information retrieval which could affect the performance of the classifier rather adversely. That is why data from before and after the movement were used for training the classifier. Moreover, the goal of the study was to evaluate the predictive performance of the BCI, and prediction of movement intention was more important than mere detection of intention after the movement had already happened. That is why while testing in a pseudo online paradigm, any intention detected within 2 seconds before the movement were only marked as true prediction. Any detection made after the event onset were disregarded from performance evaluation.

The results suggested that the average offline accuracy obtained by the happy emotion stimuli were significantly greater ($p<0.05$) than those obtained by sad and neutral emotion conditions. However, this relationship did not hold true for subjects 7 and 8, where sad stimuli resulted in better classification accuracy. The highest classification accuracy was achieved for subject 1 under happy emotion stimuli which was 97.4±1.1% and the lowest classification accuracy was achieved for subject 10 under neutral emotional state which was 82.3±2.1%. The overall classification sensitivity and specificity for all the emotion states showed no sign of biased classification as the sensitivity and specificity valuers were quite balanced as well.

In the case of pseudo online asynchronous testing, the results suggested the superiority of happy emotion stimuli over other emotion states at 95% significance level. But here too, there were some exceptions. Subjects 8, 10 achieved a greater true positive detection rate under neutral emotional state and subject 11 achieved a greater true positive detection rate under sad emotion stimuli with comparable FP/min and detection latency. The highest TPR was achieved for subject 2 which was 99.3 ± 0.4% under happy emotion stimulus. And the lowest TPR was achieved for subject 9 under sad emotion stimulus which was 64.0±7.2%.

The FP/min and detection latencies achieved under different emotional states did not show any statistically significance difference at 5% significance level. This outcome was significant because it suggested that happy emotion stimuli could enhance the true positive detection rate significantly without any deterioration in false positive detection and detection time. The detection times reported at different emotion states also suggested that the movement intentions could be detected on an average more than 1 second before the movement onset. This is promising as early detection could grant the associated assistive device much needed preparation time to adapt to the detected intention. This also would allow smooth transition

from one mode of movement to another thus resulting in natural movement and in turns successful neurorehabilitation.

Although the results suggested that happy emotion stimuli achieved overall better performances in both offline and online testing procedure, no correlation could be found between the scores assigned to the music stimuli and the corresponding classification performance. However, this is expected because emotion is a subjective phenomenon. Despite the preset scores given to the stimuli the affective effect on the individual is inherent to the participant himself. Therefore, a better way to quantify the relationship between the affective content of the stimulus and the resulting enhancement in movement intention detection performance should be investigated. One way to achieve that would be to quantify the effect of the stimuli on the neural correlates and find the correlation between the enhancement in detection accuracy and the quantified neural measurement of affective content in the stimuli. This issue will be addressed properly in future related studies.

The FP/min achieved by the study suggested that under all affective states, on an average approximately 5 to 6 false positive detections were made every minute. As decisions were made every two seconds, a total of 30 decisions were made every minute. This was a reasonable outcome in terms of FP/min. However, a better FP/min could be achieved but for that the TPR would go down dramatically. Also, it is to be noted that the detection window was [-2,0] s window corresponding to the onset of movement which included data from before the movement only. Inclusion of data from after the event onset might result in slightly better TPR and FP/min. Addition of data from after the event would remove the predictive nature of the proposed study which offered much needed preparation time for the assistive device. However, more advanced machine learning and decision-making techniques could be employed to further improve the performance of the study.

Comparison of the present study with existing studies is quite tricky. This is because there is no study which investigated into the effect of music stimuli on movement intention detection performance to the best of the authors' knowledge. Bai et al. [60] reported 40 ± 7% TPR with -620 ± 250 ms average detection latency using a [-1.5, 0] s detection window. Ibanez et al. [106] achieved a TPR of 60 ± 11% with 1.5 ± 0.1 FP/min and mean prediction period of more than 700 ms. Comparison with similar works suggested that the current method resulted in better TPR and detection times with a slightly higher FP/min. But it must be noted that the proposed study was totally predictive and decision-making criteria were different from the existing studies as well. However, extensive efforts are necessary for improving the results as well. This issue would be addressed in future extension of the study.

Investigating intelligent stimuli with targeted emotion content should have a stimulating effect on the proposed method's applicability. Although the outcomes of the current study are promising, it can be challenging to include music stimuli in clinical applications. Therefore, it would be interesting to investigate alternative methods to elicit targeted affective states in the user to enhance the chance to predict their movement intention. Moreover, the effect of emotion on more complicated movements, like gait, ankle dorsiflexion, should also be studied to find out whether the outcomes of this study are transferable and robust or not. Real-time studies are also necessary to validate the outcomes in a real-time setting. Advanced machine learning and numerical methods could also help enhance feature fusion and classification performance. The limitations of the proposed methods should be addressed extensively in future versions of the study.

7.5 Conclusion

The hypothesis of the study was to examine whether the inclusion of emotion evoking musical stimulus could result in enhanced movement intention detection performance. Analysis of EEG signals and corresponding online and offline testing suggested that happy music stimuli could work as a tool to enhance the distinguishability if movement intention from pre-movement EEG. However, further work is necessary to quantify the effect of music stimuli on neural signals. Whether there is a strict relationship between the affective content of the stimulus and the resulting detection performance is another question to look at. In general, advanced signal processing and learning techniques could be employed to enhance the current results even more. However, the current results show promising insights about the inclusion of music stimuli and its effect on movement intention, preparation and execution.

CHAPTER 8

VISION-ASSISTED TERRAIN TRANSITION PREDICTION

8.1 Background

The purpose of a powered assistive device is to reconnect the support, control, and actuation loops by interfacing with residual neuromusculoskeletal structures. This provides the immediate benefit of repairing and retraining physiological gait patterns, as well as the potential long-term benefit of recovering and retraining motor networks. The prosthesis and exoskeleton control systems involve some distinct agents which are: the environment, the user, the wearable device, and the hierarchical controller, according to Tucker et al.'s generalized control architecture [21]. There are also physical and sensory interactions between these elements. A hierarchical controller holding knowledge about the user status, the user intention, the wearable device state, as well as the state of the environment is required for movement control coordination amongst these contributing components. In response, the controller can supply the user with simulated sensory feedback and the required commands for the wearable device. Humans, by nature, have significant and volitional control over their limbs. Lower limb prosthesis must be able to respond to diverse terrains and movement modes or speeds, exactly like humans with intact motor abilities, in order to provide the user a natural mobility experience [140]. That is why it is vital to build a control system that enables for seamless operation of the connected prosthetic device while being responsive to changing environmental or topographical conditions.

8.2 Related Work

For smooth lower limb prostheses control, environmental context information can be employed to forecast human locomotor mode transition in advance. Mechanical measures [141, 142], electromyography (EMG) signals [143, 144], or inertial measurement units (IMUs) [145]— all of which are often delayed, user-dependent, and sensor position sensitive—were used to identify the locomotion mode changes. Some research has also been done on lower limb prosthesis, such as [146], who used computer vision to construct a depth sensing approach. They were able to distinguish different types of stairs using a depth camera and estimate their height, depth, and number of steps. Support vector machines (SVM) with a cubic kernel have also been used to identify different types of behaviors such as standing, walking, running, and going up or down stairs using depth sensing [147]. The terrain in front of the human was identified using a laser distance meter and an IMU-based system, which was then merged with the human's neuromuscular signals to forecast the user's locomotor task transitions. However, the laser distance meter's single-point information is insufficient to collect enough information on environmental elements [148]. Because of its informative, non-interruptive, and user-independent nature, computer vision has gotten a lot of attention in this area. Depth images were utilized to identify user movement or distinguish terrains (e.g., stairs and ramps) [149] using edge detection [146, 150], or 3-D point cloud classification [151]. Terrain recognition has also been attempted using RGB photos that are informative of terrain types [152]. Previous research has shown that scenarios with controlled modifications in the environment and human behavior can provide positive results. However, variations in the real-world environment and human behaviors must be studied for wearable robotics applications, and this remains a difficult task. Another difficulty in in-

corporating computer vision into wearable robots is the need for portability, which limits the sizes and positions of sensors and processors. Eyeglasses [148], chest [152], knee or shin [150, 151, 153], and waist have all been employed as sensor positions in current wearable robot designs to record environmental data (side [154] or front [149]).

Prediction of terrain transition on time is very critical for smooth transition between different terrains. Failure to enable timely prediction of terrain transitions can lead to increased safety hazard for the user. There can be two types of transitions that the user can go through. Type 1 occurs when the subject steps at the boundary of the two terrains and performed the next step onto the new terrain. In this case, the upcoming terrain can be clearly visible before the first step on it and predicting the transition becomes easier. The second type of transition occurs when the subject steps further away from the boundary. In this case, however, the camera captures images of the new terrain during mid swing phase of the gait and clear images appears very late and very close to the stepping moment on the new terrain. Conventional methods that rely on clean images obtained from cameras placed on higher parts of the body or through key frame selection might suffer or might be too late in predicting this type of transition. A demonstration of the two types of transitions obtained in this study are shown in fig. 8.1.

Recently, researchers used uncertainty prediction to try to forecast the environmental context for lower limb prostheses and achieved remarkable performances in predicting oncoming terrains [148, 155]. The study's findings are encouraging, however, the authors used multiple sensors to approach the problem. They used IMU sensors for gait stage recognition and to capture high quality or sharp images for inferring their model outputs. Also, their IMU based key frame selection method yielded the flat foot and early swing phase to be the most convenient period to

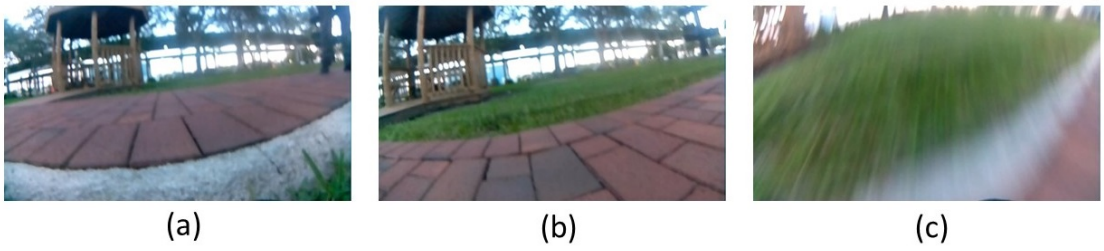

Figure 8.1: Example of two types of transitions.(a) shows a transition from grass to brick where the last step on grass is at the border of the two terrains. Here, the new terrain is very clearly visible and therefore prediction is easier. (b) and (c) show a transition from brick to grass where the last step on brick is far from the boundary between the two terrains and the mid-swing phase of the transitioning step occurs over the boundary. This results in blurry image over the new terrain and therefore makes the prediction difficult.

capture key images. This key frame selection algorithm, however, would fail in predicting transitions specially when the transition takes place at mid swing, i.e. the foot crosses the border of the two terrains while in mid or late swing stage. As a result a delayed transition prediction would take place. Moreover, the lower limb camera was placed on the knee which stays comparatively stationary than the ankle joint during gait and provides better quality images and a broader view of the upcoming terrain, thus making it comparatively easy to make accurate prediction. This also limits the usability of the system to people with amputations at or above the knee level because it seems somewhat unwanted to have an additional wearable camera system on the healthy portion of the amputated limb. As the wearable camera system cannot be concealed for continuous monitoring, placing the camera as low as possible is therefore desirable for the comfort of the user as well.

Moreover, current studies used cameras in multiple locations of the body, e.g., knee, glass and stand-alone, to create reliable labels and train their classifiers for terrain recognition and prediction. First of all, usage of multiple sensors requires additional effort in data handling, synchronization and adds to the computational

complexity of the system. The usage of multiple cameras may lead to improved classification accuracy but has the possibility of hindering the portability of the system by increasing the power and computational requirements [156]. In other studies involving autonomous driving systems, cameras and LiDARs (light detection and ranging) have been used to improve the reliability and accuracy of dynamic object perception [157]. Compared to existing studies, this study, investigated the incorporation of computer vision into a low latency asynchronous terrain transition prediction and control system for prosthetic devices in the face of varied terrains outside of the lab using a single camera placed in front of the user's ankle.

8.3 Current Study

In this study, we proposed an environmental context recognition framework for lower limb prostheses, which can detect the type of terrain and also predict any oncoming terrain transitions before the completion of the first step on the new terrain. The task is extremely challenging due to the need to utilize images severely affected by motion blur obtained under extremely dynamic conditions at the ankle joint. In contrast to previous work on clear or good quality images by placing the camera on a high body position and/or key frame selection, our task needs to handle blurred images or low quality images. We cannot ascertain whether the previous related work will still have good performance due to the worsened images. In this study we want to investigate performance of conventional approach and potentially develop an efficient method that can deal with low quality images in highly dynamic situations. For that purpose, we used a multi-frame decision fusion approach to enable early and accurate terrain transition prediction despite extreme motion blur. We considered five different types of terrains: asphalt, brick, concrete, grass and gravel for this

study. The usage of chip-on-board, portable, light weight, low-power raspberry pi device with wearable fish-eye camera mounted on the ankle of a healthy user enabled the continuous capture of surrounding environment. The camera was placed on the ankle to closely monitor the terrain type. Convolutional neural networks were designed using transfer learning [158] with shufflenet to recognize the terrain type at each frame of the video. Additionally, different frame rates were considered to monitor how the performance of the system changed in response to lowered frame rates. Moreover, the system performance was evaluated on five different terrain transition pairs, namely: grass-gravel, brick-grass, grass-asphalt, asphalt-gravel, and brick-concrete. The performance of the transition recognition system was evaluated using percentage of true positive detection, average detection time, and false positive detection rate.

8.4 Materials and Methods

8.4.1 Experimental Protocol

One healthy subject participated in the study. The participant provided informed, written consent to participate in our research approved by the Institution Review Board (IRB) of florida International University During the experiment, a lower limb device. The lower limb device was attached in front of the ankle of the participant. The device contained a Raspberry Pi 3 Model B, and a fisheye pi camera for wider view. The PiCamera recorded video at 25 FPS with a resolution of 1280×720. Data recorded by the camera was stored to an SD card in the Raspberry Pi. Figure 8.2 shows the construction of the used computer vision system and its placement on the user's body.

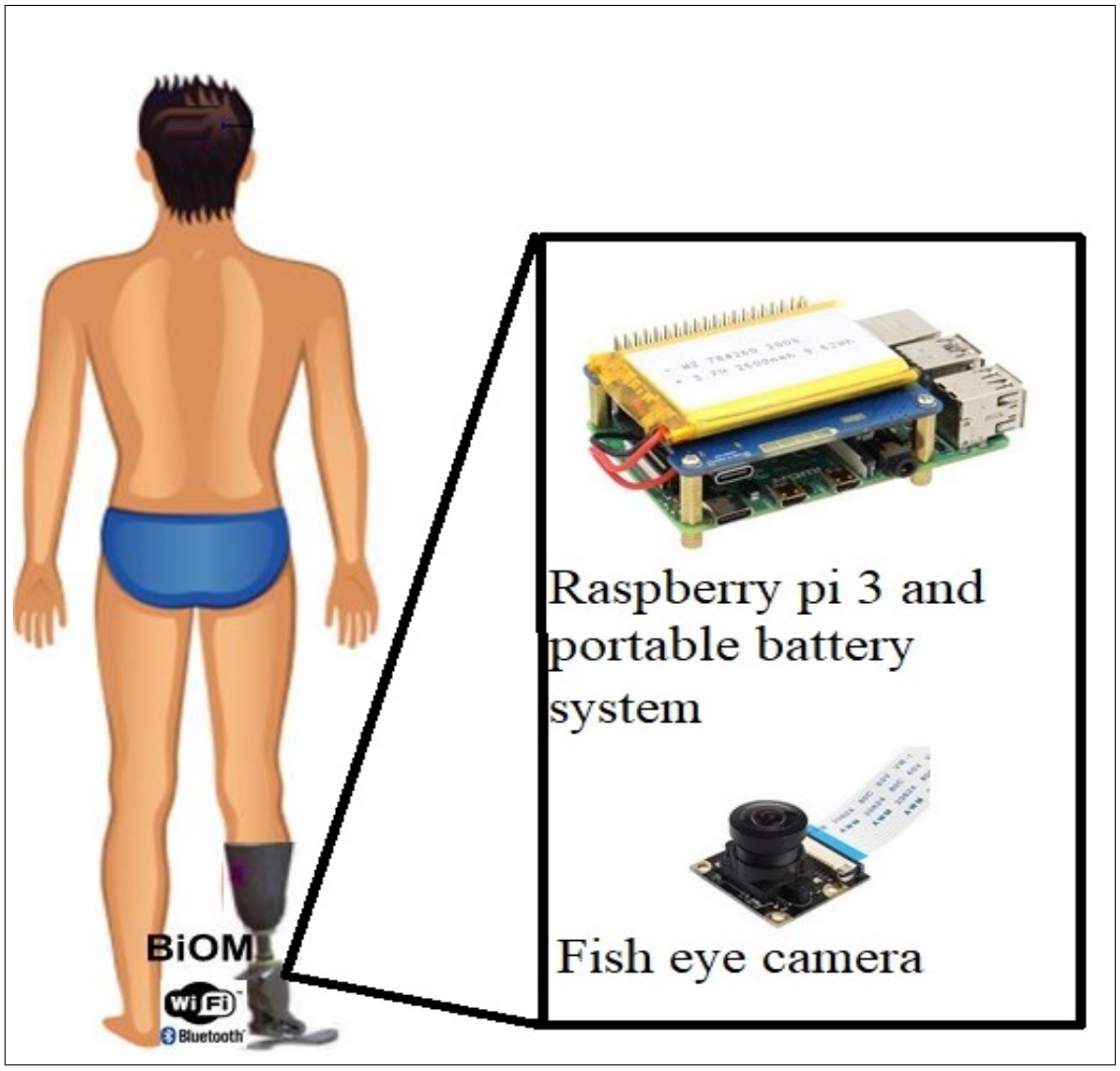

Figure 8.2: The portable camera system used in this study and its potential placement on a lower limb prosthesis. The system included a raspberry pi model 3 equipped with a portable battery system and a fish eye camera.

The participant walked freely in the Engineering campus of Florida International University in three difference sessions. Figure 8.3 show the examples of outdoor sites. The data set totals around 50 minutes of recording. The collection includes around 70000 RGB images— 13000 for brick, 17000 for grass, 14000 for asphalt, 14000 for concrete, and 11000 for gravel— from approximately 50-minute long video.

Figure 8.3: Example of outdoor sites for data collection. The first image shows grass and brick terrains, the second one shows asphalt, gravel and grass while the third portion shows the intersection of brick and concrete.

8.4.2 Image Preprocessing

The impact of foot contact during the stance phase and movement induced blur during the swing phase of gait would substantially degrade the image quality as the camera was placed at such a low elevation from the ground as the ankle. The image clarity could be considerably diminished, which had the potential of lowering the performance of the terrain recognition system based on computer vision and deep learning. Previous research has demonstrated that the foot accelerates at a virtually constant rate during the rest state of gait and as a result, the risk of image sharpness degradation is at an all-time low at this moment [148]. The flat foot of a gait cycle is defined as the time between when the foot initially strikes the ground

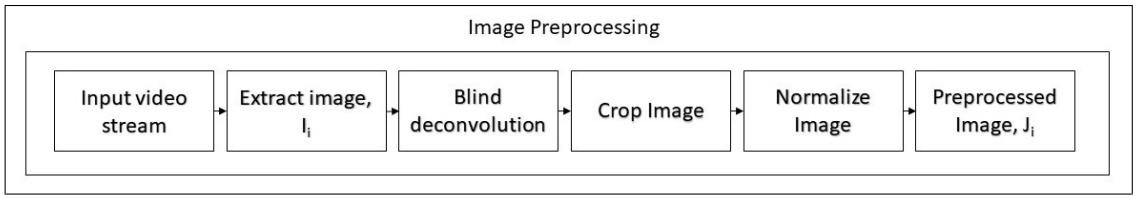

Figure 8.4: Image Preprocessing Pipeline.

and when the toes leave the floor. As the ankle moves periodically with the gait states, it is quite easy to detect the moment of flatfoot or rest state from an image sequence collected from the ankle camera. As stated before, the image quality at or close to the rest state, i.e. the double pivot, flat foot and early swing, is significantly better compared to the images collected at mid swing. Moreover, the camera showed the background and horizon at mid swing because the ankle is curled upwards at those points of time. Unlike previous studies, we use all the images which contain even partial information about the terrain. Therefore, for training our deep learning model, it was vital to ignore the images where held no information about the terrain. For this reason, we followed the following pipeline to preprocess the obtained images before training:

- Extract image frame.
- Perform blind deconvolution to remove motion blur. We used an array of one's as an initial estimate of the point-spread function in this step.
- Crop the image to obtain the lower quadrant of the image in front of the ankle camera.
- Normalize the pixel values of the cropped image between 0 and 255.
- If the processed image contained the terrain, it was used for training the terrain recognition model. otherwise, it was ignored and termed as background image.

Figure 8.4 shows the image processing pipeline used in this study. After the end of these steps, the images were labelled as one the corresponding terrain classes: asphalt, brick, concrete, grass or gravel.

8.5 Offline Training and testing

The whole dataset were divided in training, validation and testing sets. The goal of this study was to recognize the current terrain type and predict any oncoming terrain transition before the execution of the first step on the new terrain. The dataset in this study included images collected while the person walked on steady terrains and also contained images where the subject performed transitions from one terrain to another. For the purpose of the study, we used all the images corresponding to walking on single terrain and a portion (around 70%) of the images where the person performed terrain transition for training and validation. While, the remaining image sequences were kept aside for pseudo-online testing.

We used a popular deep learning model which is compact, computation efficient and optimized for operation in mobile environments: Shufflenet. This is a convolutional neural network that is trained on more than a million images from the ImageNet database [159]. The network can classify photos into 1000 different object categories and as a result has learned a variety of rich feature representations for a variety of images.

Shufflenet is [160] an incredibly computation-efficient convolutional neural network design. It is designed for low-processing-power mobile devices (e.g., 10-150 MFLOPs). The new architecture uses two novel operations: pointwise group convolution and channel shuffle, which reduce computation costs while maintaining

accuracy. It has reported better classification accuracy in multiple tasks in mobile environents compared to mobilenets [161].

In this study, we employed transfer learning to modify the pretrained shufflenet. To enable transfer learning, the following steps were followed:

- Recognize the last learnable layer of the base model. We kept the initial network unchanged till the last fully connected layer and replaced it with a fully connected layer of 5 components in the output layer and replaced the following softmax layers to match the size of our output which is 5.
- Data augmentation was used to prevent the classifier from learning specific details of the training dataset and make the trained model more robust and generalizable. We used scaling, translation and rotation for data augmentation.
- We used adam solver [162] with a fixed learning rate of 0.0001 with a mini batch size of 128 and validation frequency of 10.
- Regularization parameter of 0.0001 and the gradient threshold method of l_2-norm [163] was used to prevent overfitting.
- The value of gradient decay factor, epsilon and Squared Gradient Decay Factor were set to 0.9, 1×10^{-8} and 0.999 respectively.

8.5.1 Pseudo Online Testing

Fig. 8.5 shows the pseudo online testing framework used in the study. After the preprocessing steps discussed before, we resized the image, I_i to $224 \times 224 \times 3$ before feeding them into the base model. Then the processed image, J_i were passed to the learned classifier, H. The classifier output, $T(i)$ held the terrain type information

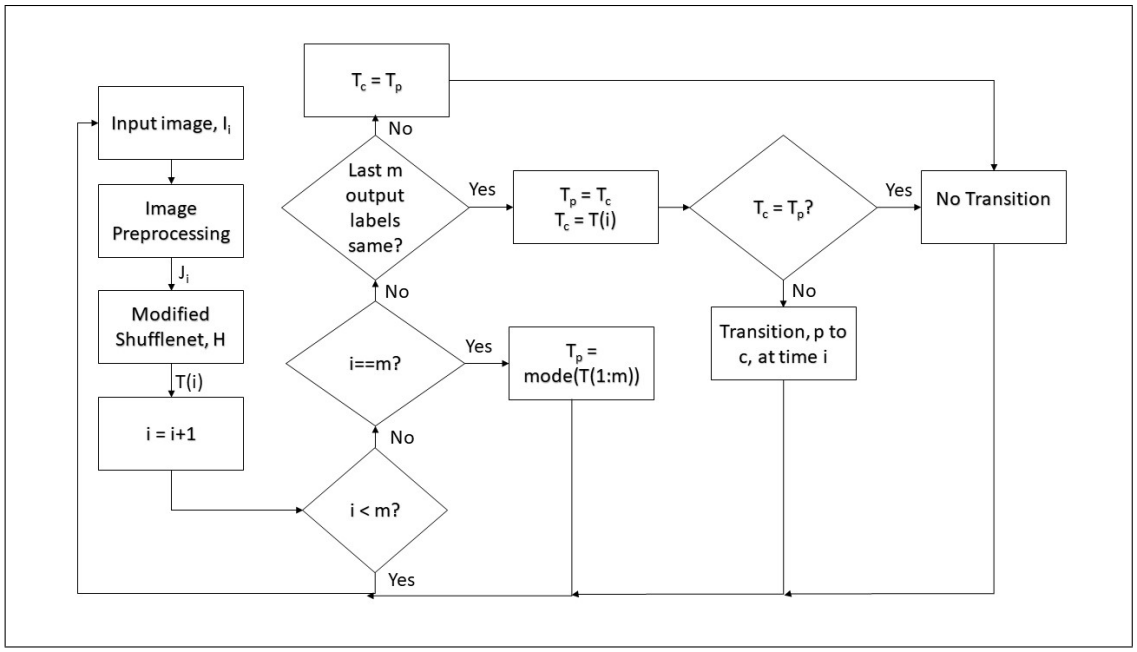

Figure 8.5: Flowchart of Pseudo-online terrain transition prediction pipeline using modified Shufflenet.

at time i. Now, because of the noisy nature of the images at midswing stage of gait, the classifier outputs at that portion were highly noisy and would result in misclassification of terrain type and would hinder the goal of the study. That is why, we introduced a simple state space based multi window decision fusion model in the inference stage to remove output noise. For this purpose, the terrain type outputs, $T(i)$ were stored and buffered for the first m number of images and after m images were classified, the output at mth image were updated as the mode of the last m classifier outputs. From the next frame onwards, the last m number of image class labels were monitored and if all of them returned the same label, only then the terrain type was updated. Otherwise, the terrain type was kept unchanged. Once the last m images were labelled as the same class, the output terrain type was updated. This process was repeated after every frame until the last frame of the video stream. This moving window decision fusion took care of the transitory noise

in classifier output resulting from movement artifacts, motion blur and rhythmic movement effect on the images specially during the midswing stage of gait.

The pseudo-online classification method was evaluated using multiple video framerates which included 25 FPS, 12.5 FPS, and 5 FPS. Clearly, recognizing the terrain transition and type of transition form lower FPS videos would be much difficult. However, the ability to recognize terrain types and terrain transitions using lower frame rates is crucial for such mobile operation. That is why, the model was evaluated using different Frame rates and the classifier performance was analyzed.

Moreover, the number of frames between two consecutive flat foots of a single leg was approximately 30-35 which amounts to nearly 1.2-1.5 seconds at 25 FPS. The choice of m is critical because too high a value would cause a faulty initiation of the system. On the other hand, a low value of m would make the system vulnerable to output noises caused by image quality. In this study, the value of m was kept at 5 for 25 FPS, 3 for 12.5 FPS, and 2 for 5 FPS.

8.6 Results and Discussion

The offline classification of terrain type was evaluated using cross validation accuracy and average validation loss. Figure8.6 shows the progression of training and validation accuracies and losses for modified Shufflenet. For both modified shufflenet and MobileNetV2, validation frequency was set to 10, which meant after every 10 iterations, the model was validated and the classification accuracy was reported.The final validation accuracy was found to be 97.66% and the final validation loss was 0.1768 for shufflenet. The training and validation accuracies were also very close, which mean the model was not overfitting the training data.

Table 8.1: Comaprison of Pseudo-online Transition Prediction Performance using proposed method and conventional method.

Transition type	Prediction latency<=-500 ms				Prediction latency<=-100 ms			
	True detection rate (%)		False positive/min		True detection rate (%)		False positive/min	
	Proposed	Conventional	Proposed	Conventional	Proposed	Conventional	Proposed	Conventional
Asphalt and gravel	90	80	1.5	40	100	90	1	26
Asphalt and grass	80	70	2	42	90	90	1	29
Brick and concrete	90	90	0	25	100	100	0	13
Grass and gravel	80	60	2	49	90	80	2	32
Brick and grass	88	76	2	37	94	88	1	21
Average	85.6	75.2	1.5	38.6	94.8	89.6	1	24.2

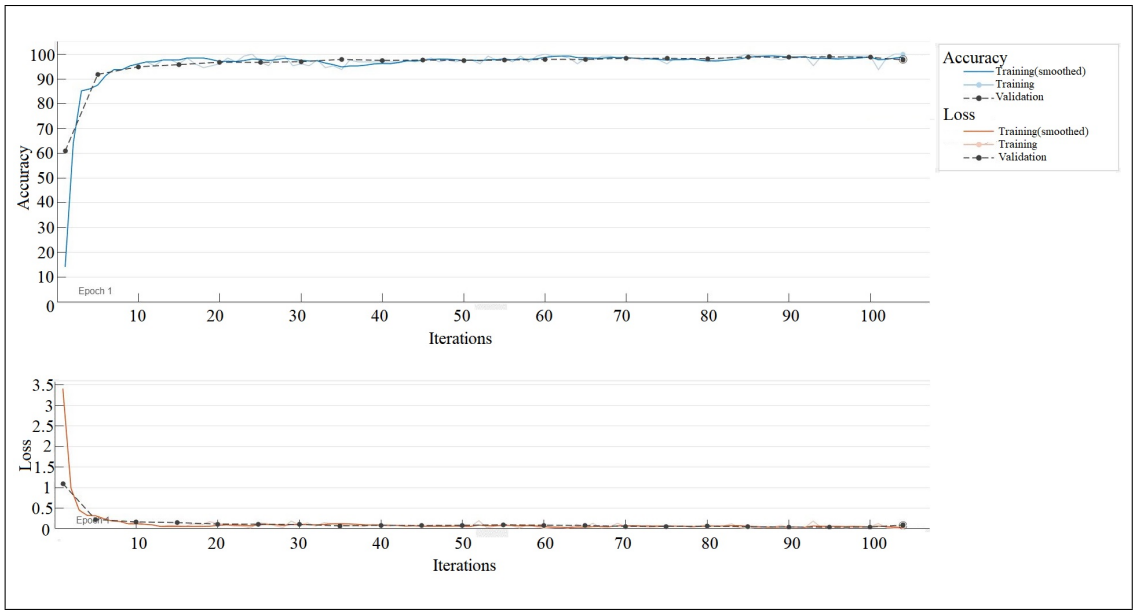

Figure 8.6: Offline Classification Results using modified Shufflenet. The final validation accuracy after 208 iterations was 97.66% and the validation loss was 0.1768.

Table 8.2: Comaprison of Pseudo-online Terrain Recognition Performance using Different Frame Rates.

Transition terrains (number of transitions)	Frame Rates	True prediction rate(%)	False prediction /min
Asphalt and Gravel (10)	25	90	1
	12.5	90	2
	5	90	1.5
Asphalt and Grass (10)	25	90	1
	12.5	80	1
	5	80	1
Brick and Concrete (10)	25	100	0
	12.5	100	0
	5	100	0
Grass and Gravel (10)	25	90	2
	12.5	80	2
	5	80	2
Brick and Grass (17)	25	94	1
	12.5	88	1.5
	5	82	3

The pseudo-online classification results are shown in table 8.2. The performance of pseudo-online classification was evaluated by number of true transition detection out of total number of transitions, number of late detection, number of missed transitions, number of false detection and the average detection time. The evaluation was done using multiple frame rates.

Table 8.2 shows some key outcomes of the study. First of all, it was found that shufflenet outperformed MobileNetV2 in terms of all the performance metrics across different frame rates. The finding was consistent with the offline classification accuracy and validation loss achieved by the two models. This outcome suggests that shufflenet was better suited for the proposed transition prediction pipeline. Moreover, it was observed that transition between brick and concrete was the easiest to predict while the most difficult task was to predict the transition between grass and gravel. This suggests that the definition of the boundary between the two terrains plays a very important role in the prediction performance. If the two terrains were very definitely separated, the system found it easier to predict the transition.

Moreover, there were two types of transitions that the subject went through. Type 1 was when the subject stepped at the boundary of the two terrains and performed the next step onto the new terrain. In this case, the upcoming terrain was clearly visible way earlier and predicting the transition was easier. The second type of transition occurred when the subject stepped further away from the boundary. In this case, however, the camera captured images of the new terrain during mid swing phase of the gait and clear images appeared very late and very close to the stepping moment on the new terrain. As a result, this type of transition was more difficult to predict. The transition between brick and grass contained a lot of examples of the second type and therefore the number of delayed and false predictions were a bit higher in that transition prediction task.

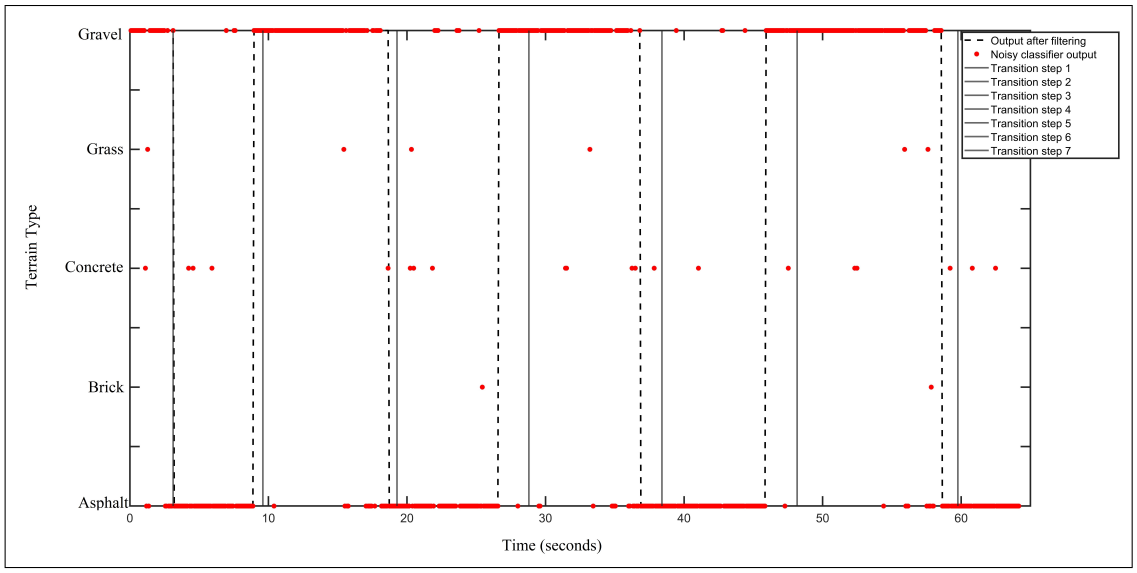

Figure 8.7: Pseudo-online terrain transition prediction example between asphalt and gravel. The figure shows that all the transitions were predicted before the actual transition step. Moreover, the output filtering method also removed some noisy classifier outputs and thus reduced false transition detection.

Figure 8.7 shows a detailed representation of a pseudo online terrain transition recognition between asphalt and gravel. The figure shows the performance of the proposed system in a one-minute segment of asphalt-gravel transition imagery. The red dots represent the classifier label of single image input. As can be seen from the figure, the classifier performed quite well on unseen test data, however, there were noisy outputs at times due to movement related noises and artifacts specially during the midswing phase of gait cycle where the images held partial information about the terrain. Our proposed pipeline of pseudo online testing removed the noisy and erroneous outputs and significantly reduced the classification errors by utilizing sliding window decision fusion. This also led to reduced false positive or false negative detection. It can also be noticed that all the transitions could be predicted on or before the completion of the step on the new terrain which is a very desirable outcome for terrain adaptive prosthesis.

Table 8.1 shows the comparison of pseudo-online classification performance using our proposed method and a conventional method. The conventional model was trained on the cleanest images obtained during the rest stage of the gait cycle only. Moreover, no multi-window decision fusion was applied to the classification results. Moreover, the comparison was performed under two different conditions. At first the minimum required prediction latency was set to -500 ms and later performances were compared at -100 ms latency as well. Hypothetically, it would be more difficult to correctly predict upcoming transitions further away from the transition boundary. Results suggest that our proposed model resulted in higher true prediction rate and lower false positive/ min in both comparison conditions. Interestingly, the number of false positive detections was much higher using the conventional method. Understandably, this model struggled to correctly recognize terrain type in the event of noisy input image appearing at swing phase of gait. Our proposed pipeline of pseudo online testing removed the noisy and erroneous outputs and significantly reduced the classification errors by utilizing sliding window decision fusion. This also led to reduced false positive or false negative detection. This improvement shows the efficacy of the multi-window decision fusion algorithm. Another interesting observation that could be made was the conventional model performed comparatively better closer to the transitioning step. It is expected because as we moved closer to the completion of the transitioning step, much clearer images appeared which helped the conventional model make more correct decisions. However, the number of false positives remained high due to the errors made during the swing phase of non-transitioning steps.

Table 8.2 shows some other key outcomes of the study. It was observed that transition between brick and concrete was the easiest to predict while the most difficult task was to predict the transition between grass and gravel. This suggests

that the definition of the boundary between the two terrains plays a very important role in the prediction performance. If the two terrains were very definitely separated, the system found it easier to predict the transition.

Table 8.2 suggests that with lower frame rate of the input video, it got difficult to predict oncoming transitions. The best performance was achieved with 25 FPS input video. However, with lowered frame rates as well, the system worked reasonably well with very little declination is performance specially at 12.5, and 5 FPS. The transition between brick and grass occurred more frequently as the brick pavement between two grass fields was very narrow. As a result it was more challenging to predict this transition at lower frame rates. The prediction times had negative average values throughout all frame rates and transition types. This outcome suggests that the modified shufflenet based terrain prediction system could predict terrain transitions 500ms to 1300ms before the transition on average. Moreover, unlike other studies, the current study only utilizes a single optimized deep learning network assisted by a simple state space based inference model which utilizes multi window decision fusion. Therefore, the size and computation requirement of the model is lesser. The outcome is very promising from a real-time monitoring and transition prediction point of view.

The proposed study was carried out in a personal computer with a NVIDIA GeForce RTX 2080 TI Graphics Card and on this system, every image was classified in approximately 10 ms. At 25, 12.5, and 5 FPS framerates, frame to frame time difference, δ is approximately 40ms, 80ms, and 200 ms. This suggests that the execution time suggests that the proposed algorithms could run without causing any frame to frame overlap or execution delay. Moreover, the system showed robust performance in the event of diminishing frame rates which suggested its efficacy in performing at lower frame rates and therefore in reducing power and computational

requirements. Recently few studies have employed deep learning models on embedded platforms [148, 155] with similar processing times. Our proposed systems also shows promise to be implemented in real time using embedded platforms. This task should be carried out in future versions of this study.

An approach of dynamic frame selection based on the gait stage information obtained from the IMU sensors was used in [155]. Moreover, a combination of Bayesian neural network and Bayesian gated recurrent units (BGRU) was used to detect terrain types. However, our study suggested that the images obtained during the mid swing phase of gait were mostly affected by motion blur and noise. And that part of gait only constitute around 20% of the whole gait cycle. The rest of the cycle produced comparatively less noisy and usable image. That is why, we hypothesized that instead of spending computational power and adding sensor networks for recognizing noise free images, desirable system performance could be achieved by simply filtering out noisy outputs of the model due to blurred and low-quality inputs. For that purpose, we introduced a simple multi-window decision fusion algorithm which smoothed out noisy prediction of the model based on previous output states. The results suggested that the proposed methodology performed remarkably well even in low frame rates.

Comparsion with current studies is quite tricky. Because, no other studies reported transition prediction accuracies and detection latencies in online or pseudo-online scenarios to the knowledge of the authors. Moreover, previous studies either used multiple sensor networks like IMU, LiDar, lasers, multiple cameras to capture environmental information. However, as discussed earlier, usage of multiple sensors and cameras pose the problem of synchronicity and increase computational load. Moreover, previous studies used cameras places on or above the knee level [148, 155]. It is desired to place the camera system as low as possible from a user's

point of view so that the system does not create inconvenience and discomfort in long term usage. Moreover, the knee joint is comparatively more stable during gait phases. Increased motion artifacts makes terrain transition prediction from ankle camera system more challenging. Despite these challenges, the proposed method showed very good classification accuracy of 97.66% in a 5-class classification problem which is comparable to previous studies. However, unlike previous works, this study only utilized a single camera system and the used model was also comparatively simpler. The proposed model utilized the fact that the midswing phase of gait was responsible for most of the blurred images, however, midswing constituted only 20% of the whole gait cycle [164]. Inspired by this fact, we hypothesized that instead of allocating computational resources behind finding key frames, a desired level of output could be achieved by filtering out noisy classifier outputs at midswing by using a simple multi window decision fusion. The results of the study validated the hypothesis by portraying robust transition prediction performance even at low frame rates. This is a promising outcome in terms of applicability in real-time assistive systems.

8.7 Conclusion

In this study, we suggested an environmental context identification framework for lower limb prosthesis, which can recognize terrain type and predict any upcoming terrain transitions before the completion of the first step on the new terrain. Unlike previous studies, the work utilized information from blurred images and removed the noise in model outputs using a sliding-window decision fusion approach. For this study, we looked at five distinct types of terrain: asphalt, brick, concrete, grass, and gravel. The continuous capture of the surrounding environment was made possible

by using a chip-on-board, portable, light-weight, low-power Raspberry Pi system with a wearable fish-eye camera mounted on the ankle of a healthy user. To distinguish the terrain type at each frame of the video, a convolutional neural network was created using a modified shufflenet. Different frame rates were also investigated in order to see how the system's performance altered as the frame rate was reduced. The technology was also tested on five various terrain transition pairs, including grass-gravel, brick-grass, grass-gravel, asphalt-gravel, and brick-concrete. The true positive detection metrics, average detection time, and false positive detection rate were used to assess the performance of the transition recognition system. Comparison with a convention model trained using high quality images obtained at the rest state of gait revealed that the proposed method resulted in higher true positive rate and lower false positive detection/ min. The outcomes of this study is a highly accurate terrain recognition and transition prediction framework which can predict the oncoming terrain transition from 500 ms to 1300 ms before the first step on the new terrain despite using highly blurred images obtained in extremely dynamic conditions, and thus shows promise to be used in real-time adaptive assistive technologies.

BIBLIOGRAPHY

[1] N. Sharma and L. G. Cohen, "Recovery of motor function after stroke," *Developmental Psychobiology*, vol. 54, no. 3, pp. 254–262, 2012.

[2] R. Bonita and R. Beaglehole, "Recovery of motor function after stroke.," *Stroke*, vol. 19, no. 12, pp. 1497–1500, 1988.

[3] Centers for Disease Control and Prevention, "Difficulties in physical functioning among adults aged 18 and over, by selected characteristics: United States, 2014," tech. rep., 2014.

[4] K. Ziegler-Graham, E. J. MacKenzie, P. L. Ephraim, T. G. Travison, and R. Brookmeyer, "Estimating the prevalence of limb loss in the united states: 2005 to 2050," *Archives of physical medicine and rehabilitation*, vol. 89, no. 3, pp. 422–429, 2008.

[5] M. Owings and L. J. Kozak, *Ambulatory and inpatient procedures in the United States, 1996*. No. 139, US Department of Health and Human Services, Centers for Disease Control and Prevention, National Center for Health Statistics, 1998.

[6] E. Buch, C. Weber, L. G. Cohen, C. Braun, M. A. Dimyan, T. Ard, J. Mellinger, A. Caria, S. Soekadar, A. Fourkas, *et al.*, "Think to move: a neuromagnetic brain-computer interface (bci) system for chronic stroke," *Stroke*, vol. 39, no. 3, pp. 910–917, 2008.

[7] A. R. Donati, S. Shokur, E. Morya, D. S. Campos, R. C. Moioli, C. M. Gitti, P. B. Augusto, S. Tripodi, C. G. Pires, G. A. Pereira, *et al.*, "Long-term training with a brain-machine interface-based gait protocol induces partial neurological recovery in paraplegic patients," *Scientific reports*, vol. 6, no. 1, pp. 1–16, 2016.

[8] J.-M. Belda-Lois, S. Mena-del Horno, I. Bermejo-Bosch, J. C. Moreno, J. L. Pons, D. Farina, M. Iosa, M. Molinari, F. Tamburella, A. Ramos, *et al.*, "Rehabilitation of gait after stroke: a review towards a top-down approach," *Journal of neuroengineering and rehabilitation*, vol. 8, no. 1, pp. 1–20, 2011.

[9] J. T. Gwin, K. Gramann, S. Makeig, and D. P. Ferris, "Removal of movement artifact from high-density eeg recorded during walking and running," *Journal of neurophysiology*, vol. 103, no. 6, pp. 3526–3534, 2010.

[10] J. Wagner, T. Solis-Escalante, P. Grieshofer, C. Neuper, G. Müller-Putz, and R. Scherer, "Level of participation in robotic-assisted treadmill walking modulates midline sensorimotor eeg rhythms in able-bodied subjects," *NeuroImage*, vol. 63, no. 3, pp. 1203 – 1211, 2012.

[11] K. Y. Nam, H. J. Kim, B. S. Kwon, J.-W. Park, H. J. Lee, and A. Yoo, "Robot-assisted gait training (lokomat) improves walking function and activity in people with spinal cord injury: a systematic review," *Journal of NeuroEngineering and Rehabilitation*, vol. 14, p. 24, Mar 2017.

[12] M. Nakanishi, Y. Wang, Y.-T. Wang, Y. Mitsukura, and T.-P. Jung, "A high-speed brain speller using steady-state visual evoked potentials," *International Journal of Neural Systems*, vol. 24, no. 06, p. 1450019, 2014. PMID: 25081427.

[13] J. Li, H. Ji, L. Cao, D. Zang, R. Gu, B. Xia, and Q. Wu, "Evaluation and application of a hybrid brain computer interface for real wheelchair parallel control with multi-degree of freedom," *International Journal of Neural Systems*, vol. 24, no. 04, p. 1450014, 2014. PMID: 24694169.

[14] A. H. Do, P. T. Wang, C. E. King, S. N. Chun, and Z. Nenadic, "Brain-computer interface controlled robotic gait orthosis," *Journal of NeuroEngineering and Rehabilitation*, vol. 10, no. 1, pp. 1–7, 2013.

[15] M. A. Lebedev and M. A. L. Nicolelis, "Brain-Machine Interfaces: From Basic Science to Neuroprostheses and Neurorehabilitation," *Physiological Reviews*, vol. 97, no. 2, pp. 767–837, 2017.

[16] J. L. Contreras-Vidal and R. G. Grossman, "NeuroRex: A clinical neural interface roadmap for EEG-based brain machine interfaces to a lower body robotic exoskeleton," *Proceedings of the Annual International Conference of the IEEE Engineering in Medicine and Biology Society, EMBS*, pp. 1579–1582, 2013.

[17] Y. He, D. Eguren, T. P. Luu, and J. L. Contreras-Vidal, "Risk management and regulations for lower limb medical exoskeletons: a review," *Medical devices (Auckland, NZ)*, vol. 10, p. 89, 2017.

[18] M. Arazpour, S. W. Hutchins, and M. Ahmadi Bani, "The efficacy of powered orthoses on walking in persons with paraplegia," *Prosthetics and orthotics international*, vol. 39, no. 2, pp. 90–99, 2015.

[19] J. M. Antelis, L. Montesano, A. Ramos-Murguialday, N. Birbaumer, and J. Minguez, "Continuous decoding of intention to move from contralesional hemisphere brain oscillations in severely affected chronic stroke patients," in *2012 Annual International Conference of the IEEE Engineering in Medicine and Biology Society*, pp. 4099–4103, Aug 2012.

[20] E. López-Larraz, J. M. Antelis, L. Montesano, A. Gil-Agudo, and J. Minguez, "Continuous decoding of motor attempt and motor imagery from eeg activity in spinal cord injury patients," in *2012 Annual International Conference of the IEEE Engineering in Medicine and Biology Society*, pp. 1798–1801, Aug 2012.

[21] M. R. Tucker, J. Olivier, A. Pagel, H. Bleuler, M. Bouri, O. Lambercy, J. d. R. Millán, R. Riener, H. Vallery, and R. Gassert, "Control strategies for active lower extremity prosthetics and orthotics: a review," *Journal of neuroengineering and rehabilitation*, vol. 12, no. 1, pp. 1–30, 2015.

[22] J. d. R. Millán, R. Rupp, G. Mueller-Putz, R. Murray-Smith, C. Giugliemma, M. Tangermann, C. Vidaurre, F. Cincotti, A. Kubler, R. Leeb, *et al.*, "Combining brain–computer interfaces and assistive technologies: state-of-the-art and challenges," *Frontiers in neuroscience*, p. 161, 2010.

[23] J. R. Millán, F. Renkens, J. Mourino, and W. Gerstner, "Noninvasive brain-actuated control of a mobile robot by human eeg," *IEEE Transactions on biomedical Engineering*, vol. 51, no. 6, pp. 1026–1033, 2004.

[24] T. Carlson and J. d. R. Millan, "Brain-controlled wheelchairs: a robotic architecture," *IEEE Robotics & Automation Magazine*, vol. 20, no. 1, pp. 65–73, 2013.

[25] F. Sup, H. A. Varol, and M. Goldfarb, "Upslope walking with a powered knee and ankle prosthesis: initial results with an amputee subject," *IEEE transactions on neural systems and rehabilitation engineering*, vol. 19, no. 1, pp. 71–78, 2010.

[26] L. Peeraer, B. Aeyels, and G. Van der Perre, "Development of emg-based mode and intent recognition algorithms for a computer-controlled above-knee prosthesis," *Journal of biomedical engineering*, vol. 12, no. 3, pp. 178–182, 1990.

[27] Y. D. Li and E. T. Hsiao-Wecksler, "Gait mode recognition and control for a portable-powered ankle-foot orthosis," in *2013 IEEE 13th International Conference on Rehabilitation Robotics (ICORR)*, pp. 1–8, IEEE, 2013.

[28] F. Zhang, Z. Fang, M. Liu, and H. Huang, "Preliminary design of a terrain recognition system," in *2011 annual international conference of the IEEE engineering in medicine and biology society*, pp. 5452–5455, IEEE, 2011.

[29] H. Kawamoto, S. Lee, S. Kanbe, and Y. Sankai, "Power assist method for hal-3 using emg-based feedback controller," in *SMC'03 Conference Proceedings. 2003 IEEE International Conference on Systems, Man and Cybernetics. Conference Theme-System Security and Assurance (Cat. No. 03CH37483)*, vol. 2, pp. 1648–1653, IEEE, 2003.

[30] C. D. Hoover, G. D. Fulk, and K. B. Fite, "The design and initial experimental validation of an active myoelectric transfemoral prosthesis," *Journal of Medical Devices*, vol. 6, no. 1, 2012.

[31] L. Hargrove, A. Simon, R. Lipschutz, S. Finucane, and T. Kuiken, "Real-time myoelectric control of knee and ankle motions for transfemoral amputees,," *JAMA - Journal of the*, 2011.

[32] L. J. Hargrove, A. M. Simon, R. D. Lipschutz, S. B. Finucane, and T. A. Kuiken, "Real-time myoelectric control of knee and ankle motions for transfemoral amputees," *JAMA*, vol. 305, no. 15, pp. 1542–1544, 2011.

[33] C. Fleischer, C. Reinicke, and G. Hommel, "Predicting the intended motion with emg signals for an exoskeleton orthosis controller," in *2005 IEEE/RSJ International Conference on Intelligent Robots and Systems*, pp. 2029–2034, IEEE, 2005.

[34] N. Karavas, A. Ajoudani, N. Tsagarakis, J. Saglia, A. Bicchi, and D. Caldwell, "Tele-impedance based assistive control for a compliant knee exoskeleton," *Robotics and Autonomous Systems*, vol. 73, pp. 78–90, 2015.

[35] S. K. Au, P. Bonato, and H. Herr, "An emg-position controlled system for an active ankle-foot prosthesis: an initial experimental study," in *9th International Conference on Rehabilitation Robotics, 2005. ICORR 2005.*, pp. 375–379, IEEE, 2005.

[36] D. P. Ferris, K. E. Gordon, G. S. Sawicki, and A. Peethambaran, "An improved powered ankle–foot orthosis using proportional myoelectric control," *Gait & posture*, vol. 23, no. 4, pp. 425–428, 2006.

[37] H. A. Varol, F. Sup, and M. Goldfarb, "Multiclass real-time intent recognition of a powered lower limb prosthesis," *IEEE Transactions on Biomedical Engineering*, vol. 57, no. 3, pp. 542–551, 2009.

[38] E. Wentink, S. Beijen, H. Hermens, J. Rietman, and P. Veltink, "Intention detection of gait initiation using EMG and kinematic data," *Gait & Posture*, vol. 37, pp. 223–228, 2 2013.

[39] R. Atri, J. Marquez, C. Leung, M. Siddiquee, D. Murphy, A. Gorgey, W. Lovegreen, D.-Y. Fei, and O. Bai, "Smart Data-Driven Optimization of Powered Prosthetic Ankles Using Surface Electromyography," *Sensors*, vol. 18, p. 2705, 8 2018.

[40] H. H. Kornhuber and L. Deecke, "Changes in the brain potential in voluntary movements and passive movements in man: readiness potential and reafferent potentials.," *Pflugers Archiv fur die gesamte Physiologie des Menschen und der Tiere*, vol. 284, pp. 1–17, 5 1965.

[41] H. Shibasaki and M. Hallett, "What is the Bereitschaftspotential?," *Clinical Neurophysiology*, vol. 117, pp. 2341–2356, 11 2006.

[42] A. Shakeel, M. S. Navid, M. N. Anwar, S. Mazhar, M. Jochumsen, and I. K. Niazi, "A review of techniques for detection of movement intention using movement-related cortical potentials," *Computational and Mathematical Methods in Medicine*, vol. 2015, 2015.

[43] G. Pfurtscheller and A. Aranibar, "Evaluation of event-related desynchronization (ERD) preceding and following voluntary self-paced movement," *Electroencephalography and Clinical Neurophysiology*, vol. 46, pp. 138–146, 2 1979.

[44] G. Pfurtscheller and C. Neuper, "Event-related synchronization of mu rhythm in the eeg over the cortical hand area in man," *Neuroscience Letters*, vol. 174, no. 1, pp. 93 – 96, 1994.

[45] G. Cheron, M. Duvinage, C. De Saedeleer, T. Castermans, A. Bengoetxea, M. Petieau, K. Seetharaman, T. Hoellinger, B. Dan, T. Dutoit, F. Sylos Labini, F. Lacquaniti, and Y. Ivanenko, "From spinal central pattern generators to

cortical network: integrated BCI for walking rehabilitation.," *Neural plasticity*, vol. 2012, p. 375148, jan 2012.

[46] M. Severens, B. Nienhuis, P. Desain, and J. Duysens, "Feasibility of measuring event related desynchronization with electroencephalography during walking," in *2012 Annual International Conference of the IEEE Engineering in Medicine and Biology Society*, pp. 2764–2767, Aug 2012.

[47] G. Pfurtscheller and F. L. da Silva, "Event-related eeg/meg synchronization and desynchronization: basic principles," *Clinical Neurophysiology*, vol. 110, no. 11, pp. 1842 – 1857, 1999.

[48] E. Lew, R. Chavarriaga, S. Silvoni, and J. d. R. Millán, "Detection of self-paced reaching movement intention from eeg signals," *Frontiers in Neuroengineering*, vol. 5, p. 13, 2012.

[49] E. Hortal, A. Úbeda, E. Iáñez, J. M. Azorín, and E. Fernández, "EEG-Based Detection of Starting and Stopping During Gait Cycle," *International Journal of Neural Systems*, vol. 26, no. 07, p. 1650029, 2016.

[50] M. Ortiz, E. Ianez, M. Rodriguez-Ugarte, and J. M. Azorin, "Empirical mode decomposition use in electroencephalography signal analysis for detection of starting and stopping intentions during gait cycle," *RO-MAN 2017 - 26th IEEE International Symposium on Robot and Human Interactive Communication*, vol. 2017-Janua, pp. 94–100, 2017.

[51] R. Xu, N. Jiang, C. Lin, N. Mrachacz-Kersting, K. Dremstrup, and D. Farina, "Enhanced low-latency detection of motor intention from EEG for closed-loop brain-computer interface applications," *IEEE Transactions on Biomedical Engineering*, vol. 61, no. 2, pp. 288–296, 2014.

[52] C. Lin, B. H. Wang, N. Jiang, R. Xu, N. Mrachacz-Kersting, and D. Farina, "Discriminative manifold learning based detection of movement-related cortical potentials," *IEEE Transactions on Neural Systems and Rehabilitation Engineering*, vol. 24, no. 9, pp. 921–927, 2016.

[53] O. Bai, P. Lin, S. Vorbach, J. Li, S. Furlani, and M. Hallett, "Exploration of computational methods for classification of movement intention during human voluntary movement from single trial eeg," *Clinical Neurophysiology*, vol. 118, no. 12, pp. 2637 – 2655, 2007.

[54] A. Savić, R. Lontis, N. Jiang, M. Popović, D. Farina, K. Dremstrup, and N. Mrachacz-Kersting, "Movement related cortical potentials and sensory motor rhythms during self initiated and cued movements," in *Replace, Repair, Restore, Relieve – Bridging Clinical and Engineering Solutions in Neurorehabilitation* (W. Jensen, O. K. Andersen, and M. Akay, eds.), (Cham), pp. 701–707, Springer International Publishing, 2014.

[55] A. I. Sburlea, L. Montesano, and J. Minguez, "Continuous detection of the self-initiated walking pre-movement state from EEG correlates without session-to-session recalibration," *Journal of Neural Engineering*, vol. 12, no. 3, 2015.

[56] A. I. Sburlea, L. Montesano, R. Cano-De La Cuerda, I. M. Alguacil Diego, J. C. Miangolarra-Page, and J. Minguez, "Detecting intention to walk in stroke patients from pre-movement EEG correlates," *Journal of NeuroEngineering and Rehabilitation*, vol. 12, no. 1, pp. 1–12, 2015.

[57] P. Velu and V. de Sa, "Single-trial classification of gait and point movement preparation from human eeg," *Frontiers in Neuroscience*, vol. 7, p. 84, 2013.

[58] A. Presacco, L. Forrester, and J. L. Contreras-Vidal, "Towards a non-invasive brain-machine interface system to restore gait function in humans," in *2011 Annual International Conference of the IEEE Engineering in Medicine and Biology Society*, pp. 4588–4591, Aug 2011.

[59] N. Jiang, L. Gizzi, N. Mrachacz-Kersting, K. Dremstrup, and D. Farina, "A brain–computer interface for single-trial detection of gait initiation from movement related cortical potentials," *Clinical Neurophysiology*, vol. 126, no. 1, pp. 154 – 159, 2015.

[60] O. Bai, V. Rathi, P. Lin, D. Huang, H. Battapady, D.-Y. Fei, L. Schneider, E. Houdayer, X. Chen, and M. Hallett, "Prediction of human voluntary movement before it occurs," *Clinical Neurophysiology*, vol. 122, no. 2, pp. 364 – 372, 2011.

[61] J. Ibáñez, J. I. Serrano, M. D. del Castillo, L. Barrios, J. Á. Gallego, and E. Rocon, "An eeg-based design for the online detection of movement intention," in *Advances in Computational Intelligence* (J. Cabestany, I. Rojas, and G. Joya, eds.), (Berlin, Heidelberg), pp. 370–377, Springer Berlin Heidelberg, 2011.

[62] S.-H. Oh, Y.-R. Lee, and H.-N. Kim, "A Novel EEG Feature Extraction Method Using Hjorth Parameter," *International Journal of Electronics and Electrical Engineering*, pp. 106–110, 2014.

[63] M. Martin-Loeches, J. Garcia-Trapero, P. Gil, and F. J. Rubia, "Topography of mobility and complexity parameters of the EEG in Alzheimer's disease.," *Biological psychiatry*, vol. 30, pp. 1111–21, 12 1991.

[64] T. Cecchin, R. Ranta, L. Koessler, O. Caspary, H. Vespignani, and L. Maillard, "Seizure lateralization in scalp EEG using Hjorth parameters," *Clinical Neurophysiology*, vol. 121, pp. 290–300, 3 2010.

[65] A. Mert and A. Akan, "Emotion recognition from EEG signals by using multivariate empirical mode decomposition," *Pattern Analysis and Applications*, vol. 21, pp. 81–89, 2 2018.

[66] O. Turk, M. Seker, V. Akpolat, and M. S. Ozerdem, "Classification of mental task eeg records using hjorth parameters," in *2017 25th Signal Processing and Communications Applications Conference (SIU)*, pp. 1–4, May 2017.

[67] D. Winter and H. J Yack, "Emg profiles during normal human walking: stride-to-stride and inter-subject variability," *Electroencephalography and clinical neurophysiology*, vol. 67, pp. 402–11, 12 1987.

[68] J. Sebastian Marquez, R. Atri, and O. Bai, "Exploration of metrics for leg length discrepancy using a wearable gait analysis system," in *2018 40th Annual International Conference of the IEEE Engineering in Medicine and Biology Society (EMBC)*, pp. 1–4, July 2018.

[69] M. R. Siddiquee, J. S. Marquez, R. Atri, R. Ramon, R. P. Mayrand, and O. Bai, "Movement artefact removal from nirs signal using multi-channel imu data," *BioMedical Engineering OnLine*, vol. 17, no. 1, p. 120, 2018.

[70] A. Delorme and S. Makeig, "EEGLAB: an open sorce toolbox for analysis of single-trail EEG dynamics including independent component anlaysis," *Journal of Neuroscience Methods*, vol. 134, pp. 9–21, 2004.

[71] T. Mullen, C. Kothe, Y. M. Chi, A. Ojeda, T. Kerth, S. Makeig, G. Cauwenberghs, and T. Jung, "Real-time modeling and 3d visualization of source dynamics and connectivity using wearable eeg," in *2013 35th Annual International Conference of the IEEE Engineering in Medicine and Biology Society (EMBC)*, pp. 2184–2187, July 2013.

[72] C. Chang, S. Hsu, L. Pion-Tonachini, and T. Jung, "Evaluation of artifact subspace reconstruction for automatic eeg artifact removal," in *2018 40th Annual International Conference of the IEEE Engineering in Medicine and Biology Society (EMBC)*, pp. 1242–1245, July 2018.

[73] M. Chaumon, D. V. Bishop, and N. A. Busch, "A practical guide to the selection of independent components of the electroencephalogram for artifact correction," *Journal of Neuroscience Methods*, vol. 250, pp. 47–63, 2015.

[74] J. A. Palmer, K. Kreutz-Delgado, and S. Makeig, "Amica: An adaptive mixture of independent component analyzers with shared components," *Swartz Center for Computatonal Neursoscience, University of California San Diego, Tech. Rep*, 2012.

[75] A. Delorme, J. Palmer, J. Onton, R. Oostenveld, and S. Makeig, "Independent EEG Sources Are Dipolar," *PLoS ONE*, vol. 7, p. e30135, 2 2012.

[76] S.-H. Hsu, L. Pion-Tonachini, J. Palmer, M. Miyakoshi, S. Makeig, and T.-P. Jung, "Modeling brain dynamic state changes with adaptive mixture independent component analysis," 2018.

[77] M. Ortiz, M. Rodríguez-Ugarte, E. Iáñez, and J. M. Azorín, "Application of the stockwell transform to electroencephalographic signal analysis during gait cycle," *Frontiers in Neuroscience*, 2017.

[78] W. H. Kruskal, "Historical notes on the wilcoxon unpaired two-sample test," *Journal of the American Statistical Association*, vol. 52, no. 279, pp. 356–360, 1957.

[79] B. E. Boser, I. M. Guyon, and V. N. Vapnik, "A training algorithm for optimal margin classifiers," in *Proceedings of the Fifth Annual Workshop on Computational Learning Theory*, COLT '92, (New York, NY, USA), pp. 144–152, ACM, 1992.

[80] S. Holm, "A simple sequentially rejective multiple test procedure," *Scandinavian Journal of Statistics*, vol. 6, no. 2, pp. 65–70, 1979.

[81] L. Pion-Tonachini, S.-H. Hsu, S. Makeig, T.-P. Jung, and G. Cauwenberghs, "Real-time eeg source-mapping toolbox (rest): Online ica and source localization," in *2015 37th Annual International Conference of the IEEE Engineering in Medicine and Biology Society (EMBC)*, pp. 4114–4117, IEEE, 2015.

[82] S.-H. Hsu, T. Mullen, T.-P. Jung, and G. Cauwenberghs, "Online recursive independent component analysis for real-time source separation of high-density eeg," in *2014 36th Annual International Conference of the IEEE Engineering in Medicine and Biology Society*, pp. 3845–3848, IEEE, 2014.

[83] M. T. Akhtar, T.-P. Jung, S. Makeig, and G. Cauwenberghs, "Recursive independent component analysis for online blind source separation," in *2012 IEEE International Symposium on Circuits and Systems*, pp. 2813–2816, IEEE, 2012.

[84] S. M. S. Hasan, M. R. Siddiquee, and O. Bai, "Supervised classification of eeg signals with score threshold regulation for pseudo-online asynchronous detection of gait intention," in *2019 18th IEEE International Conference On Machine Learning And Applications (ICMLA)*, pp. 1476–1479, Dec 2019.

[85] S. M. S. Hasan, M. R. Siddiquee, and O. Bai, "Asynchronous Prediction of Human Gait Intention in a Pseudo Online Paradigm Using Wavelet Transform," *IEEE Transactions on Neural Systems and Rehabilitation Engineering*, 2020.

[86] S. M. Shafiul Hasan, M. R. Siddiquee, R. Atri, R. Ramon, J. S. Marquez, and O. Bai, "Prediction of gait intention from pre-movement EEG signals: a feasibility study," *Journal of NeuroEngineering and Rehabilitation*, 2020.

[87] L. Pion-Tonachini, K. Kreutz-Delgado, and S. Makeig, "ICLabel: An automated electroencephalographic independent component classifier, dataset, and website," *NeuroImage*, 2019.

[88] M. J. Shensa, "The Discrete Wavelet Transform: Wedding the À Trous and Mallat Algorithms," *IEEE Transactions on Signal Processing*, 1992.

[89] J. Gilles, "Empirical wavelet transform," *IEEE Transactions on Signal Processing*, 2013.

[90] I. Daubechies, J. Lu, and H. T. Wu, "Synchrosqueezed wavelet transforms: An empirical mode decomposition-like tool," *Applied and Computational Harmonic Analysis*, 2011.

[91] B. Graimann and G. Pfurtscheller, "Chapter 6 Quantification and visualization of event-related changes in oscillatory brain activity in the time-frequency domain," 2006.

[92] B. Schölkopf, "An Introduction to Support Vector Machines," in *Recent Advances and Trends in Nonparametric Statistics*, 2003.

[93] C. Shahnaz, Shoaib-Bin-Masud, and S. M. S. Hasan, "Emotion recognition based on wavelet analysis of empirical mode decomposed eeg signals responsive to music videos," in *2016 IEEE Region 10 Conference (TENCON)*, pp. 424–427, Nov 2016.

[94] M. S. Gowri G and D. P. Prasanna Raj, "EEG Feature Extraction using Daubechies Wavelet and Classification using Neural Network," tech. rep.

[95] I. Omerhodzic, S. Avdakovic, A. Nuhanovic, and K. Dizdarevic, "Energy Distribution of EEG Signals: EEG Signal Wavelet-Neural Network Classifier," *World Academy of Science, Engineering and Technology*, vol. 37, pp. 1240–1245, jul 2013.

[96] L. Guo, D. Rivero, J. Dorado, J. R. Rabuñal, and A. Pazos, "Automatic epileptic seizure detection in EEGs based on line length feature and artificial neural networks," *Journal of Neuroscience Methods*, vol. 191, pp. 101–109, aug 2010.

[97] T. Gandhi, B. K. Panigrahi, M. Bhatia, and S. Anand, "Expert model for detection of epileptic activity in EEG signature," *Expert Systems with Applications*, vol. 37, pp. 3513–3520, apr 2010.

[98] S. Kumar, M. Yadava, and P. P. Roy, "Fusion of EEG response and sentiment analysis of products review to predict customer satisfaction," *Information Fusion*, vol. 52, pp. 41–52, dec 2019.

[99] D. J. Clark, "Automaticity of walking: Functional significance, mechanisms, measurement and rehabilitation strategies," may 2015.

[100] P. Haggard, "Human volition: Towards a neuroscience of will," dec 2008.

[101] B. Libet, C. A. Gleason, E. W. Wright, and D. K. Pearl, "Time of Conscious Intention to Act in Relation to Onset of Cerebral Activity (Readiness-Potential): The Unconscious Initiation of a Freely Voluntary Act," *Brain*, vol. 106, no. 3, pp. 623–642, 1983.

[102] C. Lin, B. Wang, N. Jiang, R. Xu, N. Mrachacz-Kersting, and D. Farina, "Discriminative manifold learning based detection of movement-related cortical po-

tentials,," *IEEE Trans. Neural Syst. Rehabil. Eng*, vol. 24, no. 9, p. 921–927, 2016.

[103] S. M. Shafiul Hasan and O. Bai, "Vmd-wsst: A combined bci algorithm to predict self-paced gait intention¡sup¿*¡/sup¿," in *2021 IEEE International Conference on Systems, Man, and Cybernetics (SMC)*, pp. 3188–3193, 2021.

[104] K. Dragomiretskiy and D. Zosso, "Variational mode decomposition," *IEEE Transactions on Signal Processing*, vol. 62, pp. 531–544, feb 2014.

[105] G. Lisi and J. Morimoto, "EEG single-trial detection of gait speed changes during treadmill walk," *PLoS ONE*, vol. 10, may 2015.

[106] J. Ibáñez, J. I. Serrano, M. D. Del Castillo, J. A. Gallego, and E. Rocon, "Online detector of movement intention based on EEG - Application in tremor patients," *Biomedical Signal Processing and Control*, 2013.

[107] A. D. Nordin, W. D. Hairston, and D. P. Ferris, "Faster Gait Speeds Reduce Alpha and Beta EEG Spectral Power from Human Sensorimotor Cortex," *IEEE Transactions on Biomedical Engineering*, 2020.

[108] O. Bai, G. Kelly, D.-Y. Fei, D. Murphy, J. Fox, B. Burkhardt, W. Lovegreen, and J. Soars, "A wireless, smart EEG system for volitional control of lower-limb prosthesis," in *TENCON 2015 - 2015 IEEE Region 10 Conference*, pp. 1–6, IEEE, nov 2015.

[109] S. M. S. Hasan, M. R. Siddiquee, J. S. Marquez, and O. Bai, "Enhancement of movement intention detection using eeg signals responsive to emotional music stimulus," *IEEE Transactions on Affective Computing*, pp. 1–1, 2020.

[110] B. Blankertz, G. Curio, and K. R. Müller, "Classifying single trial EEG: Towards brain computer interfacing," in *Advances in Neural Information Processing Systems*, 2002.

[111] X. Liao, D. Yao, D. Wu, and C. Li, "Combining spatial filters for the classification of single-trial EEG in a finger movement task," *IEEE Transactions on Biomedical Engineering*, 2007.

[112] J. Lu, K. Xie, and D. J. McFarland, "Adaptive spatio-temporal filtering for movement related potentials in EEG-based brain-computer interfaces," *IEEE Transactions on Neural Systems and Rehabilitation Engineering*, 2014.

[113] E. A. Zeid, A. R. Sereshkeh, and T. Chau, "A pipeline of spatio-temporal filtering for predicting the laterality of self-initiated fine movements from single trial readiness potentials," *Journal of Neural Engineering*, 2016.

[114] K. Wang, M. Xu, Y. Wang, S. Zhang, L. Chen, and D. Ming, "Enhance decoding of pre-movement EEG patterns for brain-computer interfaces," in *Journal of Neural Engineering*, 2020.

[115] J. H. Jeong, N. S. Kwak, C. Guan, and S. W. Lee, "Decoding Movement-Related Cortical Potentials Based on Subject-Dependent and Section-Wise Spectral Filtering," *IEEE Transactions on Neural Systems and Rehabilitation Engineering*, 2020.

[116] A. Úbeda, J. M. Azorín, R. Chavarriaga, and J. del R Millán, "Classification of upper limb center-out reaching tasks by means of EEG-based continuous decoding techniques," *Journal of NeuroEngineering and Rehabilitation*, 2017.

[117] D. Pei, M. Burns, R. Chandramouli, and R. Vinjamuri, "Decoding Asynchronous Reaching in Electroencephalography Using Stacked Autoencoders," *IEEE Access*, 2018.

[118] J. Meng, S. Zhang, A. Bekyo, J. Olsoe, B. Baxter, and B. He, "Noninvasive Electroencephalogram Based Control of a Robotic Arm for Reach and Grasp Tasks," *Scientific Reports*, 2016.

[119] P. Ofner, A. Schwarz, J. Pereira, and G. R. Müller-Putz, "Upper limb movements can be decoded from the time-domain of low-frequency EEG," *PLoS ONE*, 2017.

[120] N. Tang, C. Guan, K. Ang, K. Phua, and E. Chew, "Motor imagery-assisted brain-computer interface for gait retraining in neurorehabilitation in chronic stroke," *Annals of Physical and Rehabilitation Medicine*, 2018.

[121] J. H. Jeong, M. H. Lee, N. S. Kwak, and S. W. Lee, "Single-trial analysis of readiness potentials for lower limb exoskeleton control," in *5th International Winter Conference on Brain-Computer Interface, BCI 2017*, 2017.

[122] D. Liu, W. Chen, K. Lee, R. Chavarriaga, F. Iwane, M. Bouri, Z. Pei, and J. D. R. Millan, "EEG-Based Lower-Limb Movement Onset Decoding: Continuous Classification and Asynchronous Detection," *IEEE Transactions on Neural Systems and Rehabilitation Engineering*, 2018.

[123] L. Yao, N. Mrachacz-Kersting, X. Sheng, X. Zhu, D. Farina, and N. Jiang, "A Multi-Class BCI Based on Somatosensory Imagery," *IEEE Transactions on Neural Systems and Rehabilitation Engineering*, 2018.

[124] H. Yang, C. Guan, C. C. Wang, and K. K. Ang, "Detection of motor imagery of brisk walking from electroencephalogram," *Journal of Neuroscience Methods*, 2015.

[125] Y. Zhang, S. Prasad, A. Kilicarslan, and J. L. Contreras-Vidal, "Multiple kernel based region importance learning for neural classification of gait states from EEG signals," *Frontiers in Neuroscience*, 2017.

[126] K. Lee, D. Liu, L. Perroud, R. Chavarriaga, and J. d. R. Millán, "A brain-controlled exoskeleton with cascaded event-related desynchronization classifiers," *Robotics and Autonomous Systems*, vol. 90, pp. 15–23, 2017.

[127] K. M. Naugle, C. J. Hass, J. Joyner, S. A. Coombes, and C. M. Janelle, "Emotional state affects the initiation of forward gait," *Emotion*, 2011.

[128] S. A. Coombes, J. H. Cauraugh, and C. M. Janelle, "Emotion and movement: Activation of defensive circuitry alters the magnitude of a sustained muscle contraction," *Neuroscience Letters*, 2006.

[129] K. S. Park, C. J. Hass, B. Fawver, H. Lee, and C. M. Janelle, "Emotional states influence forward gait during music listening based on familiarity with music selections," *Human Movement Science*, 2019.

[130] K. M. Naugle, C. J. Hass, D. Bowers, and C. M. Janelle, "Emotional state affects gait initiation in individuals with Parkinson's disease," *Cognitive, Affective and Behavioral Neuroscience*, 2012.

[131] L. Avanzino, G. Lagravinese, G. Abbruzzese, and E. Pelosin, "Relationships between gait and emotion in Parkinson's disease: A narrative review," 2018.

[132] M. Chen and J. A. Bargh, "Consequences of automatic evaluation: Immediate behavioral predispositions to approach or avoid the stimulus," 1999.

[133] K. L. Duckworth, J. A. Bargh, M. Garcia, and S. Chaiken, "The automatic evaluation of novel stimuli," *Psychological Science*, 2002.

[134] P. M. Niedenthal, "Embodying emotion," 2007.

[135] S. N. Haber, "The primate basal ganglia: Parallel and integrative networks," in *Journal of Chemical Neuroanatomy*, 2003.

[136] K. Takakusaki, N. Tomita, and M. Yano, "Substrates for normal gait and pathophysiology of gait disturbances with respect to the basal ganglia dysfunction," in *Journal of Neurology*, 2008.

[137] T. Eerola and J. K. Vuoskoski, "A comparison of the discrete and dimensional models of emotion in music," *Psychology of Music*, 2011.

[138] M. Halaki and K. Gi, "Normalization of EMG Signals: To Normalize or Not to Normalize and What to Normalize to?," in *Computational Intelligence in Electromyography Analysis - A Perspective on Current Applications and Future Challenges*, InTech, oct 2012.

[139] D. Schubring and H. T. Schupp, "Affective picture processing: Alpha- and lower beta-band desynchronization reflects emotional arousal," *Psychophysiology*, vol. 56, p. e13386, apr 2019.

[140] T. Yan, M. Cempini, C. M. Oddo, and N. Vitiello, "Review of assistive strategies in powered lower-limb orthoses and exoskeletons," *Robotics and Autonomous Systems*, vol. 64, pp. 120–136, 2015.

[141] H. A. Varol, F. Sup, and M. Goldfarb, "Multiclass real-time intent recognition of a powered lower limb prosthesis," *IEEE Transactions on Biomedical Engineering*, vol. 57, no. 3, pp. 542–551, 2009.

[142] H. Huang, F. Zhang, L. J. Hargrove, Z. Dou, D. R. Rogers, and K. B. Englehart, "Continuous locomotion-mode identification for prosthetic legs based on neuromuscular–mechanical fusion," *IEEE Transactions on Biomedical Engineering*, vol. 58, no. 10, pp. 2867–2875, 2011.

[143] H. Huang, T. A. Kuiken, R. D. Lipschutz, *et al.*, "A strategy for identifying locomotion modes using surface electromyography," *IEEE Transactions on Biomedical Engineering*, vol. 56, no. 1, pp. 65–73, 2008.

[144] M. T. Farrell and H. Herr, "A method to determine the optimal features for control of a powered lower-limb prostheses," in *2011 Annual International Conference of the IEEE Engineering in Medicine and Biology Society*, pp. 6041–6046, IEEE, 2011.

[145] D. Novak and R. Riener, "A survey of sensor fusion methods in wearable robotics," *Robotics and Autonomous Systems*, vol. 73, pp. 155–170, 2015.

[146] N. E. Krausz, T. Lenzi, and L. J. Hargrove, "Depth sensing for improved control of lower limb prostheses," *IEEE Transactions on Biomedical Engineering*, 2015.

[147] H. A. Varol and Y. Massalin, "A feasibility study of depth image based intent recognition for lower limb prostheses," in *Proceedings of the Annual International Conference of the IEEE Engineering in Medicine and Biology Society, EMBS*, 2016.

[148] B. Zhong, R. Luiz da Silva, M. Li, H. Huang, and E. Lobaton, "Environmental Context Prediction for Lower Limb Prostheses With Uncertainty Quantification," *IEEE Transactions on Automation Science and Engineering*, 2020.

[149] T. Yan, Y. Sun, T. Liu, C. H. Chcung, and M. Q. H. Meng, "A Locomotion Recognition System Using Depth Images," in *Proceedings - IEEE International Conference on Robotics and Automation*, 2018.

[150] Y. Massalin, M. Abdrakhmanova, and H. A. Varol, "User-independent intent recognition for lower limb prostheses using depth sensing," *IEEE Transactions on Biomedical Engineering*, 2018.

[151] K. Zhang, C. Xiong, W. Zhang, H. Liu, D. Lai, Y. Rong, and C. Fu, "Environmental Features Recognition for Lower Limb Prostheses Toward Predictive Walking," *IEEE Transactions on Neural Systems and Rehabilitation Engineering*, 2019.

[152] B. Laschowski, W. McNally, A. Wong, and J. McPhee, "Preliminary design of an environment recognition system for controlling robotic lower-limb prostheses and exoskeletons," in *IEEE International Conference on Rehabilitation Robotics*, 2019.

[153] J. P. Diaz, R. L. Da Silva, B. Zhong, H. H. Huang, and E. Lobaton, "Visual Terrain Identification and Surface Inclination Estimation for Improving Human Locomotion with a Lower-Limb Prosthetic," in *Proceedings of the Annual International Conference of the IEEE Engineering in Medicine and Biology Society, EMBS*, 2018.

[154] M. Liu, D. Wang, and H. Helen Huang, "Development of an Environment-Aware Locomotion Mode Recognition System for Powered Lower Limb Pros-

theses," *IEEE Transactions on Neural Systems and Rehabilitation Engineering*, 2016.

[155] B. Zhong, R. L. da Silva, M. Tran, H. Huang, and E. Lobaton, "Efficient environmental context prediction for lower limb prostheses," *IEEE Transactions on Systems, Man, and Cybernetics: Systems*, 2021.

[156] B. Laschowski, W. McNally, A. Wong, and J. McPhee, "Comparative analysis of environment recognition systems for control of lower-limb exoskeletons and prostheses," in *2020 8th IEEE RAS/EMBS International Conference for Biomedical Robotics and Biomechatronics (BioRob)*, pp. 581–586, IEEE, 2020.

[157] W. Zhang, H. Zhou, S. Sun, Z. Wang, J. Shi, and C. C. Loy, "Robust multi-modality multi-object tracking," in *Proceedings of the IEEE/CVF International Conference on Computer Vision*, pp. 2365–2374, 2019.

[158] K. Weiss, T. M. Khoshgoftaar, and D. Wang, "A survey of transfer learning," *Journal of Big data*, vol. 3, no. 1, pp. 1–40, 2016.

[159] J. Deng, W. Dong, R. Socher, L.-J. Li, K. Li, and L. Fei-Fei, "Imagenet: A large-scale hierarchical image database," in *2009 IEEE Conference on Computer Vision and Pattern Recognition*, pp. 248–255, 2009.

[160] X. Zhang, X. Zhou, and M. Lin, "ShuffleNet: An Extremely Efficient Convolutional Neural Network for Mobile Devices,"

[161] A. G. Howard, M. Zhu, B. Chen, D. Kalenichenko, W. Wang, T. Weyand, and M. Andreetto, "MobileNets: Efficient Convolutional Neural Networks for Mobile Vision Applications,"

[162] D. P. Kingma and J. Ba, "Adam: A method for stochastic optimization," *CoRR*, vol. abs/1412.6980, 2015.

[163] C. Cortes, M. Mohri, and A. Rostamizadeh, "L2 regularization for learning kernels," *arXiv preprint arXiv:1205.2653*, 2012.

[164] R. Di Gregorio and L. Vocenas, "Identification of gait-cycle phases for prosthesis control," *Biomimetics*, vol. 6, no. 2, p. 22, 2021.

VITA

S M SHAFIUL HASAN

2021	M.Sc., Electrical Engineering Florida International University Miami, Florida
2019	M.Sc., Electrical and Electronic Engineering Bangladesh University of Engineering and Technology Dhaka, Bangladesh
2016	B.Sc., Electrical and Electronic Engineering Bangladesh University of Engineering and Technology Dhaka, Bangladesh

PUBLICATIONS AND PRESENTATIONS

Castellanos, A., Ysea-Hill, O., Lin, C., Hasan, S., Bai, O. and Ruiz, J.G., 2021. Identifying veterans at risk for dementia using claims-based electronic health record data and machine learning. Alzheimer's & Dementia, 17, p.e052636.

Lin, C., Hasan, S.S. and Bai, O., 2021, November. Robotic Navigation with Human Brain Signals and Deep Reinforcement Learning. In 2021 4th International Conference on Robotics, Control and Automation Engineering (RCAE) (pp. 278-283). IEEE.

Hasan, S.S. and Bai, O., 2021, October. VMD-WSST: A Combined BCI Algorithm to Predict Self-paced Gait Intention. In 2021 IEEE International Conference on Systems, Man, and Cybernetics (SMC) (pp. 3188-3193). IEEE.

Hasan, S.S., Marquez, J.S., Siddiquee, M.R., Fei, D.Y. and Bai, O., 2021. Preliminary Study on Real-time Prediction of Gait Acceleration Intention from Volition-Associated EEG Patterns. IEEE Access, 9, pp.62676-62686.

Hasan, S.S., Siddiquee, M.R., Atri, R., Ramon, R., Marquez, J.S. and Bai, O., 2020. Prediction of gait intention from pre-movement EEG signals: a feasibility study. Journal of neuroengineering and rehabilitation, 17(1), pp.1-16.

Hasan, S.S., Siddiquee, M.R., Marquez, J.S. and Bai, O., 2020. Enhancement of movement intention detection using EEG signals responsive to emotional music stimulus. IEEE Transactions on Affective Computing.

Hasan, S.S., Siddiquee, M.R. and Bai, O., 2020. Asynchronous prediction of human gait intention in a pseudo online paradigm using wavelet transform. IEEE Transactions on Neural Systems and Rehabilitation Engineering, 28(7), pp.1623-1635.

Siddiquee, M.R., Hasan, S.S., Marquez, J.S., Ramon, R.N. and Bai, O., 2020. Accurate vigilance detection during gait by using movement artifact removal. IEEE Access, 8, pp.51179-51188.

Marquez, J.S., Hasan, S.M., Siddiquee, M.R., Luca, C.C., Mishra, V.R., Mari, Z. and Bai, O., 2020. Neural correlates of freezing of gait in Parkinson's disease: an electrophysiology mini-review. Frontiers in neurology, p.1303.

Siddiquee, M.R., Atri, R., Marquez, J.S., Hasan, S.M., Ramon, R. and Bai, O., 2020. Sensor location optimization of wireless wearable fnirs system for cognitive workload monitoring using a data-driven approach for improved wearability. Sensors, 20(18), p.5082.

Hasan, S.S., Siddiquee, M.R. and Bai, O., 2019, December. Supervised classification of eeg signals with score threshold regulation for pseudo-online asynchronous detection of gait intention. In 2019 18th IEEE International Conference On Machine Learning And Applications (ICMLA) (pp. 1476-1479). IEEE.

Shafiul Hasan, S.M., 2019. Emotion recognition based on statistical modeling of EMD-DWT transformed EEG signals responsive to music videos.

Shahnaz, C. and Hasan, S.S., 2016, November. Emotion recognition based on wavelet analysis of Empirical Mode Decomposed EEG signals responsive to music videos. In 2016 IEEE Region 10 Conference (TENCON) (pp. 424-427). IEEE.